BYPASSABLE ESSENTIAL GENES AFFECTING REGULATION OF
HETEROCHROMATIN SILENCING IN *S. POMBE*

By

EVE SAMANTHA REILLY

A dissertation submitted to the

School of Graduate Studies

Rutgers, The State University of New Jersey

In partial fulfillment of the requirements

For the degree of

Doctor of Philosophy

Graduate Program in Microbiology and Molecular Genetics

Written under the direction of

Mikel Zaratiegui

And approved by

———————————————————

———————————————————

———————————————————

———————————————————

New Brunswick, New Jersey

October 2019

ABSTRACT OF THE DISSERTATION

BYPASSABLE ESSENTIAL GENES AFFECTING REGULATION OF
HETEROCHROMATIN SILENCING IN *S. POMBE*

by EVE SAMANTHA REILLY

Dissertation Director:

Mikel Zaratiegui

The mechanisms by which epigenetic markings are generated and maintained are crucial

to ensuring genome stability and appropriate gene expression levels, therefore

understanding how chromatin states are faithfully maintained and propagated is critical.

We performed a forward genetic screen in *Schizosaccharomyces pombe* using integration

density profiling of transposable element insertions to identify modifiers of position

effect variegation (PEV), an epigenetic phenomenon characterized by heritable yet

stochastic heterochromatin spreading over a reporter gene. Interestingly, a number of

essential genes including DNA replication and repair factors were enriched within the

screen. Transposable element integration sites were subsequently used to guide the

generation of new mutant alleles in the essential candidate PEV genes *top2, top3,* and *tel2*

using CRISPR-Cas9 mediated mutagenesis; with this approach we were able to isolate

mutant alleles in all three genes affecting transcriptional silencing at heterochromatic

regions. Finally, we demonstrate that dense transposon integrations may permit bypass of

essentiality (BOE) by leveraging complex genetic interactions which suppress lethality in

bypassable essential gene mutants. These interactions may facilitate the detection of

novel phenotypes occurring as a consequence of essential gene inactivation. Essential

genes have long been under-represented using traditional genetic screening approaches;

however, a systematic approach utilizing these phenomena could potentially increase their representation in such screens to allow for future discovery and investigation of novel roles for essential genes in a number of vital cellular processes.

Acknowledgements

I am grateful to my advisor, Dr. Mikel Zaratiegui, for his support, encouragement, and expertise in conducting the work presented in this thesis. I am further thankful to Dr. Zaratiegui for his flexibility and generosity in allowing me to pursue other career development opportunities throughout my doctoral research. I would also like to thank the Zaratiegui lab members, both past and present, for their companionship, guidance, and technical discussion.

I would like to thank Dr. Sam Gu and the Gu lab members, past and present, whom have always been wonderful neighbors and are always quick to share reagents, advice, and technical discussions. I would also like to thank the rest of my thesis committee, Dr. Nancy Walworth and Dr. Marc Gartenberg, for their feedback and productive discussions.

I am grateful to Dr. Ruth Steward, who has supported me from the first day I set foot in a research laboratory and who taught me what it means to be a scientist. I am further grateful to have had a number of formal and informal mentors and role models both inside and outside of the lab. Their generosity with their time, advice, encouragement, and feedback is very much appreciated.

I would also like to thank my classmates; my peers in the incoming Molecular Biosciences Class of 2015 have made the past four years so much more enriching, and I am grateful to have gone through this graduate school journey alongside them. In addition to nurturing a positive and stimulating intellectual environment within classes and seminars they have also been a tremendous source of support outside of the lab and

iv

classroom. I would particularly like to thank Jenna Newman for her boundless positivity and encouragement throughout our lunches, ice cream dates, and Girls' Nights.

Last, but certainly not least, I would like to thank my family, who wholly encouraged my decision to go to graduate school. Without their support these past four years would not have been possible. My mother, who has always taken exceptional care of my children since my return to work shortly after my older daughter was born, is one of the most thoughtful and selfless individuals I have ever known. My husband, Joseph, is my number one cheerleader, copy editor, chief strategist, and best friend. I would like to acknowledge and express my gratitude for the countless hours they have spent on childcare, endless schedule rearrangements and emergency accommodations, and 'quick stops' at the lab so that I could continue making progress towards my degree.

Dedication

To Anna and Madison, the light of my life.

Table of Contents

LIST OF FIGURES

LIST OF TABLES

CHAPTER I: INTRODUCTION

1.1 Introduction to heterochromatin and its importance in maintaining genome stability

Epigenetic modifications organize chromatin into two distinct states- an 'open' form known as euchromatin, or 'closed' and highly compact heterochromatin. Maintaining or switching between chromatin states in a temporally and spatially defined manner is essential for coordinating gene regulation and ensuring genome stability. The term heterochromatin was originally coined to describe the differential staining of highly condensed chromosomal regions; however, the definition of heterochromatin has evolved to encompass a distinct form of chromatin endowed with specific markings, characteristics, and functional properties (Robin C. Allshire & Madhani, 2017; Heitz, 1929). Heterochromatin can be further classified into constitutive or facultative, with the former referring to regions which are stably heterochromatinized while the latter retains the ability to revert between euchromatin and heterochromatin (Trojer & Reinberg, 2007). The tightly compacted conformation of heterochromatin denies access to its underlying DNA impeding virtually all nucleic acid transactions. As a consequence, heterochromatic regions are transcriptionally silent and homologous recombination (HR) is inhibited. Regions of constitutive heterochromatin are commonly comprised of repetitive elements, non-coding regions, and chromosome features such as telomeres and centromeres; many of the above can jeopardize genome stability if not carefully regulated and/or silenced (S. I. S. Grewal & Jia, 2007; Janssen, Colmenares, & Karpen, 2018; Trojer & Reinberg, 2007). Transcriptional de-repression and/or loss of heterochromatic markings on repetitive elements, for example, can contribute to gross chromosomal

rearrangements in a variety of cancers as a result of non-allelic recombination, while centromeric heterochromatin helps to ensure chromosomal cohesion during mitosis thereby facilitating proper chromosome segregation (Bernard et al., 2001; Ting et al., 2011; Zhu et al., 2011). Another notable example is the transcriptional silencing of parasitic genomic elements such as transposons, thus limiting their ability to mobilize and colonize other genomic regions by reducing transposon expression (Robin C. Allshire & Madhani, 2017; Buchon & Vaury, 2006; Groh & Schotta, 2017). Heterochromatin also plays an important role in establishing overall nuclear architecture in addition to conferring discrete chromatin domains with functional properties such as suppression of recombination at repetitive elements (Amaral, Ryu, Li, & Chiolo, 2017; W. Zhang et al., 2015). Constitutive heterochromatin, therefore, has an important role in defending and maintaining genome integrity that is accomplished through a number of diverse mechanisms.

1.2 Constitutive heterochromatin in *Schizosaccharomyces pombe*

Schizosaccharomyces pombe, or fission yeast, has long been used as a model organism for the study of heterochromatin. *S. pombe* is a eukaryotic, single-celled organism with a compact nuclear genome consisting of three chromosomes ranging in size from 3.5-5.7 Mb. Many of the proteins and pathways contributing to heterochromatin formation and maintenance in higher-order eukaryotes are conserved in fission yeast. Genetic analysis is further simplified due to the fact that *S. pombe* spends the majority of its life cycle as haploid organism and exhibits minimal genetic redundancy, making the analysis of single genes and their contributions to these essential processes easier to parse.

The fission yeast genome houses several domains of constitutive heterochromatin which can be found at the centromeres, ribosomal DNA (rDNA), subtelomeric regions, and the mating type locus. Like most multicellular eukaryotes, fission yeast possess specialized regional centromeres which are cytologically distinct from the rest of the chromosome (Partridge, 2008). Kinetochore assembly during mitosis occurs within the central domain which is composed of a specialized, highly conserved histone H3 variant known as CENP-A (Stellfox, Bailey, & Foltz, 2013). The central domain is flanked by two regions of constitutive heterochromatin assembled over arrays of tandemly repeated non-coding satellite DNA. This arrangement is a conserved feature of nearly all regional centromeres found in higher-order eukaryotes (McKinley & Cheeseman, 2015). The heterochromatic region that flanks the kinetochore is collectively termed the pericentromere. In fission yeast the pericentromere is subdivided into two distinct repetitive domains, the inner repeats (*imr*) and the outer repeats (*otr*). The inner repeat sequence varies between chromosomes while the outer repeat sequences are closely related on all three chromosomes in *S. pombe* (Alper, Lowe, & Partridge, 2012; Chikashige et al., 1989).

Pericentromeric heterochromatin has an important structural role in ensuring proper chromosome segregation and kinetochore assembly during mitosis, therefore preservation of centromere stability is critical (Bernard et al., 2001). Repetitive elements are often inherently destabilizing, however, and so a number of mechanisms exist to maintain transcriptional and recombination repression at these regions (Bzymek & Lovett, 2001; S. I. Grewal & Elgin, 2007). RNA interference (RNAi) is the primary pathway by which pericentromeric heterochromatin is established in fission yeast (Volpe

et al., 2002). The process of RNAi-directed pericentromeric heterochromatin assembly is coupled to transcription of non-coding pericentromeric repeats by RNA Polymerase II (RNA Pol II) during S phase of the cell cycle (E. S. Chen et al., 2008; Kloc, Zaratiegui, Nora, & Martienssen, 2008). The core RNAi machinery consists of Argonaute (*ago1*), Dicer (*dcr1*), and RNA-dependent RNA polymerase (*RdRP*) (Martienssen & Moazed, 2015; Provost et al., 2002) . Double-stranded pericentromeric transcripts (dsRNA) are processed by Dicer into small interfering RNAs (siRNAs) while RdRP participates in dsRNA production and siRNA amplification (Martienssen & Moazed, 2015; Sugiyama, Cam, Verdel, Moazed, & Grewal, 2005). siRNAs are subsequently loaded onto the RITS complex which consists of the chromodomain protein Chp1, Tas3, and RNAi effector protein Ago1 (Elizabeth H. Bayne et al., 2014; DeBeauchamp et al., 2008; Martienssen & Moazed, 2015). Base-pairing between the siRNA and the nascent pericentric repeat transcripts recruits the RITS complex to the pericentromeric repeats. H3K9 methylation constitutes a second necessary recruitment signal for RITS via its chromodomain subunit Chp1 (J.-i. Nakayama, J. C. Rice, B. D. Strahl, C. D. Allis, & S. I. Grewal, 2001; Verdel et al., 2004). The chromatin-interacting RITS complex subsequently recruits the chromatin-modifying CLRC complex consisting of Clr4, Rik1, Dos1/2 (Raf1/2), and Cul4 mediated by the adaptor protein Stc1, permitting H3K9 methylation by Clr4 (E. H. Bayne et al., 2010; F. Li et al., 2005; K. Zhang, Mosch, Fischle, & Grewal, 2008). Methylated H3K9 is then bound by the chromodomain proteins Chp1, Chp2, and Swi6, facilitating formation of a repressive chromatin structure and promoting efficient RNA degradation by stabilization of the RNAi and nuclear exosome complexes as well as recruitment of additional chromatin remodeling complexes (Keller et al., 2012; Motamedi

et al., 2008). The convergence of multiple pathways at this juncture is critical to ensure heterochromatic silencing at the centromere. Swi6 and Chp2 recruit the Snf2/histone deacetylase [HDAC] repressor complex (SHREC) which contains the class II HDAC Clr3 and the Snf2 chromatin-remodeling factor homolog Mit1 in addition to silencing factors Clr1 and Clr2 (Sugiyama et al., 2007). Clr3 further aids in restricting Pol II accessibility by removing/preventing histone modifications associated with active transcription and preventing histone turnover; loss of Clr3 leads to decreased heterochromatin at pericentromeres yet produces a concomitant increase in small RNAs due to increased transcription in this region (Aygün, Mehta, & Grewal, 2013; Hansen et al., 2005). Swi6 associates with another complex containing the class I HDAC Clr6, which is semi-redundant with Clr3 yet exhibits a broader substrate specificity (Fischer et al., 2009).

Collectively, the redundancy and/or overlap in the ways in which silencing is established and maintained at centromeres underscores its importance. Paradoxically, transcription is an essential component of many of these processes. RNA Pol II preferentially transcribes pericentromeric repeat sequences at low levels beginning in the G2/M transition, coinciding with condensin and Swi6 delocalization from heterochromatic regions by H3S10phosphorylation which prevents the chromodomain of Swi6 from binding to adjacent methylated H3K9 (Ee Sin Chen et al., 2008). In S phase RNAi activity begins in earnest restoring silenced heterochromatin at the pericentromeric repeats in a process likely coupled to the passage of the replication fork; Dicer also plays an important role in facilitating release of Pol II while these processes are ongoing simultaneously to prevent clashes between the transcription and DNA replication

machinery (Castel et al., 2014; E. S. Chen et al., 2008; Kloc et al., 2008; F. Li, 2011; Zaratiegui, Castel, et al., 2011).

A number of diverse mechanisms exist for maintenance and establishment of heterochromatin domains in addition to RNAi, including nuclear exosome processing, RNA quality control surveillance, and the presence of chromatin insulators such as the tRNA genes found at the boundaries of pericentromeric outer repeats which restrict heterochromatin spreading (Chalamcharla, Folco, Dhakshnamoorthy, & Grewal, 2015; Kirkland, Raab, & Kamakaka, 2013; Reyes-Turcu, Zhang, Zofall, Chen, & Grewal, 2011). While RNAi components localize to rDNA, which are partially heterochromatinized, their primary purpose appears to be in management of replication-transcription collisions and suppression of recombination (R. C. Allshire & Ekwall, 2015; Castel et al., 2014). Finally, RNAi appears to be dispensable at subtelomeric heterochromatin, another major region of constitutive heterochromatin in fission yeast (Kanoh, Sadaie, Urano, & Ishikawa, 2005). Instead, subtelomeric heterochromatin is the product of a concerted effort between chromatin remodelers, histone chaperones, and cohesins for establishment and maintenance of silenced chromatin at chromosome ends (Buchanan et al., 2009; Dheur, Saupe, Genier, Vazquez, & Javerzat, 2011; Kanoh et al., 2005; Steglich et al., 2015).

In this study we describe a screen for mutants affecting the integrity and spreading of heterochromatin at the pericentromeric outer repeats. As described in greater detail in the following chapters, we found that a number of genes encoding products known to be involved in heterochromatin formation and maintenance- *swi6, dos1/2, rik1-* were significantly enriched in the screen, indicating that the selection was successful and

validating the overall approach. Gene ontology (GO) analysis further confirmed that genes emerging as significantly enriched from the screen are over-represented in biological processes known to be involved in chromatin silencing. Thus, the genetic screen described in this study enables robust identification of genes affecting heterochromatin at silenced loci. We also identified a number of candidate genes for follow up which do not have a known function in centromeric silencing, suggesting that this approach can facilitate identification of novel genes involved in heterochromatin maintenance. Going forward, the approach described in this study can be leveraged to enhance our understanding of the complexities and regulation of heterochromatin domains by identification of novel genes contributing to centromeric silencing.

1.3 The influence of replication fork management and DNA repair on chromatin status

One of the most important open questions in epigenetics is how heterochromatic marks are faithfully inherited by subsequent generations after disruption by the replication fork during DNA replication. It has been suggested that replication fork stalling can promote changes in the local chromatin environment which influence fork management and gene expression in subsequent cell cycles (Fournier, Kumar, & Stirling, 2018; Rowlands, Dhavarasa, Cheng, & Yankulov, 2017). The nature of these changes, however, and their underlying mechanisms are still poorly understood. In human cells, the histone chaperone Asf1 shows an increase in bound histones bearing the H3K9me1 PTM when replication is globally impaired which are promptly incorporated upon resumption of DNA replication (Huang et al., 2015; Jasencakova et al.). Conversely, in *C. elegans*, impaired DNA replication has been linked to global chromatin de-repression

and subsequent inheritance of epigenetic alterations for several generations before silencing is re-established (Klosin et al., 2017). In *S. pombe*, Brc1 stabilizes stalled replication forks in pericentromeric heterochromatin and this activity has also been demonstrated to be important for maintaining heterochromatin and transcriptional repression of the pericentromeres (Lee, Rozenzhak, & Russell, 2013; Williams et al., 2010; Young Lee & Russell, 2013). Replication stress has also been proposed to drive epigenetic plasticity in cancer cells, which may in turn contribute to tumorigenesis (Alabert & Groth, 2012; Jasencakova & Groth, 2010; Nikolov, 2015). Taken together, these findings and many others not specifically referenced here reinforce the coordination between replication and chromatin assembly in response to replicative stress (for review, see (Alabert & Groth, 2012; H. He, Gonzalez, Zhang, & Li, 2014; Khurana & Oberdoerffer, 2015; Rowlands et al., 2017)).

The nature of this relationship appears to be complex, however, as replicative stress has paradoxically been linked to both decreases and increases in heterochromatic markings- or in some circumstances has been shown to have no effect at all- indicating that the epigenetic effect and nature of the stressor is likely context dependent. In the instance of the former, one of the prevailing theories is that replication slowing or stalling prior to fork re-start can adversely impact histone recycling and subsequent inheritance of histone modifications, which are important for re-establishment of chromatin states in the wake of the replication fork (Jasencakova et al.; Reveron-Gomez et al., 2018; Šviković & Sale, 2017). The minichromosome maintenance (MCM) helicase subunit MCM2 has the ability to bind H3-H4 tetramers containing any H3 variant, and it has been suggested that this activity may transfer histone variants deposited during previous replication cycles or

"old" post-translationally modified nucleosomes to facilitate chromatin re-assembly and promote histone recycling in the wake of the replication fork (Huang et al., 2015). Similarly, assays using synthetic sequences which approximate unwound DNA after replication fork passage demonstrated that the single-strand binding protein RPA directly binds H3-H4 and promotes DNA-(H3-H4) complex assembly on nearby double-stranded DNA (S. Liu et al., 2017). In the same study, the authors note that MCM2 and its interactions with histone chaperones facilitates disassembly of parental H3-H4 prior to DNA replication, and that RPA subsequently binds single-stranded DNA (ssDNA) after the unwinding of double-stranded DNA (dsDNA) by MCM. Thus, replication factors work in concert to coordinate histone deposition and recycling during replication-coupled nucleosome assembly (S. Liu et al., 2017). The replisome itself, therefore, is directly involved in ensuring the fidelity of epigenetic inheritance, underscoring the importance of replication-coupled chromatin assembly.

A related theory postulates that replisome disassembly to allow for DNA repair and/or recombination may lead to the loss of heterochromatin-specific replication factors (Haijin He et al., 2017; F. Li, 2011; Zaratiegui, Castel, et al., 2011). In *Schizosaccharomyces pombe* the catalytic subunit of DNA polymerase epsilon (Cdc20), the leading strand polymerase, interacts directly with a silencing complex containing Dos2, Rik1, and Mms19 thus facilitating replication-coupled heterochromatin formation (F. Li, 2011; F. Li et al., 2005). Additionally, replication of heterochromatic regions appears to diverge from their euchromatic counterparts early in the process of DNA replication, as replication factors have been observed to act in concert with heterochromatin proteins during the initial stages of replication origin activation to

regulate the timing of DNA replication (Hayashi, Takahashi, Nakagawa, Nakayama, & Masukata, 2009; Richet et al., 2015; Talbert & Henikoff, 2016). The specific regulation of heterochromatin replication origin firing and the described physical interactions between the canonical replisome and heterochromatin deposition machinery indicate that heterochromatin and euchromatin replication may employ distinct mechanisms to ensure the maintenance of their respective epigenetic marks.

Parsing the function of the replication fork complex and DNA repair factors in heterochromatin maintenance and inheritance using classical forward and reverse genetics is challenging due to the fact that many DNA replication factors are essential for viability. For the purpose of this study, therefore, we focused on genes with a described role in DNA replication, recombination, and repair to probe their relationship with heterochromatin formation and maintenance. Going forward, the mutants described in this work- as well as the overall approach- can be utilized for a mechanistic dissection of the pathways contributing to epigenetic modulation as a product of replicative stress and/or aberrant DNA repair.

1.4 Next-generation genetic screening approaches for identification of heterochromatin modifiers

Early studies recognized the differential chromosomal staining between heterochromatin and euchromatin as a reflection of the degree of condensation exhibited by the two chromatin states; however, the link between chromatin conformation and gene expression was not recognized until early studies in Drosophila described a phenomenon known as position effect variegation (PEV) in which differential expression of a gene

was linked to encroaching or receding pericentric heterochromatin (Muller & Muller, 1930; Zhimulev, Belyaeva, Fomina, Protopopov, & Bolshakov, 1986). Since its discovery in *Drosophila* PEV has been used as a tool to study heterochromatin formation in a number of organisms including yeasts, flies, and mammals (R. C. Allshire & Ekwall, 2015; Blewitt & Whitelaw, 2013; Elgin & Reuter, 2013). PEV is typically assayed via a forward genetics approach utilizing a reporter gene as a readout of PEV at a given locus followed by mutagenesis to identify mutants exhibiting enhancement or suppression of variegation. Although the general structure of PEV screens is fairly straightforward, this framework has been repurposed throughout the last several decades for use in a number of different organisms using a diversity of reporters and mutagenesis techniques to facilitate a thorough dissection of the mechanisms and factors underlying the complex process of heterochromatin formation, maintenance, and inheritance.

While traditional genetic screening in the manner described above has been remarkably fruitful, there are several notable limitations to such approaches which limit their overall resolution. Screening through a number of organisms to identify individuals with a PEV phenotype can be time- and resource-intensive, and retroactive identification and enrichment of causal alleles can be challenging (Forsburg, 2001; Irvine et al., 2009). As an example, an early PEV forward genetic screen in fission yeast (centromere: suppressor of PEV, *csp*) successfully yielded alleles in all RNAi machinery components but their identification via complementation assays was prevented by the inherent genetic instability of the reporter gene in the context of de-condensed heterochromatin. The discovery of the involvement of RNAi in heterochromatin silencing had to wait for a

reverse genetic analysis which then enabled identification of the original corresponding *csp* alleles (Karl Ekwall, Cranston, & Allshire, 1999).

Further, the majority of candidate alleles identified in screens using diploid organisms such as *Drosophila* exert a dominant effect and are homozygous lethal (Elgin & Reuter, 2013). Recessive alleles, therefore, are presumably under-represented as a consequence of the essential status of many of the genes involved in PEV pathways. While model organisms such as *Schizosaccharomyces pombe* have the advantage of a primarily haploid life cycle, making it easier to identify recessive alleles within a screen, the same restriction is likely to apply (Karl Ekwall et al., 1999; Forsburg, 2001; Irvine et al., 2009).

As researchers approach saturation of the accessible screening 'space' afforded by traditional genetic screens there has been an increasing push for the design and implementation of more versatile and high-throughput screening approaches. One solution developed in a number of model organisms has been the use of high-throughput transposon mutagenesis coupled with next-generation sequencing to identify insertion sites at the population level, which can then be mapped back to their respective genome to identify genes have been disproportionately affected (Guo et al., 2013; Kool & Berns, 2009; A. H. Michel et al., 2017; van Opijnen & Camilli, 2013). While this approach often generates a higher number of candidate genes and often results in a greater density of mutations as a product of transposon activity, it too has its own limitations, most notably the lack of actionable mutants for candidate follow-up. Many model organisms have readily available deletion and/or mutant libraries comprised of non-essential genes; however, studying essential genes using traditional genetics approaches is challenging

due to the difficulty in obtaining mutants in such genes. In this work we describe a novel implementation of a genetic screen for PEV suppressors utilizing positive selection and transposable-element mediated mutagenesis in *S. pombe* followed by a simple CRISPR-based mutagenesis approach for generation of mutations in candidate essential genes exhibiting a PEV phenotype for follow-up analysis.

Equally challenging is identification of essential genes affecting cellular processes of interest, as essential genes tend to be absent from genetic screens unless alleles exhibit a dominant phenotype. Transposon-based insertion profiling has been used to reveal the identity of essential genes in bacteria and yeast based on the premise that insertions in genes which are functionally important for growth quickly disappear from vegetatively growing cells at the population level, as they are rapidly selected against due to their negative effects on the fitness of the organism (Chao, Abel, Davis, & Waldor, 2016; Grech et al., 2019; A. H. Michel et al., 2017). Generally, in transposition-based fitness screens the prevalence of an insertion is tied to its effect on fitness in a given growth condition (Chao et al., 2016). This phenomenon is distinct from conditional essentiality, in which a subpopulation of genes is only rendered essential in particular growth conditions; a requirement for the ability to proliferate and survive is a staple of virtually any genetic screen (Tong et al., 2004). Thus, this limitation is universal to the conduct and application of genetic screens.

Although genetic suppression is a familiar concept, a recent study in fission yeast found that monogenic suppressors rendering essential genes dispensable are far more pervasive than originally appreciated (J. Li et al., 2019). The authors of the study coined the term 'bypassable' to describe this subpopulation of essential genes, referring to the

associated phenomenon as 'bypass of essentiality (BOE)'. In the present study we describe a screen in which a number of essential genes were enriched in transposable element insertions, and we demonstrate that many of the insertion events are likely to generate null alleles of the affected gene(s). We advance the hypothesis that the persistence and enrichment of insertions in essential genes may be explained by BOE interactions which allow cells carrying lethal alleles to maintain viability thereby allowing conditional selection to act upon them; in this instance, selection for mutants exhibiting enhanced PEV. Going forward, identification and exploitation of bypassable essential genes may facilitate a more nuanced dissection of the pathways and processes that many of these essential genes participate in; further, these genetic interactions have the potential to unlock a large portion of the genetic 'screening space' available to researchers when performing genetic screens such as the one described in this study.

1.5 Transposable elements and their effects on genome stability and structure

Transposable elements (TEs), also known as jumping genes, are mobile DNA sequences that possess the ability to move throughout the genome. TEs have successfully colonized a staggering diversity of host organisms and comprise a major portion of many eukaryotic genomes (Guillaume Bourque et al., 2018). TEs are often characterized as parasitic genomic elements; however, many studies have reinforced the finding that TEs and their activities are often at the heart of the development and evolution of gene regulatory networks within their host organisms at the genetic level; additionally, there are many described instances of TE proteins becoming 'domesticated' and performing vital cellular functions within their hosts (Hugh P Cam, Noma, Ebina, Levin, & Grewal, 2008; Mateo & Gonzalez, 2014; Pastuzyn et al., 2018). The impact of TEs permeate

many aspects of genome evolution, function, and disease, therefore the nature of their contributions to these vital processes is an area of active investigation.

While much of the condemnation of the mutagenic potential of transposons stems from the threat of transposon mobilization into protein coding or regulatory sequences, thereby disrupting the normal activity of these loci, silenced and/or dormant transposons pose their own threat to genomic stability. In addition to the genetic burden of additional genetic material to be duplicated in the process of DNA replication, multiple copies of a transposon within a host genome can increase the potential for non-allelic homologous recombination (NAHR) (G. Bourque, 2009; Hedges & Deininger, 2007). Large genomes are particularly susceptible to these effects, as they do not exhibit the same transposable element copy number constraints affecting compact genomes (Kidwell, 2002). Indeed, a staggering 45% of the human genome is comprised of TEs, thus the potential for these illicit recombination events is highly relevant to human health and disease (Belancio, Deininger, & Roy-Engel, 2009; Lander et al., 2001). Accordingly, TE-mediated NAHR has been implicated in a number of human pathologies including acute myelogenous leukemia, von Hippel-Lindau syndrome, familial breast cancer, and has been found to significantly contribute to structural variation in human genomes (Belancio et al., 2009; Korbel et al., 2007).

Interestingly, transcription has been demonstrated to play a major role in influencing the recombinogenic potential of repetitive elements, particularly in the context of DNA replication (Ponnari Gottipati, Cassel, Savolainen, & Helleday, 2008; P. Gottipati & Helleday, 2009; Takeuchi, Horiuchi, & Kobayashi, 2003; Zaratiegui, Vaughn, et al., 2011). It has been proposed that the mechanism underlying transcription-associated

recombination is stimulation of recombination by conflicts between DNA replication and transcription machinery (Aguilera & Gaillard, 2014; Aguilera & García-Muse, 2012; Prado & Aguilera, 2005). Stable RNA-DNA hybrids known as R loops can occur as a consequence of these encounters, which can further threaten genome integrity (Aguilera & García-Muse, 2012; Gavaldá, Gallardo, Luna, & Aguilera, 2013). In this study we investigate a potential role for replication-transcription collisions at Tf2 transposon bodies in fission yeast and their influence on transposon mobilization. While Tf2 transposons are unique in their preference for mobilization via an integrase-independent mechanism utilizing HR, the interplay between replication and transcription at sites of transposon integration and their proposed modulation of the recombinogenicity of these loci may be generally informative regarding the consequences of such encounters.

1.6 Transposable element integration site preferences and analysis

TEs exhibit a staggering diversity of integration site preferences, influenced by factors such as chromatin environment, sequence, gene density, and other genomic features such as promoters and protein coding sequences(Bowen, Jordan, Epstein, Wood, & Levin, 2003; Esnault & Levin, 2015; Sultana, Zamborlini, Cristofari, & Lesage, 2017). Transposable element integration site preferences are often shaped by competing selective forces, as the continued propagation of the transposon is essential for its survival yet transposon activity can often be deleterious to its host. This selective pressure can in turn influence transposon integration site preferences to promote insertion in regions where their presence is neutral with respect to the fitness of the host yet they retain the ability to propagate themselves (Guillaume Bourque et al., 2018; Bushman, 2003). One such example is the independently evolved targeting of Pol III gene

promoters by retrotransposons found in slime molds, budding, and fission yeast (Guo, Singh, & Levin, 2015; Spaller, Kling, Glöckner, Hillmann, & Winckler, 2016; Sultana et al., 2017). Similarly, the integration site preferences of the budding yeast transposon Ty5 are directly influenced by the condition of the host cell: when resources and nutrients are readily available, phosphorylation of Ty5 integrase directs integration into silent chromatin; conversely, under stress conditions phosphorylation of Ty5 integrase is reduced and Ty5 integration events are subsequently distributed throughout the genome (Dai, Xie, Brady, Gao, & Voytas, 2007; Zou, Ke, Kim, & Voytas, 1996). Left unconstrained, the mutagenic potential of transposons can often be deleterious to their host; however, this relationship exemplifies the successful incorporation of transposon activities into the adaptive response of the host to changing environmental conditions, where their mutagenic potential is better suited to benefit host survival (Oliver & Greene, 2009). Collectively, the integration site preferences of transposons and their mobilization has played a significant role in shaping gene regulatory networks and genome structure (Guillaume Bourque et al., 2018; Feschotte, 2008; Rey, Danchin, Mirouze, Loot, & Blanchet, 2016).

One of the barriers to analysis of transposon integration site preference is the unwavering force of natural selection. Often there is a disconnect between pre-insertion biases and post-insertion selection; this discrepancy was made apparent in a recent study of L1 retrotransposons in human cells, where it was found that newly induced L1 retrotransposition events exhibited a markedly different profile than that of endogenous L1 elements (Sultana et al., 2019). Thus, analysis of de novo transposon insertions is a powerful tool for disentangling insertion site preferences and natural selection. A

previous study from our laboratory had uncovered a role for Sap1, a DNA binding factor

that regulates replication fork progression, in guiding Tf1 retrotransposon insertion site

selection. The Tf2 transposon, despite the high sequence conservation with Tf1, exhibits

a very different behavior in preferring to mobilize by HR. In this study we generate for

the first time a profile of de novo Tf2 insertions to better understand the integration site

preferences of Tf2 retrotransposons in fission yeast. Construction of Tf2 insertion

libraries is technically challenging due to the preference of Tf2 for recombination with

pre-existing endogenous Tf2 elements in a phenomenon known as 'integration site

recycling (ISR)'; indeed, it has been suggested that ISR is another example of balancing

host survival with retrotransposon mobilization and propagation (Hoff, Levin, & Boeke,

1998). Further, we investigate the reliance of Tf2 on the host factor Sap1 and its

replication fork barrier activity for integration into fission yeast genomes via HR.

CHAPTER II. IDENTIFICATION OF BYPASSABLE ESSENTIAL GENES AFFECTING HETEROCHROMATIN IN S. POMBE

2.1 Introduction

Genetic screens have long been powerful tools for discovering and characterizing gene function. The success of such approaches is typified by the long tradition of screening for modulators of a phenomenon known as position effect variegation (PEV) in the fruit fly, *Drosophila Melanogaster* (Elgin & Reuter, 2013). Position effect variegation (PEV), first observed in *Drosophila*, is an epigenetic phenomenon characterized by variable expression of a reporter gene due to stochastic heterochromatic spreading with stable inheritance of these expression patterns once they are established (Elgin & Reuter, 2013; Schultz, 1950; Spofford, 1967). Over 150 genes have been identified as PEV modulators in Drosophila using a variety of screening approaches (Elgin & Reuter, 2013). Similarly, PEV has been observed and well-studied in the highly tractable model organism *Schizosaccharomyces pombe* (R. C. Allshire & Ekwall, 2015; K. Ekwall & Ruusala, 1994; Thon, Cohen, & Klar, 1994; Thon & Klar, 1992).

Many of the PEV mutants identified in *Drosophila* are homozygous lethal yet exhibit a dominant phenotype, making them detectable by traditional screening methods used in diploid organisms (Elgin & Reuter, 2013). *S. pombe* is primarily a haploid unicellular organism, therefore even recessive phenotypes are readily detectable. Essential genes, however, are often underrepresented in genetic screens since most model organisms are highly sensitive to loss or impaired function of essential gene products, particularly in haploid organisms. Previously, transposon-based integration profiling has

been utilized to identify essential genes in haploid eukaryotic organisms (Guo et al.,

2013). In this approach cells carrying transposon insertions are allowed to grow for many

generations; the transposon insertion sites present in the final cell population are

subsequently identified by high throughput sequencing. ORFs with lower integration

densities at the conclusion of the screen corresponded with genes reported to be essential,

while ORFs with higher densities corresponded with nonessential genes (Grech et al.,

2019; Guo et al., 2013). It is challenging to screen for phenotypes associated with

essential genes outside of their effect on viability, however, given their importance in a

number of cellular processes essential for survival (Bertomeu et al., 2018; Rousset et al.,

2018; Wang et al., 2015). Interestingly, it was recently reported that many essential genes

in *S. pombe* exhibit "bypassability", a phenomenon in which essential genes are rendered

non-essential by monogenic suppressors (J. Li et al., 2019).

We conducted a screen utilizing transposable element-mediated mutagenesis in *S.*
pombe coupled with positive selection for mutants exhibiting suppressed PEV.

Subsequent identification of transposon insertion sites after multiple rounds of selection

and integration profiling revealed enrichment of a number of essential genes. Cloning-

free CRISPR/Cas9 mutagenesis was then deployed in a small-scale secondary screen to

isolate novel mutants in essential genes *top2, top3, and tel2* exhibiting a PEV phenotype

informed by the location of insertions which emerged in the primary screen. Interestingly,

reconstructing *Hermes* integrations in DNA topoisomerases *top2* and *top3* which

occurred in the primary screen revealed that single insertion events in these genes are

lethal. We hypothesize that the enrichment of select essential gene mutants as a

consequence of positive selection may be a product of "bypass of essentiality" (BOE) (J.

Li et al., 2019) as a result of dense transposon integrations, and that these complex genetic interactions may enable detection of phenotypes which would otherwise be missed via traditional screening approaches.

2.2 Materials and Methods

Yeast Strains

The S. pombe strains used in this study are listed in Table 2.4. The strains used for Hermes mutagenesis, cloning-free CRISPR mutagenesis, and construction of *top2::Hermes* and *top3::Hermes* alleles as well as generation of *Hermes* and *rqh1Δ* double mutants are described below.

Hermes Mutagenesis Screen

A strain carrying a pericentromeric *ade6+* reporter, TV312, was sequentially transformed with plasmids pHL2578 and pHL2577 carrying the Hermes transposase and transposon, respectively. A 5 mL culture of the plasmid transformed strain was grown overnight and used to inoculate 50 mL of EMM –leu –ura –B1 at a starting OD of .05 and incubated until saturation was reached (OD 2.0-5.0) and serially passaged until approximately 12% integration was reached. Integration was monitored by plating approximately 1,000 cells from each passage on EMM+leu+ura+FOA+B1 and YES+FOA+G418 and measuring the proportion of colonies on each plate (colony number on EMM+leu+ura+FOA+B1 divided by colony number on YES+FOA+G418) to gauge the overall transposition frequency. After the final passage the mutagenized culture was then used to inoculate a 500 mL of EMM+leu+ura+FOA+B1 to OD .25 and grown until saturation to select against the donor plasmid. This culture was then washed, harvested, and used to inoculate

a 500 mL culture of YES+FOA+G418 to OD .25 to select for cells with integration events. Once grown to saturation, the insertion-carrying culture was used to inoculate 500 mL of EMM+DO-ADE+B1 to an OD of .15 to select for cells in which the ade6+ reporter was de-repressed. The remainder of the culture was washed, harvested, and reserved for genomic DNA extraction to prepare a library of Hermes insertions with flanking genomic DNA for high-throughput sequencing (referred to as Library 0, see *Hermes Insertion Library Preparation for High-Throughput Sequencing*). The mutagenized cells were passaged 3 times in media lacking adenine with the remainder after inoculation reserved for library preparation by harvesting and freezing collected cells at -80 C. The cultures derived from each round of selection for loss of *ade6+* silencing are referred to as Library 1, 2, and 3.

Hermes Insertion Library Preparation for High-Throughput Sequencing

A Hermes insertion library for high-throughput sequencing was prepared as previously described (Guo et al., 2013). Briefly, genomic DNA was extracted and digested with the restriction endonuclease MseI. Linker ligation was performed using linkers containing MseI restriction site overhangs. Finally, linker-ligated genomic DNA fragments were used to amplify genomic sequences flanking Hermes integration sites, using an oligonucleotide hybridizing near the end of the Hermes terminal inverted repeat (TIR-R) and another oligonucleotide corresponding to the MseI-ligated linker. These oligonucleotides add, respectively, the P5:TruSeqv2 and P7 Illumina adapter sequences in their 5' ends, generating Illumina HiSeq 2500 compatible custom libraries. Amplified DNA was size selected by running the amplification products on a 2% agarose gel, excising all bands within the 200-600 bp range, and gel extraction of the size-selected

fragments. Samples were pooled and sequenced by Admera (Piscataway, NJ) using an Illumina HiSeq 2500 platform with 20% PhiX spike-in to compensate for low initial sequence complexity.

Mapping Hermes Integration Sites Onto the S. Pombe Genome

The FASTQ files were stripped of adapter and Hermes ITR-R sequences with cutadapt v1.8.1, then mapped to the *Schizosaccharomyces pombe* ENSEMBL ASM294 v2 genome assembly with Bowtie v2.0.6. Mapped reads were filtered with Samtools v1.3.1 by chromosome to exclude reads mapping to the Mitochondrial genome and by quality > 5 to remove low quality mappers and repetitive sequences.

Statistical analysis of Hermes screen data

Read counts in each of the 4 libraries were normalized to reads per million mapped reads to account for library differences, assigned to the coding sequences (including introns) of protein coding genes, and normalized by gene size. In parallel, we generated a control set of regions with neutral effect on fitness as identified by a recent survey of saturated Hermes transposition data by merging adjacent Hidden Markov Model states 4 and 5 intervals larger than 50bp (Grech et al., 2019). We then selected for analysis genes with at least one insertion in each selection step and at least 5 average insertions per selection step, to remove genes with low insertion counts. Out of 5118 total genes, 3760 passed this filter. To quantify the changes in insertion frequencies for each gene in the selected cultures, we calculated the log-transformed fold increase in normalized read number in each successive selection step and then assigned Z-scores calculated with respect to the average and standard deviation of changes in the neutral control regions to account for

loss of observed insertions by random bottlenecks and gains of infrequent observed insertions by removal of high frequency insertions upon selection that increase the representation of the insertion libraries. Z scores from each selection step were averaged with equal weights, and their associated probabilities were calculated taking into account their covariance. The associated probabilities were adjusted for multiple testing using the Benjamini-Hochberg procedure to control the False Discovery Rate at α=0.05. The frequencies of essential and by-passable essential genes were evaluated by Fisher exact test. All statistical analyses were performed in R v3.4.4 with Bioconductor packages. GO term enrichment analysis was performed with the PUMA tool using Fisher exact test and FDR adjustment.

Cloning-Free CRISPR Mutagenesis

For CRISPR/Cas9-mediated mutagenesis we used the cloning-free split-*ura4* system described in (X.-R. Zhang, He, Wang, & Du, 2018). sgRNAs were designed using the Benchling CRISPR guide RNA generation tool, which provides on-target and off-target scores based on previously published studies; sgRNAs were selected based on the following conditions: 1) proximity to Hermes-enriched regions in the targeted gene, 2) high on-target score, and 3) high off-target score to maximize on-target cleavage and minimize off-target Cas9 activity, respectively (Doench et al., 2016; Hsu et al., 2013). To generate Cas9 and sgRNA containing fragments for yeast transformation, *pDB4280* was linearized by NotI digestion to generate the gapped plasmid containing the Cas9 coding sequence and the 5' part of the *ura4* marker. The PCR template for sgRNA insert amplification was prepared by digesting with Not1 to generate a ~1.3 kb fragment containing the 3' part of the *ura4* marker, the hammerhead ribozyme sequence, and the

sgRNA scaffold sequence. To generate sgRNAs specific to genes of interest, the sgRNA template was subsequently amplified with Phusion polymerase and a primer pair including an oligo with homology to the sgRNA template in addition to sgRNA specific target sequence. The sgRNA-containing fragments were then gel extracted for transformation.

Strain ZB2116 was then transformed by electroporation (J. M. Murray, Watson, A. T., and Carr, A.M., 2016) with 30ng of the gapped *ura4* plasmid in addition to 200 ng of the intended sgRNA-containing fragment and plated on EMMG+DO-ADE,URA+10 mg/L adenine. Plates were monitored over the course of 2-3 weeks for the emergence of white or pink colonies. Colonies with a putative silencing defect were then struck out to single colonies on YEA to allow for loss of the Cas9-expressing plasmid and a 1 kb fragment surrounding each Cas9 cleavage site was amplified from a single representative colony by colony PCR and analyzed by Sanger sequencing to identify mutations occurring as a result of DSB repair at the Cas9 cleavage point; streaking out to single colonies was essential to avoid contamination with wild type cells once selection for the Cas9/sgRNA-expressing plasmid was removed. Any colonies which appeared to carry a mutation of interest were subsequently re-amplified for glycerol storage and further phenotypic analysis.

Serial dilution spot assays

Cells were grown overnight in liquid YEA to an OD_{600} of ~2.0. 100 uL of each sample was removed and diluted in 1 mL of sterile water for precise determination of the sample OD_{600} before harvesting 1 mL of cells, washing in 1 mL of sterile water, and

resuspending in an adequate volume of sterile water for a final OD_{600} of 10.0. Three ten-fold serial dilutions were prepared for each sample to a final OD_{600} of .01 in 96-well cell culture plates. Cells were subsequently transferred to the appropriate yeast media plates using a freshly sterilized pin frogger; plates were incubated at 32° C unless otherwise indicated and imaged after 3-5 days.

RNA preparation, Reverse Transcription, and qPCR

5 mL yeast cultures were grown overnight, washed, and harvested. Bulk RNA was isolated for reverse transcription and analysis using a Direct-Zol Miniprep RNA purification kit (Zymo Research) or by hot acid phenol RNA extraction following the protocol outlined in (Bahler & Wise, 2017). For RNA purifications performed using the Direct-Zol Miniprep kit cell pellets were resuspended in 300 mL of the provided TRI reagent and dispensed into 2 mL screw cap tubes with approximately 500 uL of glass beads. Cells were lysed in TRI Reagent by bead beating undr the following conditions: 4 cycles of 2.5 minutes each carried out at 4° C, followed by a 2 minute rest on ice in between cycles. The remaining steps were carried out according to the manufacturer's instructions. Reverse transcription was subsequently performed using SuperScript VILO Master Mix (Invitrogen) according to the manufacturer's instructions. qPCR reactions were set up using KAPA SYBR FAST qPCR Master Mix (2x) according to the manufacturer's instructions and run on a Mastercycler ep realplex Real-time PCR System (Eppendorf) for analysis.

ChIP-qPCR

Chromatin immunoprecipitation was performed as previously described with some modifications (H. P. W. Cam, Simon, 2016). 100 mL of cells were grown overnight to an OD_{600} of 0.5-0.8 and fixed with freshly prepared 1% formaldehyde for 10 minutes. Cells were lysed by bead beating in lysis buffer under the following conditions: 4 cycles of 2.5 minutes each carried out at 4° C, followed by a 2 minute rest on ice in between cycles. Immunoprecipitations were carried out with approximately 15-25 ug of input chromatin in a total reaction volume of 250 ul with 2 ug of ChIP Grade Anti-Histone H3 (di methyl K9) antibody (ab1220, Abcam). Antibody incubation and washing steps were all carried out in Eppendorf Protein LoBind microcentrifuge tubes; after elution of cross-linked chromatin from Dynabeads Protein G (Invitrogen) reverse cross-linking and all subsequent steps were carried out using Eppendorf DNA LoBind microcentrifuge tubes.

After immunoprecipitation, samples were analyzed by qPCR as described in the previous section. IP qPCR signals were normalized against input samples for each primer position to ensure that potential expansion or contraction of the repeat sequences analyzed does not affect quantification.

Reconstruction of Hermes integrations in top2 *and* top3

Plasmids containing the desired Hermes integration, target site duplications (TSDs), and several hundred base pairs of sequence flanking each respective integration site were constructed by Gibson assembly. A Hermes TIR-*kanMX6* fragment was obtained by amplifying the construct by PCR directly from pHL2577 using the primers indicated in TABLE. The homology fragments flanking the integration site were obtained by amplifying the homologous sequences directly from a wild type 972 strain, and target site

duplications were introduced in the appropriate orientation via the primers used to amplify the fragments. After the desired plasmids were constructed and sequenced to ensure sequence fidelity the fully assembled homology regions plus Hermes cassette were amplified by PCR directly from each plasmid as a complete transforming fragment, gel purified, and transformed into diploid fission yeast by electroporation. Diploid yeast were stably obtained by mating strains DG14 and DG21, which carry complementary ade6 alleles (ade6-210 and ade6-216, respectively), on malt extract at 28° C for approximately 16 hours and streaking pre-meiotic cells onto EMMG+DO-ADE to select for ade6+ wild type diploids.

DAPI staining

Yeast were grown overnight at 32° C or 37° C as indicated in YEA to an OD_{600} of ~1.0 before harvesting, washing, and fixing cells in cold 70% ethanol. Fixed cells were then harvested and mounted on glass microscope slides as described in Hagan et. al. (2016) (Hagan, 2016) and imaged on a Zeiss Apotome.2.

2.3 Results

2.3.1 Identification of PEV mutants by transposable element-mediated mutagenesis

We performed a forward genetic screen using the Hermes transposon for mutagenesis of vegetatively growing cells to identify genes affecting PEV of a pericentromeric reporter. Hermes has previously been demonstrated to exhibit high levels of activity in S. pombe and 33-50% of Hermes insertions occur in ORFs, making it an efficient tool for mutagenesis in fission yeast (Evertts, Plymire, Craig, & Levin, 2007; Guo et al., 2013). Previously, Hermes integration profiling has been used to probe for

essential genes and genomic elements by identifying regions in which insertions are depleted (Grech et al., 2019; Guo et al., 2013; A. H. Michel et al., 2017). These essential loci are often readily identifiable in dense maps of transposon integration, as insertions affecting loci required for cell division and proliferation will naturally be selected against by growing mutagenized cell populations for many generations (Grech et al., 2019; Guo et al., 2013). For the purposes of this study we asked whether the same approach could be repurposed to utilize positive selection to enrich for insertions in genes contributing to a phenotype of interest, namely PEV.

Cells carrying a pericentromeric *ade6+* reporter were co-transformed with plasmids carrying the Hermes transposase and a plasmid bearing the Hermes terminal inverted repeats (TIRs) flanking a *kanMX6* cassette which confers resistance to the antibiotic G418. The presence of the *ade6+* reporter, which confers prototrophy for adenine when the reporter gene is expressed, enables screening and selection for cells exhibiting loss of PEV at the typically repressed pericentromeric locus. Transposition was then permitted to occur for approximately 12 days (roughly 135 generations) as cells were grown and serially passaged in liquid media (Figure 2.1a, Figure 2.11). Transposition was monitored by plating a small number of cells after each passage and measuring the proportion of colony forming units bearing at least one Hermes insertion until approximately 12% of all cells in the final culture carried one or more Hermes insertions. To select for cells exhibiting loss of silencing of the *ade6+* reporter the final culture was placed through three rounds of selection in media lacking adenine, conferring a growth advantage to cells carrying an insertion effecting de-repression of *ade6+*. Ongoing selection was confirmed by plating a small amount of cells taken from each

culture and analyzing the ratio of colonies exhibiting repression and de-repression of the

ade6+ reporter by scoring the number of colonies which appeared red or white,

respectively, on media with a low concentration of adenine (Figure 2.1b). Insertion

libraries for identification of Hermes integration sites by high-throughput sequencing

were prepared as previously described in Guo et. al. (2013) from the liquid culture prior

to selection for *ade6+* de-repression as well as after each of three passages in selective

media for a total of four insertion libraries, allowing for analysis and identification of

genes which are successively enriched with each selective passage.

We then asked whether we could successfully identify genes with a known role in

heterochromatic silencing by analyzing gene integration densities following each round

of selection. Insertion libraries were first processed by normalization to reads per million

mapped reads to account for variation between sequencing runs. Reads were then

assigned to coding sequences of protein coding genes and further normalized to gene

size. To confirm the effect of the selection a control set of loci described as having a

neutral effect on fitness identified in a recent survey of saturated Hermes transposition

data were generated for comparison (Grech et al., 2019). Genes with fewer than one

insertion and/or less than 5 average insertions per selection step were filtered to eliminate

genes with low insertion frequency; 3,760 genes (out of 5,118 total protein coding genes)

were analyzed after making it past this filter. Previous studies have found that average

integration density is lower in essential genes, reflecting their functional importance;

despite this effect 1,050 essential genes made it past the low insertion frequency filtering

step (Grech et al., 2019; A. H. Michel et al., 2017). Changes in insertion frequencies in

genes were calculated by determining the log-transformed fold increase in normalized

read number after each round of selection and normalized to changes in neutral control regions. This analysis allowed for generation of a list of "significantly enriched" (p < .05) and "mildly enriched" (p < 0.1) genes produced by selection for mutants exhibiting a PEV phenotype (Figure 2.1c, Table 2.1).

The results of the integration profiling analysis revealed that many genes with a known role in pericentromeric silencing and/or heterochromatin formation and maintenance were significantly enriched within the screen, thereby validating the overall approach (Figure 2.1d). Notably, the top scoring gene in the screen is the Heterochromatin Protein 1 homolog Swi6; further, all components of the H3K9 methylation complex CLRC were detected as significantly enriched (Table 2.1). Gene ontology (GO) analysis demonstrated enrichment among top-scoring candidate PEV genes of a number of biological processes known to collaborate in ensuring pericentromeric silencing including chromatin silencing at centromere (GO:0030702, p=.004); chromatin silencing by small RNA (GO:0031048, p=.006); and regulation of histone H3-K9 methylation (GO: 0051570, p=.01) (summarized in Table 2.2).

Remarkably, 25% (67/263) of genes which emerged as significantly enriched are also annotated as being essential for vegetative growth in fission yeast. Previous studies analyzing transposon integrations in bacteria and yeast have found that essential genes tend to exhibit lower overall insertion density and unique insertion count, with the majority of insertions restricted to the 3' ends of genes and noncoding regions (UTRs) (Chao et al., 2016; Guo et al., 2013; A. H. Michel et al., 2017). We then asked whether insertions in essential genes exhibited the same profile in the presence of positive selection for insertions affecting PEV. Plotting average read density across all of the

genes which passed filtering criteria indeed revealed peaks in the 5' and 3' ends of both essential and non-essential genes (Figure 2.2a). Further, insertions tended to be depleted in the body of essential genes within the un-selected cohort while read density remained fairly high across the body of non-essential genes, thus the average read densities in both essential and non-essential genes showed separable profiles. Analysis of read density within genes which emerged from the screen as significantly enriched, however, revealed a markedly different profile (Figure 2.2b). The peaks present at 3' gene ends disappeared while the peak at the 5' gene end remained in both essential and non-essential genes. Insertions were more evenly distributed across gene bodies in essential genes, mirroring that of their non-essential counterparts. Further, mean read densities increased in both groups with each round of selection while the difference between mean read densities in essential and non-essential genes decreased with each selective passage. Taken together, these results suggest that selecting for mutations affecting PEV increases the representation of insertions which are more likely to elicit functional consequences in both essential and non-essential genes.

2.3.2 Reconstruction of essential gene ORF Hermes insertions reveals that solo insertions are lethal and recessive with respect to silencing

After finding that insertions in essential genes were successively enriched in the PEV screen, we examined several possible explanations: first, that insertions in the coding sequences of essential genes were producing hypomorphic gene products; alternately, we speculated that haploid cells in which one of the copies of an essential gene was inactivated by Hermes insertion during the G2 stage may be spontaneously diploidizing, allowing for the persistence of Hermes insertions in essential genes (Lynch

et al., 2008). In this scenario, a loss of silencing phenotype due to a dominant or haploinsufficient Hermes insertion allele could explain their enrichment when selecting for *ade6+* reporter de-repression.

To test each of these possibilities we selected two genes, *top2* and *top3*, and precisely re-created Hermes insertions which had appeared in the primary PEV screen (Figure 2.3a, Figure 2.12 a,b). *top2* and *top3* both have an extensively documented requirement for viability, eliminating the possibility that their essential gene status could be a product of mis-annotation, and both were mildly enriched in the initial Hermes screen (p=.09 and .08, respectively) (Goodwin, Wang, Toda, Norbury, & Hickson, 1999; Goto & Wang, 1984; Win, Goodwin, Hickson, Norbury, & Wang, 2004). Top2 and Top3 have well described roles in management of DNA topological states during DNA replication, homologous recombination, and mitosis (Yves Pommier, Sun, Huang, & Nitiss, 2016). There are several described instances of DNA replication and/or repair factors participating in heterochromatin formation and maintenance, but the nature and extent of their relationship is poorly understood (Jahn et al., 2018; F. Li, 2011; Miller et al., 2017). Thus, *top2* and *top3* were selected for further analysis.

Hermes alleles which had emerged from the PEV screen were precisely reconstructed by transforming diploid yeast carrying a pericentromeric *ura4+* reporter with DNA fragments containing the Hermes*::KanMX6* cassette in the orientation in which it had inserted in the screen and the appropriate target site duplications as they would have been generated by a true transposition event (referred to going forward as *top2::Hermes ins 1* and *ins 2* and *top3::Hermes ins 1* and *ins 2*). Homology arms spanning the regions immediately adjacent to the insertion point were included in the

fragment for efficient and non-disruptive targeting by HR to the desired integration site. Diploids carrying one of the four Hermes alleles were then plated on ME to induce sporulation followed by tetrad dissection to assess the lethality of the newly introduced Hermes insertion. Diploids carrying Hermes alleles in *top2* and *top3* were all sporulation competent, although they produced the occasional tetrad deviating from the expected 2:2 lethality pattern, instead producing variable numbers of germinated spores (0-4) (Figure 2.3b). None of the spores which successfully germinated were G418 resistant, however, indicating that all four Hermes alleles are lethal in haploid cells. The abnormal germinated colony number and deviation from the typical 2:2 segregation pattern associated with lethal alleles may be the result of a dominant or haploinsufficient chromosome segregation defect, as such defects have previously been associated with impaired topoisomerase activity (Goodwin et al., 1999; Kaur, De Muyt, & Lichten, 2015; Mengoli et al., 2014; Win et al., 2004).

After finding that all four *top2::Hermes* and *top3::Hermes* alleles were recessive lethal, we tested whether the alternative scenario- spontaneous diploidization combined with a dominant or haploinsufficient silencing defect- could potentially explain the persistence and enrichment of these insertions. We were unable to detect a silencing defect in diploids carrying any of the four Hermes alleles by serial dilution spotting assays or qRT-PCR quantification of relative *dg, dh,* and *ura4+* reporter expression, however (Figure 2.13a,b). Thus, by reconstructing Hermes insertions in *top2* and *top3* we found that all four insertions produce recessive lethal alleles with respect to viability and PEV, therefore the contingencies proposed above cannot adequately explain their continued enrichment upon selection in the initial screen.

2.3.3 Screening and detection of PEV defects in bypassable essential genes

These findings presented a paradox, as the continued enrichment for cells carrying insertions in essential genes such as *top2* and *top3* throughout multiple rounds of selection (approximately 21 generations) following 135 generations of unselected proliferation appears incompatible with the lethality presumably and experimentally associated with such insertions. In instances where onset of lethality is delayed following mutagenesis, the prolonged period over which the cultures in this study were subject to multiple rounds of selection makes such a contingency insufficient to explain the continued enrichment of lethal alleles. Further, we did not observe a dominant silencing defect following reconstruction of solo insertions in *top2* and *top3* in diploid yeast which might explain their persistence.

In a phenomenon recently coined as a 'bypass of essentiality' (BOE), digenic genetic interactions rendering essential genes dispensable were reported to occur with fairly high frequency in mutagenized cells based on the finding that 27% of the essential genes tested on the left arm of chromosome II in *S. pombe* exhibited bypassability (J. Li et al., 2019). We posited that the presence of insertions in essential genes might be explained by one or multiple 'background' insertions or suppressors permitting bypass of essentiality.

To evaluate the possibility that BOE allowed for the persistence of Hermes insertions in essential genes, we compared genes which had emerged as significantly enriched ($p < .05$) from our Hermes PEV screen to the summary of bypassable genes provided in (J. Li et al., 2019). Of the 142 essential genes on the left arm of Chromosome

II in *S. pombe* analyzed by Li et. al. we analyzed 111 for enrichment in the Hermes PEV screen. Interestingly, we found that essential genes within the cohort analyzed by Li et. al. which subsequently emerged as significantly enriched for loss of silencing in the Hermes PEV screen show a higher probability of being bypassable: of the 9 essential genes significantly enriched ($p < .05$) in the PEV screen, 5 were described by Li et. al. as bypassable and 4 were found to be non-bypassable. Of the 102 non-significant genes analyzed in the Hermes PEV screen which overlap with those analyzed by Li et. al,. 23 were found in the latter study to be bypassable while 79 were found to be non-bypassable (Fisher exact test, $p=.04$, Odds ratio 4.22, 95% CI [.83-23.14]). Thus, the finding that 'bypassability' is frequently associated with essential genes which emerged as significantly enriched from the Hermes PEV screen strongly suggested that these essential genes may be surviving throughout the screen via their co-occurrence with extragenic lethality suppressors. Further, the putative BOE which could occur by conducting the screen to a relatively high density may enable phenotypes such as defective silencing associated with otherwise 'essential' genes, which are typically underrepresented in genetic screens of a similar nature, to emerge by allowing the continued proliferation of essential gene mutants following Hermes disruption. One well described example of BOE is the suppression of lethality associated with *top3+* gene disruption by ablating the RecQ type DNA helicase *rqh1+* (Goodwin et al., 1999); we also noted that Rqh1 was also mildly enriched in our initial Hermes screen ($p = .14$).

To directly test this possibility we knocked out *rqh1* in diploids carrying one of the two *top3::*Hermes alleles to approximate the effect of a null allele generated by a Hermes integration event and/or spontaneous mutation. Tetrad dissections were

subsequently performed on *rqh1Δ top3::*Hermes diploids. Each tetrad again produced

variable numbers of germinated colonies, ranging from 1-3 successfully germinated

colonies per tetrad. Once more we were unable to isolate any single *top3::*Hermes

mutants for either allele (*ins1* or *ins2*); however, we successfully obtained several double

mutants carrying both *rqh1Δ* and *top3*::Hermes indicating suppression of the lethality

associated with both *top3::*Hermes *ins1* and *ins2* by *rqh1Δ*.

We then asked whether the presence of inactivating mutations in both *rqh1* and

top3 suppressed the putative loss-of-silencing phenotype associated with *top3::*Hermes in

addition to suppression of cell lethality. Analysis of *dg* and *dh* expression in double

mutants revealed increased pericentromeric repeat expression relative to the wild type

strain and *rqh1Δ*, indicating that while *rqh1Δ* suppresses the lethality of *top3::*Hermes

ins1 and *ins2* it does not suppress the loss of silencing generated by inactivating

mutations in *top3* (Figure 2.3c). Further, the observation that lethality and loss of

silencing are separable phenotypes in *rqh1Δ top3* double mutants may provide insight

into the biological origins of these phenotypes. The physical interaction between Top3

and RecQ-like DNA helicases is highly conserved in eukaryotes; through their combined

efforts crossover formation is suppressed in mitotic cells by promoting resolution of

double Holliday junctions, an activity which has been proposed to be important for

resolution of converging replication forks (Fabre, Chan, Heyer, & Gangloff, 2002;

Gangloff, McDonald, Bendixen, Arthur, & Rothstein, 1994; Ira, Malkova, Liberi, Foiani,

& Haber, 2003; Suski & Marians, 2008). The mechanism by which Top3 impacts

heterochromatic silencing, therefore, is presumably distinct from its canonical activity in

the resolution of recombination structures and could potentially be a product of

unresolved or delayed resolution of stalled replication forks or may be related to a function of Top3 that is independent of Rqh1. Intriguingly, Top3 in humans and budding yeast has been demonstrated to dissolve D loops as a potential anti-recombination mechanism; further, this activity appears to be independent of the RecQ homolog in budding yeast, Sgs1 (Fabre et al., 2002; Fasching, Cejka, Kowalczykowski, & Heyer, 2015; Gangloff et al., 1994; Mundbjerg et al., 2015). Suppression of recombination is critical at fission yeast centromeres, as signaling of DNA repair by homologous recombination at stalled forks leads to a subsequent loss of accompanying histone modifications (Zaratiegui, Castel, et al., 2011). Taken together, these results demonstrate that complex genetic interactions such as BOE can permit survival of cells carrying inactivating mutations in essential genes to allow for detection of other phenotypes which are otherwise undetectable in traditional genetic screens. Identification of such interactions, moreover, may facilitate a more nuanced dissection of phenotypes of interest by genetic or other means.

Overall, 25% of the genes which were classified as 'significantly enriched' ($p <$ .05) in the Hermes PEV screen are annotated in Pombase as being incompatible with vegetative growth in single allele deletions. In this study we demonstrate that a subpopulation of the alleles generated in essential genes during Hermes-mediated mutagenesis may be lethal in isolation; the distribution of insertions in essential gene bodies further suggests that it is unlikely that all of the alleles which emerged within this population of essential genes in our initial screen can be dismissed as hypomorphic alleles. Thus, bypassable essential genes are more likely to be enriched by positive

selection for a phenotype of interest within genetic screens such as the one described in this study, potentially as a result of suppressors emerging within mutagenized cells.

2.3.4 Generation of novel essential gene mutants using cloning free CRISPR

Given that the nature of the Hermes screen precluded recovery of individual mutants of interest once all libraries had been analyzed, we set out to test whether we could generate silencing defective mutants in candidate essential PEV genes using CRISPR/Cas9-mediated mutagenesis. The cloning free CRISPR system (X.-R. Zhang et al., 2018) is a flexible platform for rapid deployment of CRISPR/Cas9 gene editing technology and allowed us to rapidly screen through several genes as a proof-of-principle sub-screen. In summary, a short fragment containing the gRNA expression cassette is generated by PCR and co-transformed with a restriction-digested vector containing the Cas9 expression cassettes. Short homologies and a marker gene split between the PCR product and the digested vector permit direct assembly by homologous recombination *in vivo* of a functional CRISPR/Cas9 mutagenesis plasmid. Since the digested vector is universal, multiple targeting gRNAs can be rapidly generated and tested. Cas9 targeting was carried out in a strain carrying a pericentromeric *ade6+* reporter to permit rapid visual screening of Cas9-resistant colonies for identification of mutations affecting heterochromatin integrity. In this experimental setup, colonies in which the reporter is de-repressed by Cas9-induced mutations affecting pericentromeric silencing would be expected to appear white or pink while mutations with no effect on silencing would remain red in appearance on low adenine media (Figure 2.4a). PAM sites with optimal guide sequences in proximity to insertions which emerged from the screen were

identified and used for Cas9 targeting. The targeted genes and locations are summarized in (Table 2.3).

Rik1 and Dcr1 are both non-essential genes with a well-described role in heterochromatin formation and maintenance; accordingly, virtually all sgRNAs targeting both genes produced a number of silencing defective colonies. To confirm that the loss of silencing correlated with a CRISPR-induced mutation in the target gene, several representative strains were sequenced revealing single base pair deletions near the CRISPR target site which produced frameshifts in their respective gene coding sequences.

top2 and *top3* were once again selected from the candidate essential PEV genes for independent targeting by several sgRNAs in addition to the significantly enriched essential gene *tel2* (p = .03). Tel2 plays an important role in the Mrc1-mediated replication checkpoint in fission yeast (Shikata, Ishikawa, & Kanoh, 2007; Takai, Xie, de Lange, & Pavletich, 2010; Xu et al., 2019). In budding yeast Tel2 participates in regulation of telomere length and PEV at the telomeres; however, we did not find any publications addressing a role for Tel2 in maintenance of centromeric heterochromatin in either organism (Runge & Zakian, 1996).

Any Cas9/sgRNA-expressing colonies appearing pink or white on low adenine media were patched to YEA before amplifying and sequencing an ~1 kb region surrounding the sgRNA target site to identify CRISPR-induced mutations. Of the six sgRNAs targeting *top2*, one produced a lysine to glutamine mutation corresponding with derepression of the *ade6+* reporter. Two sgRNAs were deployed to target *top3*. One

sgRNA did not produce any silencing defective colonies while the other produced

multiple mutations associated with impaired *ade6+* repression. Further, several of the

top3 mutations appeared independently in multiple colonies. All of the top3 mutant

colonies appeared small and pink, suggesting they exhibited a mild silencing defect and

viability defect; however, the apparent viability defect was partially alleviated by

patching the colonies to YEA to allow for loss of the Cas9-sgRNA expressing plasmid.

Finally, one of 6 sgRNAs targeting *tel2* independently produced two silencing defective

colonies bearing identical deletions of three base pairs resulting in the conversion of

sequential asparagine and glutamic acid residues to a single lysine residue.

The newly isolated mutant alleles and affected domains are summarized in

(Figure 2.4a, Figure 2.14). *top2^{K388Q}* affects a conserved lysine residue in the ATPase

domain which has been found to be SUMOylated in fission yeast (Køhler et al., 2015)

(Figure 2.14b). *top3^{S69del}* and *top3^{E70K}* affect residues in the Toprim (Topoisomerase-

primase) domain which do not appear to be conserved themselves but are located

between two highly conserved hydrophobic residues (Figure 2.14c). *top3^{E70Y71D}* affects

the same glutamic acid residue at position 70 in addition to a a moderately conserved

tyrosine residue found in bacterial Top3 and human Top3ß (FIG). Finally, *tel2^{N765E766K}*

affects an arginine residue found in both budding and fission yeast which appears to

reside outside of any annotated protein domains (Figure 2.14a).

2.3.5 Top2, Tel2, and Top3 mutant alleles exhibit replicative stress and mitotic defects

After isolation and identification of our CRISPR mutant alleles we set out to

characterize the mutant phenotypes in the context of *top2*, *top3*, and *tel2*'s previously

described roles in DNA replication, repair, and checkpoint activation (Goodwin et al., 1999; Goto & Wang, 1984; Mengoli et al., 2014; Shikata et al., 2007; Win et al., 2004; Xu et al., 2019). We subsequently noted that two of the *top3* mutants (*top3^{S69del}* and *top3^{E70Y71D}*) and *tel2^{N765E766K}* exhibited a significant growth defect when grown at 37° C (Figure 2.5a, Figure 2.8d), therefore we analyzed the phenotype of these genes at both restrictive and permissive temperatures.

Visualization of yeast cells grown overnight at 37° C and 32° C revealed that at the permissive temperature the cell morphology of each of the mutant cells appeared mostly normal, with a slight increase in the proportion of elongated cells observed in all three *top3* mutants in addition to an increase in the number of vacuolar structures visible inside the cells (Figure 2.5). At 37° C, however, the majority of *top3^{S69del}* and *top3^{E70Y71D}* cells appeared massively elongated, while the elongation phenotype did not show any appreciable difference in the other mutants compared to cells grown at 32° C (Figure 2.5). Taken together, we concluded that all three *top3* mutants appear to be undergoing cell cycle arrest as a consequence of initiation of an intact DNA damage checkpoint, most likely indicative of varying levels of unresolved replicative stress; the cellular morphology of *tel2^{N765E766}* and *top2^{K388Q}* appeared mostly normal notwithstanding a subtle increase in the proportion of elongated cells in *top2^{K388Q}*.

Given that *top2, top3,* and *tel2* all have described roles in DNA replication and repair we assayed the mutant alleles for sensitivity to various genotoxic agents, a hallmark of DNA replication, checkpoint, and/or repair defective mutants (Figure 2.6). Camptothecin is a topoisomerase 1 inhibitor that leads to a buildup of torsional stress by trapping Top1-DNA cleavage complexes which can in turn serve as further impediments

to the replication fork (L. F. Liu et al., 2000; Y. Pommier et al., 2006; Vesela, Chroma, Turi, & Mistrik, 2017). Hydroxyurea inhibits the ribonucleotide reductase enzyme thereby depleting cellular dNTPs and inhibiting DNA replication in S phase (Koc, Wheeler, Mathews, & Merrill, 2004; Slater, 1973). Methyl methanesulfonate (MMS) is an alkylating agent which causes the formation of secondary structures which impede replication fork progression, therefore sensitivity to MMS has often been observed in strains with defective checkpoint responses or repair or in certain replisome mutants (Lundin et al., 2005; Ranatunga & Forsburg, 2016; Vesela et al., 2017).

$tel2^{E765N766K}$ exhibited a significant drop in viability at the restrictive temperature after exposure to any of the three genotoxic agents assayed as well as a mild loss of viability when exposed to hydroxyurea at a permissive temperature, indicating mild ongoing replicative stress exacerbated by shifting to restrictive temperature. $top2^{K388Q}$ and $top3^{E70K}$ were insensitive to all of the genotoxins tested, while $top3^{S69del}$ and $top3^{E70Y71D}$ exhibited a slight sensitivity to HU at the permissive temperature which became more pronounced after shifting to the restrictive temperature in addition to mild sensitivity to CPT and MMS at higher concentrations (FIG).

DAPI staining of all mutant strains grown at 32° C revealed chromosome segregation defects such as lagging chromosomes and abnormally partitioned chromosomal material in $top2^{K388Q}$ and $top3$ mutants in accordance with previously described $top2$ and $top3$ mutant phenotypes (Figure 2.7). Many $tel2^{N765E766K}$ mutant cells exhibited the 'cell untimely torn (*cut*)' phenotype characterized by initiation of cytokinesis/septation prior to complete nuclear division commonly observed among mitotic and checkpoint defective mutants (Griffiths, Uchiyama, Nurse, & Wang, 2000;

Uemura & Yanagida, 1984; Yanagida, 1998). The *cut* phenotype was also observed in the *top2^{K388Q}* and *top3* mutants, presumably as a consequence of abnormal chromosome segregation. The severity and penetrance of these phenotypes increased at the restrictive temperature, with the majority of *top3^{S69del}* and *top3^{E70Y71D}* mutant cells lacking any recognizable nuclear structure and often appearing as massively elongated multiseptate cells (Figure 2.7).

Although the penetrance of the observed morphological differences and sensitivity to DNA damaging agents varied, all of the mutants analyzed exhibited signs of replicative stress and/or mitotic defects in accordance with mutant phenotypes previously associated with the affected genes (Goodwin, Wang, Toda, Norbury, & Hickson, 1999; Goto & Wang, 1984; Mengoli et al., 2014; Win, Goodwin, Hickson, Norbury, & Wang, 2004). The extent of the defects in *top2^{K388Q}*, however, were mild and only became apparent after visualizing cell nuclei by DAPI staining; the same was true for *top3^{E70K}* despite the fact that it shares an affected residue with *top3^{E70Y71D}*. The morphologically normal appearance of *tel2^{N765E766K}* combined with the apparent replicative stress suggested by its sensitivity to genotoxic agents and decreased overall viability suggests defective checkpoint activation in this mutant, consistent with its previously described role in activation of the DNA replication checkpoint by phosphorylation of the replication checkpoint adaptor protein Mrc1 (Shikata et al., 2007; Xu et al., 2019; Zhao & Russell, 2004). Thus, the newly isolated mutant alleles recapitulate many of the same phenotypes previously attributed to the affected genes and presumably affect at least one or several of the canonical functions associated with each gene.

2.3.6 Mutants generated by CRISPR-Cas9 mediated mutagenesis in essential genes tel2*,* top2*, and* top3 *exhibit loss of heterochromatin and transcriptional de-repression*

All of the mutants of interest had been isolated because they appeared to affect *ade6+* reporter silencing, therefore we performed a more formal analysis of the newly generated mutants to characterize the extent and nature of the silencing defect in each mutant. Streaking out each mutant to single colonies on low adenine media to assess the uniformity of reporter de-repression revealed that each mutant exhibited slightly higher variegation frequency than the wild type parent strain, with $tel2^{N765E766K}$ exhibiting the most dramatic increase in variegation rates (Figure 2.8a,b,c). Given that the majority of the mutations produced DNA replication, repair, and/or checkpoint defects we confirmed that the change in reporter expression in white colonies was attributable to epigenetic changes and not the result of a mutator phenotype. Picking colonies appearing white on low adenine media, patching them onto rich media for approximately 40 generations, and streaking them back onto low adenine media confirmed that nearly all of the previously white colonies had fully or partially reverted back to a heterochromatinized state with freshly struck out cells appearing pink or red (not shown) (Loeb, Springgate, & Battula, 1974; Serero, Jubin, Loeillet, Legoix-Né, & Nicolas, 2014; Sohl, Ray, & Sweasy, 2015). Consistent with a PEV defect, reporter silencing appeared less static in all three mutants (Figure 2.8b). The difference in reporter expression was subtler and more difficult to detect by traditional serial dilution spotting assays on YE media and/or synthetic media with low adenine at 32° C; we speculate that this may be due in part to the mildness of the defect and/or the unstable nature of the alleles and their stochastic effect on reporter silencing, or may represent a differential loss of silencing between the reporter and

endogenous pericentromeric heterochromatin. The apparent silencing defect is more

pronounced in temperature sensitive mutants $top3^{S69del}$, $top3^{E70Y71D}$, and $tel2^{N765E766K}$ at

restrictive temperature, however, producing a noticeable change in reporter expression

indicating that the loss of silencing phenotype is enhanced in conjunction with the loss of

viability at restrictive temperatures (Figure 2.8d). The $dcr1^{565fs}$ allele generated in the

previous CRISPR mutagenesis screen is included in this and subsequent analyses as a

positive control, as it exhibited a near-complete loss of silencing at the centromere

(Figure 2.8d, Figure 2.10).

dg and dh repeats are found in the outer pericentromeric region of all three

chromosomes in *S. pombe*; while dg and dh repeat number varies between chromosomes

the repeat sequence itself is well conserved (Alper et al., 2012; Chikashige et al., 1989)

(Figure 2.10). To determine whether $top2, top3,$ or $tel2$ mutants exhibit a more general

defect in heterochromatic silencing we analyzed the expression of the pericentromeric

repeats dg and dh in each mutant (Figure 2.9a,b). $top2, top3,$ and $tel2$ mutants showed a

modest increase in dg and dh expression at 32° C while $dcr1^{565fs}$ produced a considerable

increase in repeat expression (Figure 2.9a). Given that repeat contraction and/or

expansion is not uncommon at repetitive elements, particularly under conditions of

aberrant transcription and in replication and recombination defective mutants, we

analyzed genomic DNA for copy number differences that might explain the apparent

increase (T. Kobayashi & Ganley, 2005; Takehiko Kobayashi, Heck, Nomura, &

Horiuchi, 1998; Salim et al., 2017). While there were slight fluctuations in copy number

which may suggest that copy number at repetitive elements is more elastic in $top2, top3,$

and *tel2* mutant backgrounds, there was nothing which would adequately explain the observed increase in transcription (Figure 2.15).

We then analyzed whether pericentromeric heterochromatin levels were affected in each mutant in addition to de-repression of pericentromeric transcripts by comparing relative H3K9me2 levels at the pericentromeric repeats in each of the newly isolated mutants by ChIP-qPCR. Dimethylated H3K9me2 is the primary heterochromatic mark in fission yeast and is typically enriched in heterochromatic domains including the pericentromeric repeats (J. Nakayama, J. C. Rice, B. D. Strahl, C. D. Allis, & S. I. Grewal, 2001; Yamada, Fischle, Sugiyama, Allis, & Grewal, 2005); with the exception of *top2^{K388Q}*, which showed only a modest reduction, all mutants tested exhibited a clear decrease in H3K9me2 at *dg* and *dh* repeats (Figure 2.9c).

In addition to the pericentromeric repeats, other major regions of constitutive heterochromatin include the mating type locus, subtelomeric regions, and ribosomal DNA repeats. To determine whether the silencing defects exhibited by the *top2, top3,* and *tel2* mutants are restricted to the pericentromeric region or affect heterochromatic domains more broadly we analyzed the effect of each mutation at ribosomal DNA. Similar to what was observed at the pericentromeric repeats there was a significant reduction in H3K9me2 enrichment at rDNA in all three *top3* mutants and *tel2^{N765E766K}* (Figure 2.9d). Thus, loss of heterochromatic markings appears consistent between RNAi-responsive heterochromatin at both the pericentromere and rDNA repeats in *top3* and *tel2* mutants.

Maintenance and establishment of subtelomeric heterochromatin is distinct from the RNAi-dependent heterochromatin found within pericentromeric and ribosomal DNA repeats, and so we asked whether heterochromatin levels were also affected at the subtelomeric regions. Each essential gene mutant was crossed into a series of subtelomeric *ura4+* reporters which are typically repressed to different degrees depending on their proximity to the chromosome end and subject to serial dilution spotting assays; the reporter/mutation combinations tested are summarized in (Table 2.4). In each reporter/mutant combination there was either no visible change in reporter silencing or, in the case of $top2^{K388Q}$ and $top3^{E70Y71D}$, the effect was stochastic and varied between experiments, sometimes appearing to elicit increased reporter silencing and at other times an apparent decrease in reporter silencing (not shown). Interestingly, although $tel2^{N765E766K}$ has a strong effect on pericentromeric reporter silencing, there was no observable effect on subtelomeric reporter expression. *tel2* mutants in budding yeast exhibit a telomeric position effect variegation phenotype, which may suggest that the effect of this allele is specific to certain classes of constitutive heterochromatin or that *tel2* does not influence subtelomeric PEV in fission yeast despite its role in maintenance of telomere length (Runge & Zakian, 1996; Xu et al., 2019). More work is needed to characterize the molecular phenotypes of each mutant at the subtelomeres; taken together, these results may suggest that loss of heterochromatin in $tel2^{N765E766K}$, $top3^{E70K}$, $top3^{S69del}$, and $top3^{E70Y71D}$ is unique to RNAi-dependent heterochromatin. With this limited data other confounding factors such as increased *ura4+* reporter instability in subtelomeric heterochromatin cannot be ruled out, however.

RNAi is the primary pathway by which heterochromatin is established in *S. pombe* at the pericentromeric and ribosomal DNA repeats (Volpe et al., 2002). With the exception of $top2^{K388Q}$ all of the mutants analyzed in this study exhibited pericentromeric and rDNA heterochromatin silencing defects, therefore we investigated whether the RNAi pathway or siRNA biogenesis was perturbed by isolation and high-throughput sequencing of siRNAs from each mutant. Pericentromeric siRNAs were unaffected in $top2^{K388Q}$, suggesting that the core RNAi pathway remains intact in this mutant. $tel2^{N765E766K}$, $top3^{E70K}$, $top3^{S69del}$, and $top3^{E70Y71D}$ all showed an increase in siRNAs (Figure 2.10).

Taken together, these observations suggest that the core RNAi pathway is preserved in all mutants. The increase in siRNAs observed at *dg* and *dh* repeats in $tel2^{N765E766K}$, $top3^{E70K}$, $top3^{S69del}$, and $top3^{E70Y71D}$ are presumably a product of increased pericentromeric transcript production; the accompanying reduction in heterochromatin suggests that recruitment of chromatin modifying enzymes has been decoupled from RNAi activity in these mutants in a manner reminiscent of *clr3* histone deacetylase (HDAC) mutants in fission yeast (Yamada et al., 2005). RNAi and chromatin assembly occur in a self-reinforcing positive feedback loop, therefore even minor interference in either of these essential processes can substantially affect heterochromatic silencing. Paradoxically, however, the same relationship is not observed in $top2^{K388Q}$ despite the fact that pericentromeric transcript expression also increases. More work is needed to more thoroughly dissect the relationship between the loss of transcriptional silencing observed in these mutants and their effect on heterochromatin levels; going forward, however, these alleles and the general approach described in this study may provide a

much-needed platform for a mechanistic dissection of the candidate genes included in this study and their contribution to the observed heterochromatin and transcriptional silencing defects.

2.4 Discussion

This study describes a novel implementation of Hermes integration density profiling utilizing positive selection to identify genes affecting PEV of a pericentromeric heterochromatin reporter, followed by CRISPR/Cas9-directed mutagenesis of candidate essential and non-essential genes. The combination of a saturated Hermes insertion screen with CRISPR/Cas9 directed mutagenesis constitutes a mixed forward/reverse genetics agile approach leveraging the rapid identification of candidate genes in TE insertion screens with the flexibility obtained by mutagenesis using CRISPR/Cas9. With this combined approach we were able to identify and obtain novel alleles in essential genes contributing to heterochromatin silencing for further analysis.

We identified a number of genes with a known role in centromeric silencing which were significantly enriched within the Hermes PEV screen, confirming robust selection for PEV modifiers using the approach described herein. We also found that insertions affecting essential genes involved in DNA replication, repair, and recombination, in addition to a number of other essential cellular processes, were similarly enriched. Previous screens have uncovered a role for DNA replication and repair components in heterochromatin maintenance; however, many essential genes have been necessarily precluded from such analysis as a consequence of their requirement for viability (Elizabeth H. Bayne et al., 2014; Jahn et al., 2018). Reconstruction of several Hermes

insertions which emerged from the screen revealed that that they were lethal alleles, suggesting that similar integration events in essential gene ORFs are also likely to impact viability. We were also able to rule out the possibility that these insertions may have been propagated in pseudodiploid cells and enriched as a consequence of a dominant PEV phenotype.

We hypothesize that the appearance and persistence of these lethal alleles may be explained by extragenic suppressors arising either spontaneously or through independent Hermes insertion events in other genomic locations. With this line of reasoning we demonstrated that a known suppressor of *top3* mutant lethality, *rqh1Δ*, did not similarly suppress the loss of silencing associated with *top3* mutants. Taken together, the findings reported here suggest that as the principles underlying essentiality bypass are revealed and the complex genetic interactions occurring as a result are better understood these phenomena may be further exploited to allow for detection of novel phenotypes associated with essential genes. Suppressors have previously been used to probe the involvement of essential gene in cellular pathways; a systematic application of these principles can be leveraged in the design and deployment of next-generation genetic screens (Ben-Shahar et al., 2008; Du & Novick, 2002; J. Li et al., 2019). The outcome of the screen described in this study, moreover, suggests that the use of positive selection facilitates the enrichment of insertions eliciting functional consequences in essential genes. Going forward, identification of methods to accelerate and promote the occurrence of essentiality suppressors may enhance this approach and lend itself to a pipeline whereby essential genes affecting a phenotype of interest can be rapidly identified

followed by generation of a panel of alleles informed by screen outcomes to probe the underlying mechanism.

Li et. al. (2019) noted that 'bypassable' essential genes often correlated with slow spore lethality and relatively high transposon insertion densities when cells were mutagenized with the Hermes transposon (J. Li et al., 2019). Since the loss of viability in those instances is often delayed (ie. spores are capable of generating microcolonies before growth cessation) there is a small window of opportunity for extragenic suppressors to arise. Given that the screen as described utilizes a plasmid based transposon system, multiple copies of the transposon may be available for integration at any given time potentially resulting in multiple insertions within a single cell. Further, given that many of the mutagenized genes which emerged have known roles in DNA replication, repair, and recombination, it is possible that spontaneous mutation rates may have been globally accelerated due to alteration or impairment of these essential cellular processes prior to onset of lethality (Kokoska et al., 1998; V. F. Liu, Bhaumik, & Wang, 1999; Morrison & Sugino, 1994; Tubbs & Nussenzweig, 2017). By analyzing and identifying the molecular underpinnings influencing the conversion of essential genes into non-essential genes, researchers can undertake a rational approach to the design and optimization of genetic screens which are less restricted by the 'essential' status of genes. Many essential genes are intimately involved in a number of complex cellular processes and pathways, yet their multifaceted function is obscured outside of their requirement for survival. In this study we provide evidence that BOE may be exploited for screening purposes to facilitate the identification of essential genes contributing to a phenotype of interest, thereby broadening the available 'genetic screening space'.

Further, Li. et. al. report that 26% of the bypassable genes identified in their study were only uncovered by point mutations or insertion alleles and would have been missed without their two-pronged approach utilizing both chemical mutagenesis and transposable element insertion. Our work has shown that CRISPR-Cas9 can also be deployed to generate point mutations in non-essential and essential genes which retain viability but exhibit novel phenotypes of interest. Therefore, the use of alternate complementary mutagenesis approaches such as the CRISPR-Cas9 induced mutagenesis described in this work may enhance the coverage of the BOE suppressor mutation space by expanding the genetic toolkit available to researchers. A further advantage of generating alleles with the CRISPR/Cas9 system is that the mutations obtained can provide potential insights into the mechanism of action. As an example, while the majority of Cas9 sgRNAs directed against *top2* did not produce any viable mutants with an apparent silencing defect, we noted that the sole *top2* mutant identified- *top2^{K388Q}*- eliminates a previously described SUMOylation site in the K loop of its ATPase domain (Køhler et al., 2015). It has been proposed that the interaction of this region with DNA triggers ATP hydrolysis and subsequent release of DNA from the enzyme (Køhler et al., 2015; Schmidt, Osheroff, & Berger, 2012). Top2 functions in maintaining and establishing chromatin topology during DNA replication, transcription, and chromosome segregation by unwinding and disentangling DNA throughout these processes, which generate considerable amounts of topological distortion. This activity is accomplished by cleavage of double-stranded DNA through a transesterification reaction, generating a transient covalently bound DNA-protein cleavage complex (Top2cc) which is subsequently cleared after re-ligation of cleaved DNA (Wei et al., 2017). It has been

proposed that Top2 SUMOylation may be an important mechanism for regulation of Top2cc in instances where these DNA adducts persist by promoting their degradation (Hall & Goralski, 2018; Wei et al., 2017). Interestingly, topoisomerase poisons which lock the enzyme in the closed covalently bound state by blocking ATP hydrolysis have also been demonstrated to impair reformation of facultative heterochromatin in human cells (Miller et al., 2017). In fission yeast, the SUMO E3 ligase *pli1* promotes Top2 SUMOylation; *pli1* was also identified in a genetic screen for mutants exhibiting heterochromatin silencing defects and has been previously demonstrated to play a role in heterochromatic silencing at the centromeres and telomeres in fission yeast (Jahn et al., 2018; Xhemalce, Seeler, Thon, Dejean, & Arcangioli, 2004). Taken together, these results may suggest that the heterochromatin silencing defects associated with the *top2* mutant described in this study and *pli1* may share the same mechanistic origin in SUMOylation-mediated regulation of Top2 processing; more follow up is needed to determine the nature of the relationship between these genes and their pursuant effect on heterochromatic silencing. The use of CRISPR/Cas9-directed mutagenesis can facilitate the production of unique alleles in essential genes which, unlike the use of random mutagenic agents, can easily be recovered for further analysis when using a candidate approach. Going forward, combining these alleles with established suppressors may permit surgical dissection of the affected essential processes to disentangle the contributions of essential genes to a number of vital cellular processes.
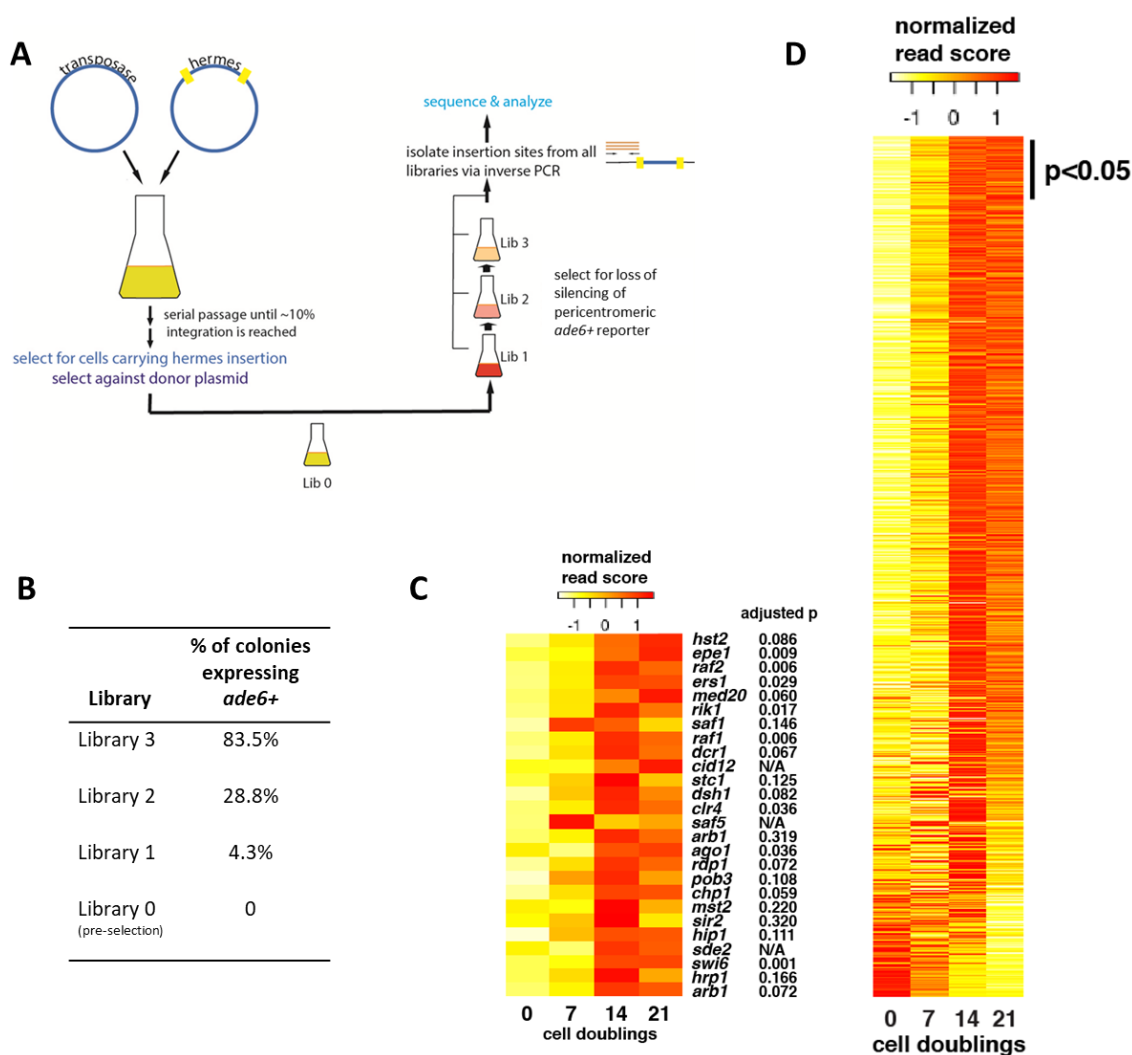
Figure 2.1. Hermes PEV Screen Overview. A. Schematic of the PEV screen. Cells were co-transformed with a transposase-expressing and transposon-containing plasmids and transposition was induced for ~12 days (135 generations) before selecting for cells carrying genomic Hermes integration events and placing the Hermes-enriched cell population through several rounds of positive selection for pericentromeric *ade6+* reporter re-repression. B. Table showing the proportion of white (ie. *ade6+*-expressing) cells after each round of selection for reporter de-repression. C. Heat map showing Z-scores for genes annotated as affecting centromeric silencing; p values are indicated to the right. Z scores reflect normalized read counts per gene. D. Heat map showing the Z-score for all genes passing filter throughout each round of selection. Significantly enriched genes (p < .05) are indicated on the right. Z scores reflect normalized read counts per gene.
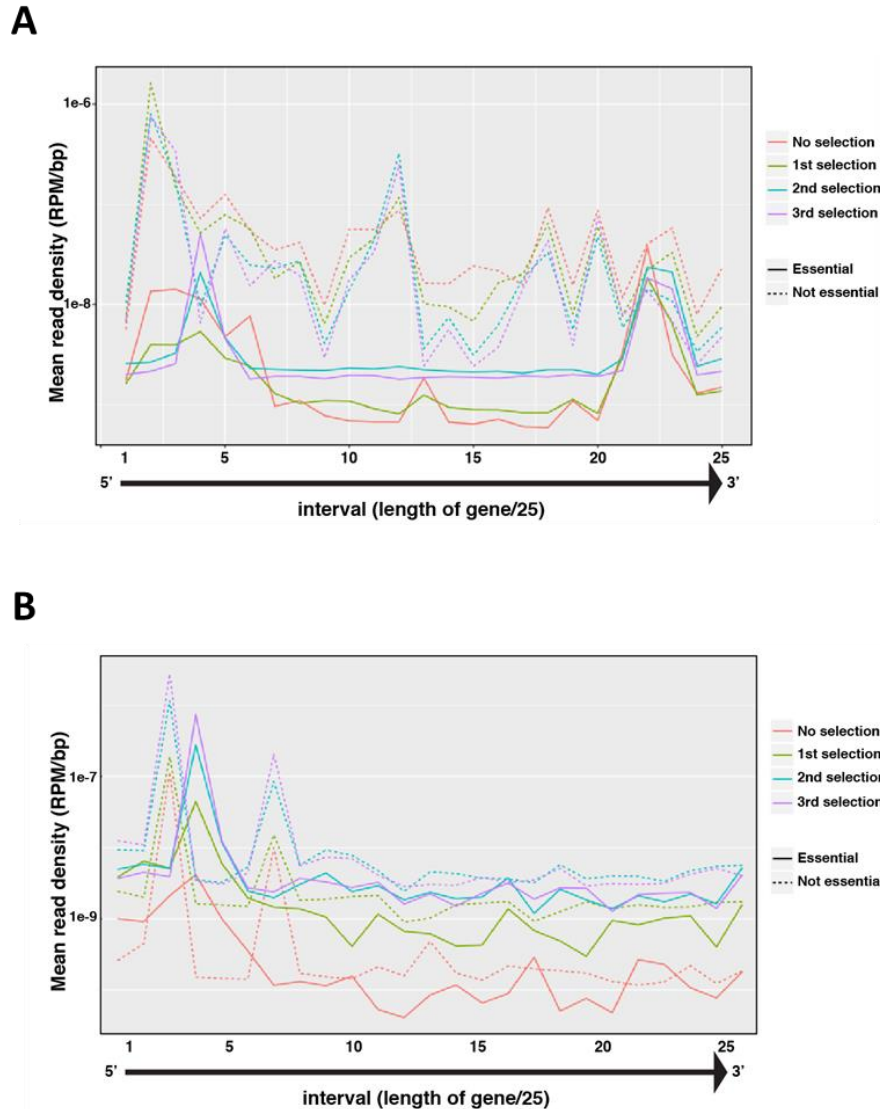
Figure 2.2. Genes which are significantly enriched within the Hermes PEV screen have increased integration site read density within both essential and non-essential gene ORFs.
A. Mean read density from all four libraries (pre-selection in addition to three sequential post-selection libraries) plotted over both essential (solid lines) and non-essential genes (dashed lines) for all genes passing the described filtering criteria (n= 3,760). Reads are evenly distributed across the majority of non-essential genes, while reads in essential genes show peaks in the 5' and 3' gene ends. B. Mean read density from all four libraries (pre-selection in addition to three sequential post-selection libraries) plotted over both essential (solid lines) and non-essential genes (dashed lines) which were considered significantly enriched in the PEV screen (n= 263). Reads in both essential and non-essential genes show a peak in the 5' ends of genes which becomes more prominent with each round of selection, while the separation between read distribution in the body of essential and non-essential genes decreases relative to the overall population of analyzed genes.
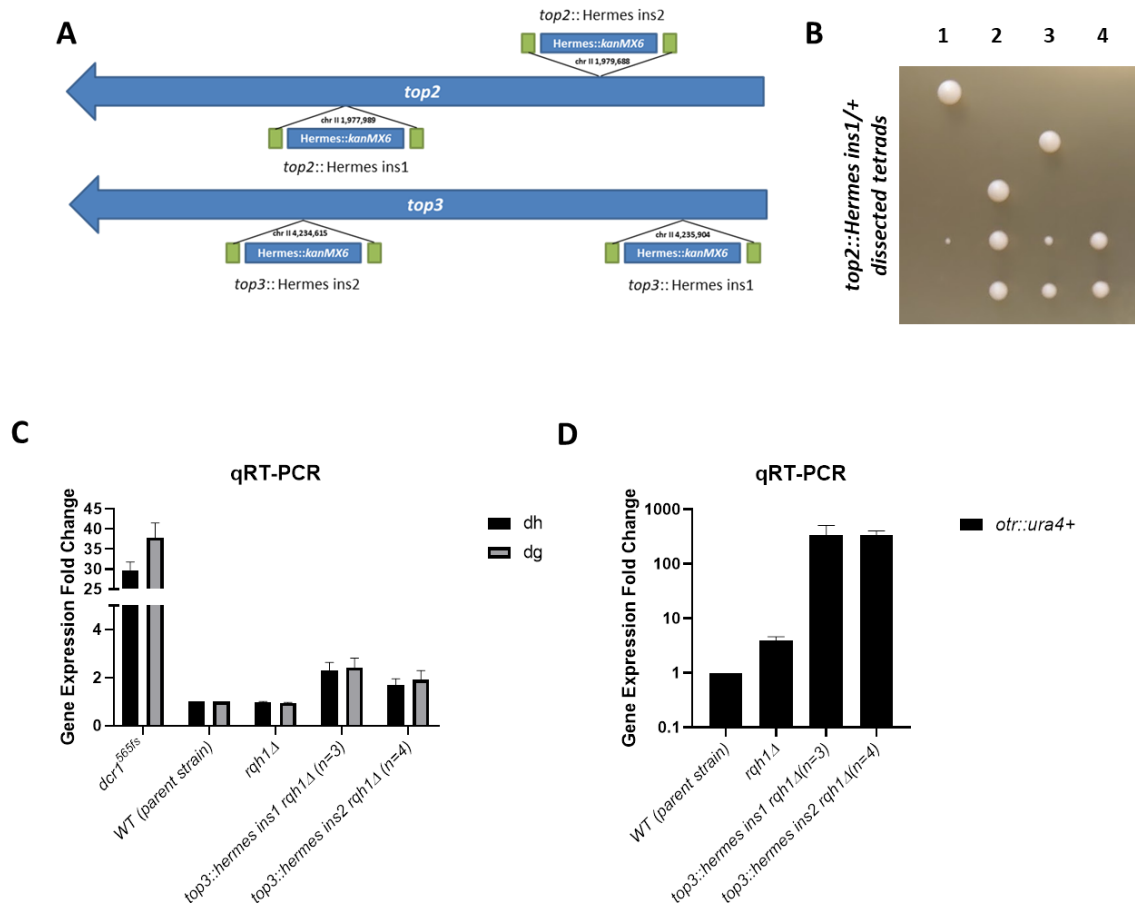
Figure 2.3. Rqh1 knockout suppresses the lethality associated with *top3::*Hermes mutant alleles but does not suppress the associated silencing defect. A. Schematic showing insertion points of Hermes fragments for reconstruction of Hermes alleles in *top2* and *top3*. Integration sites are indicated. B. Diploids carrying Hermes insertions in *top2* or *top3* were sporulated on ME and plated on YEA for 6 hours at 32° C prior to dissection of tetrads. Dissected Hermes-carrying tetrads occasionally produced variable numbers of sporulated colonies but none carrying a Hermes insertion, indicating that all four *top2::*Hermes and *top3::*Hermes alleles tested are lethal. Pictured is a representative image of four dissected tetrads sporulated from *top2::Hermes* diploids. Each row indicated contains a dissected tetrad. C. Analysis of *dg* and *dh* transcript expression by qRT-PCR in *rqh1Δ top3::*Hermes double mutants. *rqh1* was knocked out in diploids carrying one of the two *top3::Hermes* insertions (*ins1* or *ins2*) and *dg* and *dh* expression was analyzed in several transformants from each respective genotype; the number of transformants analyzed is indicated next to the strain name, qPCR reactions for each transformant were set up in triplicate. *dg* and *dh* expression was consistently increased in all transformants tested, the average of all trials is shown here. All strains shown in this experiment were grown at 32° C in rich media (YEA) prior to RNA extraction. Error bars= SEM. D. Analysis of *otr::ura4+* pericentromeric reporter expression in the same *rqh1Δ top3::*Hermes double mutants. Error bars=SEM.
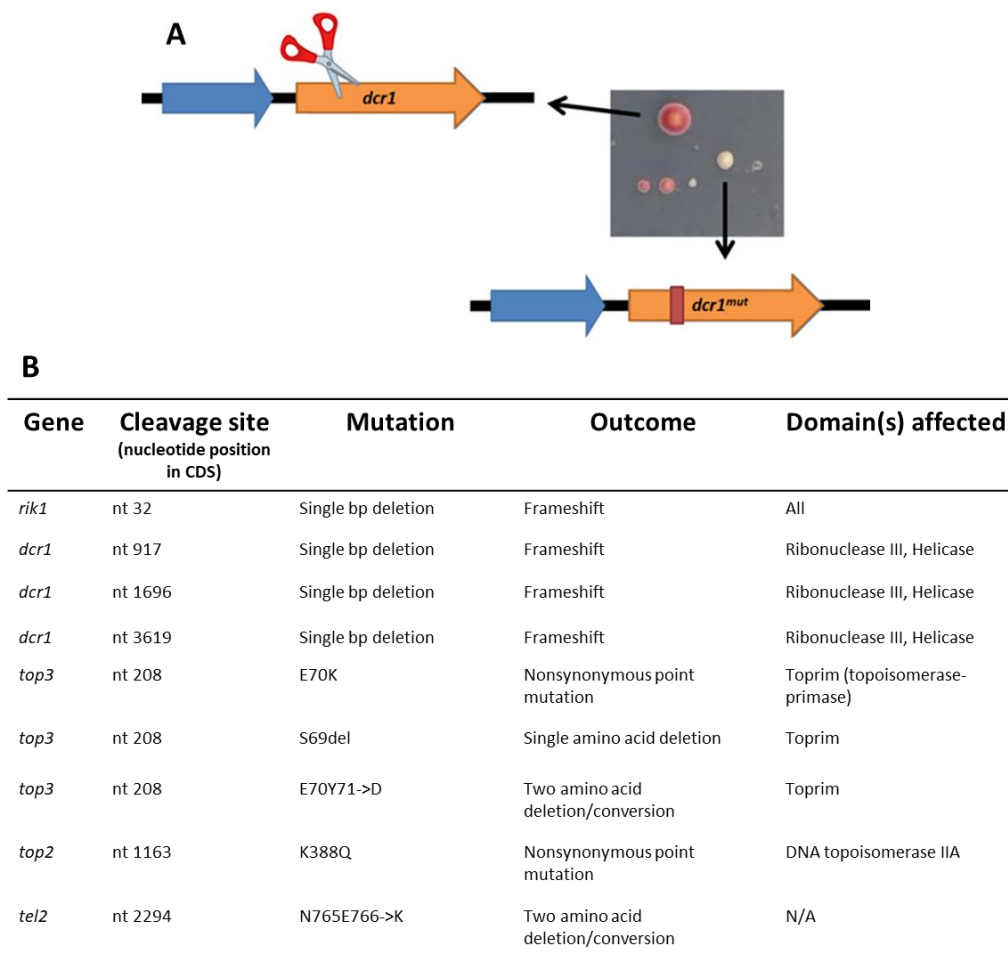
Figure 2.4. CRISPR—Cas9 mutagenesis overview. A. Cells carrying a pericentromeric *ade6+* reporter were transformed with single sgRNAs targeting regions carrying a PAM site and predicted to have high cleavage efficiency and low off-target activity closest to the location of insertions which emerged from the Hermes screen. Transformed cells were then plated on low adenine-containing media to facilitate identification of colonies with a reporter silencing defect by appearance (inset, cells transformed with a plasmid encoding Cas9 and sgRNA targeting *dcr1*). Colonies appearing pink or white were isolated and a region surrounding the PAM site was amplified and sent for Sanger sequencing to identify any mutations which may have been produced by Cas9 cleavage and repair. B. Summary of the mutants which emerged as a result of CRISPR-Cas9 mediated mutagenesis. The location of the cleavage site is indicated with respect to the start of the coding sequence as well as the mutation and its effect on the protein amino acid sequence and any affected domains.

B

Gene	Cleavage site (nucleotide position in CDS)	Mutation	Outcome	Domain(s) affected
rik1	nt 32	Single bp deletion	Frameshift	All
dcr1	nt 917	Single bp deletion	Frameshift	Ribonuclease III, Helicase
dcr1	nt 1696	Single bp deletion	Frameshift	Ribonuclease III, Helicase
dcr1	nt 3619	Single bp deletion	Frameshift	Ribonuclease III, Helicase
top3	nt 208	E70K	Nonsynonymous point mutation	Toprim (topoisomerase-primase)
top3	nt 208	S69del	Single amino acid deletion	Toprim
top3	nt 208	E70Y71->D	Two amino acid deletion/conversion	Toprim
top2	nt 1163	K388Q	Nonsynonymous point mutation	DNA topoisomerase IIA
tel2	nt 2294	N765E766->K	Two amino acid deletion/conversion	N/A

Figure 2.5. *top3* **CRISPR mutant alleles exhibit signs of replicative stress.** A. Fission yeast grown on YEA at 32° C (upper panels) and 37° C (lower panels). *top3* mutants appear elongated, with an increase in visible vacuolar structures; the elongation phenotype increases significantly upon shifting temperature sensitive (ts) alleles to the restrictive temperature.
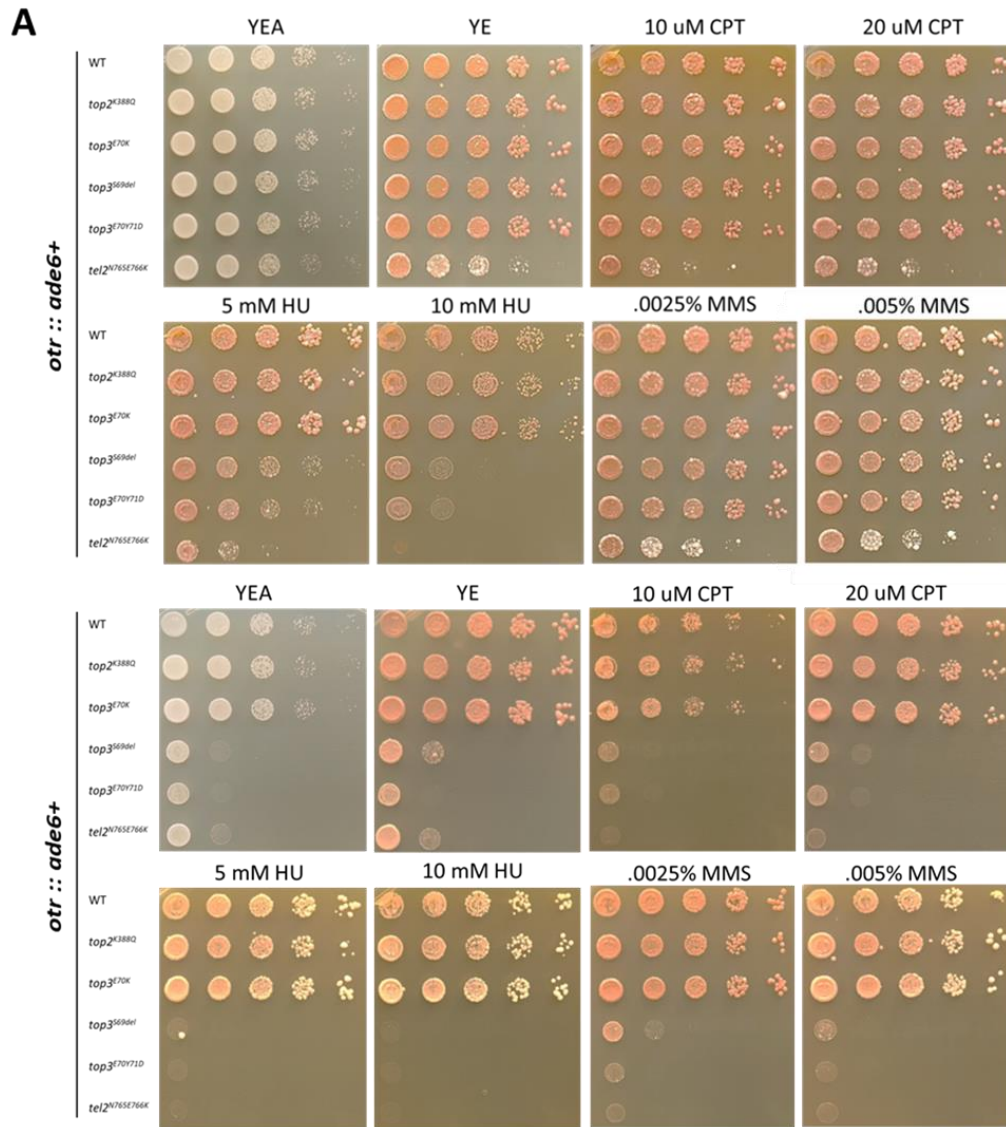
Figure 2.6. *top3* and *tel2* CRISPR mutant alleles exhibit sensitivity to genotoxic agents. A. Upper panel series: Serial dilutions of indicated mutant alleles grown at 32° C and spotted on plates with DNA damaging agents added (genotoxin and concentration is indicated above each image, plates were imaged after 3-5 days). *top2^{K388Q}* and *top^{3E70K}* are relatively insensitive to Camptothecin (CPT), hydroxyurea (HU), and MMS. The remaining temperature sensitive *top3* and *tel2* alleles show sensitivity to hydroxyurea at the permissive temperature; *tel^{2N765E766K}* shows slight sensitivity to CPT. Lower panel series: The same dilutions spotted on plates with DNA damaging agents and incubated at 37° C. At the restrictive temperature, *top3^{S69del}*, *top3^{E70Y71D}*, and *tel2^{N765E766K}* all exhibit a mild sensitivity to CPT and MMS and a strong sensitivity to HU.

A
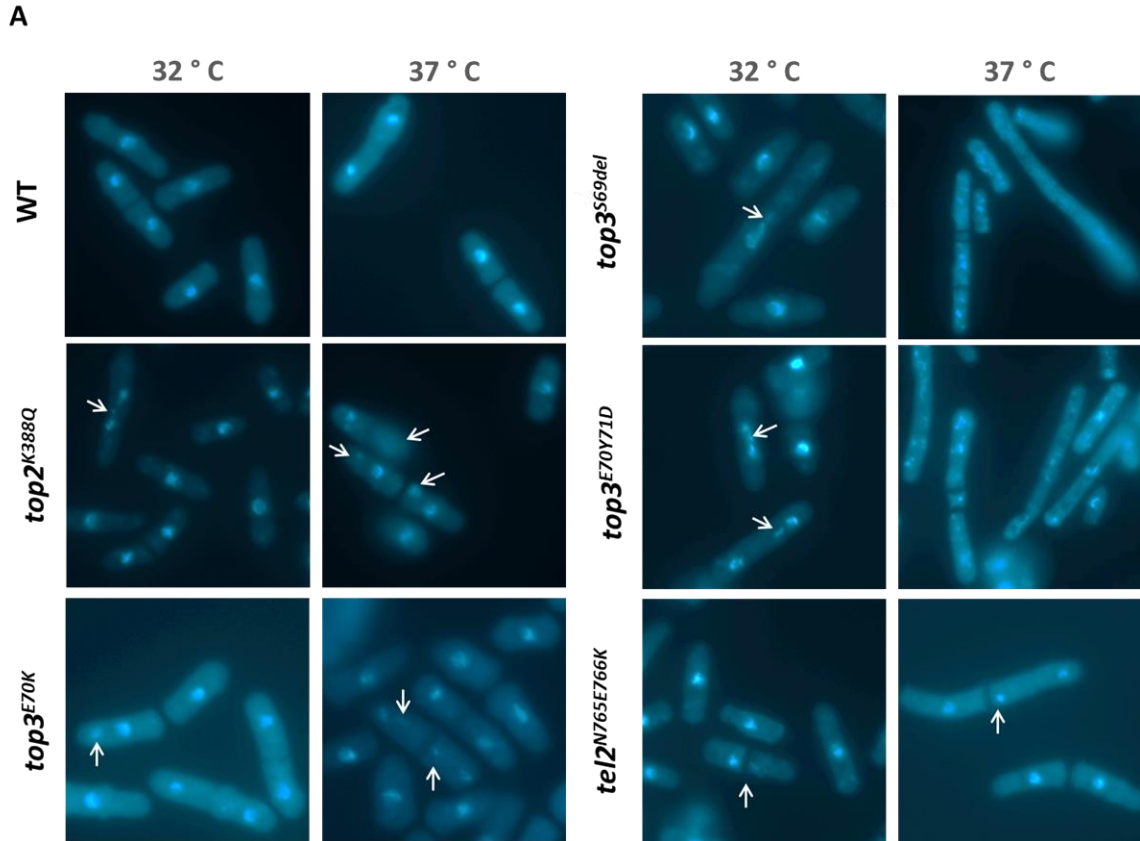
Figure 2.7. CRISPR mutant alleles exhibit chromosome segregation and mitotic defects. A. DAPI staining of *S. pombe* cells reveals chromosome segregation and mitotic defects in *top2, top3,* and *tel2* mutants. Cells were grown at both 32° and 37° C; representative images are shown for each strain. *top3*^{S69del} and *top3*^{E70Y71D} appear as massively elongated, multiseptate, and multinucleate structures with fragmented nuclear material dispersed throughout the cell. Abnormal nuclear structures (lagging chromosomes, anaphase bridges, unequally or prematurely segregated chromosomal material) are indicated with arrows.
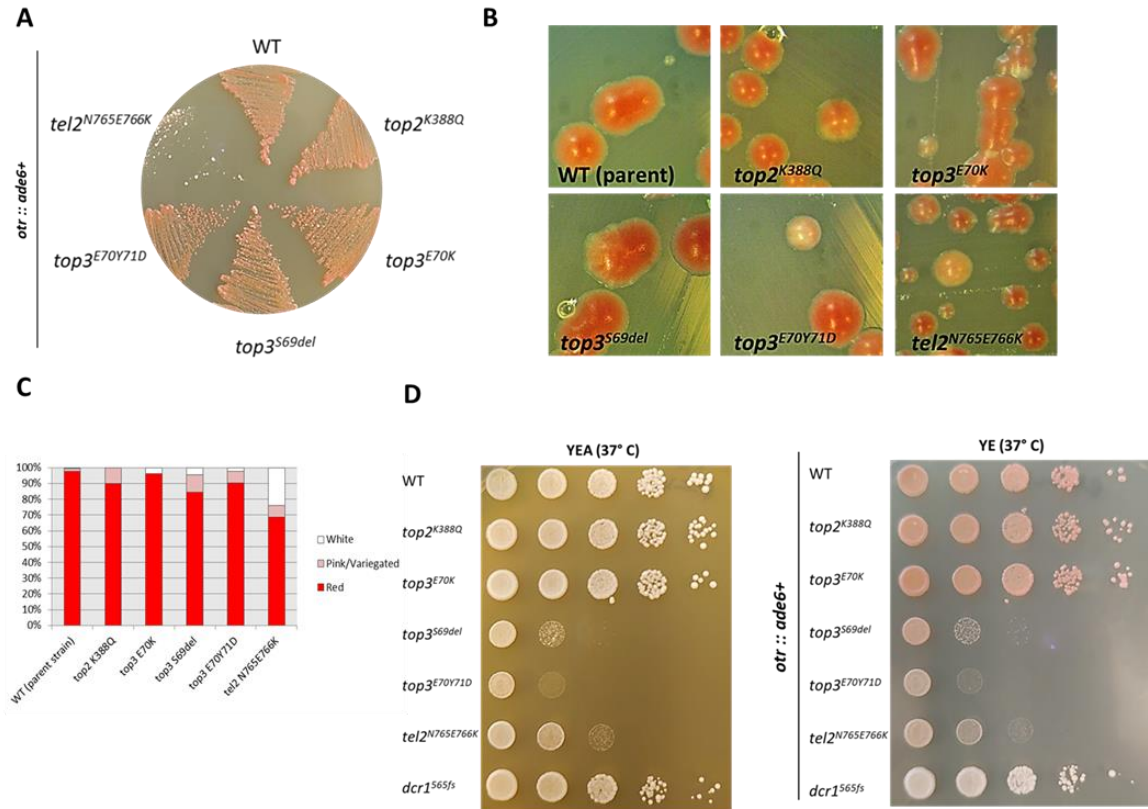
Figure 2.8. *top2, top3, and tel2* **mutants exhibit** *ade6+* **reporter de-repression and increased variegation.** A. CRISPR mutant strains struck out on YE. A slight increase in the number of white (*ade6+* expressing) colonies is visible. B. Reporter expression appears visually dynamic within colonies in *top2, top3,* and *tel2* mutants, indicating increased variegation. C. *top2, top3, and tel2* mutants exhibit increased variegation rates. The proportion of red, white, and pink/variegated colonies were counted in strains struck out to single colonies on low adenine (10 mg/L) containing media.
D. Serial dilution spotting assays revealed that several of the isolated mutants are temperature-sensitive alleles (*top3^{S69del}, top3^{E70Y71D}, tel2^{N765E766K}*); left panel. Temperature-sensitive alleles grown at the restrictive temperature appear pale pink or white, indicating de-repression of the pericentromeric *ade6+* reporter; right panel. Cells were plated on YEA and YE and incubated at 37° C (restrictive temperature) for 3-5 days before imaging.
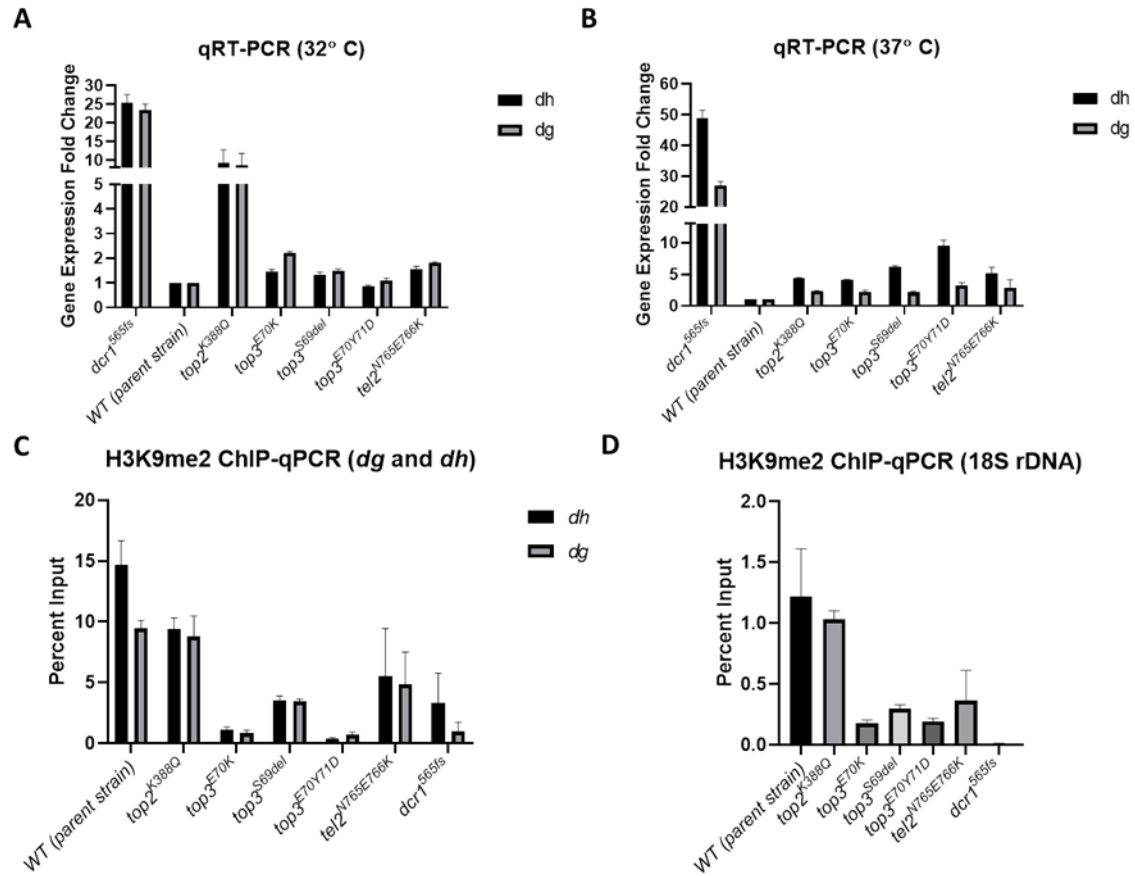
Figure 2.9. Molecular characterization of the pericentromeric silencing defect exhibited by *tel2*, *top2*, and *top3* mutants. A. qRT-PCR showing *dg* and *dh* expression levels in cells grown in rich media (YEA) overnight at 32° C prior to RNA extraction. Error bars=SEM. B. Analysis of *dg* and *dh* expression levels by qRT-PCR in cells grown in rich media (YEA) overnight at 37° C prior to RNA extraction. Error bars=SEM. C. ChIP-qPCR analyzing H3K9me2 enrichment at *dg* and *dh* repeats in cells grown in rich media (YEA) overnight at 32° C prior to ChIP. Data shown are representative of two IP replicates with each replicate assayed by qPCR in triplicate. IP signal shown is normalized to input and the euchromatic locus *act1*. Error bars=SEM. D. ChIP-qPCR analyzing H3K9me2 enrichment at *18S rDNA* repeats in cells grown in rich media (YEA) overnight at 32° C prior to ChIP. Data shown are representative of two IP replicates with each replicate assayed by qPCR in triplicate. IP signal shown is normalized to input and the euchromatic locus *act1*. Error bars=SEM.

chromosome I

chromosome II

chromosome III
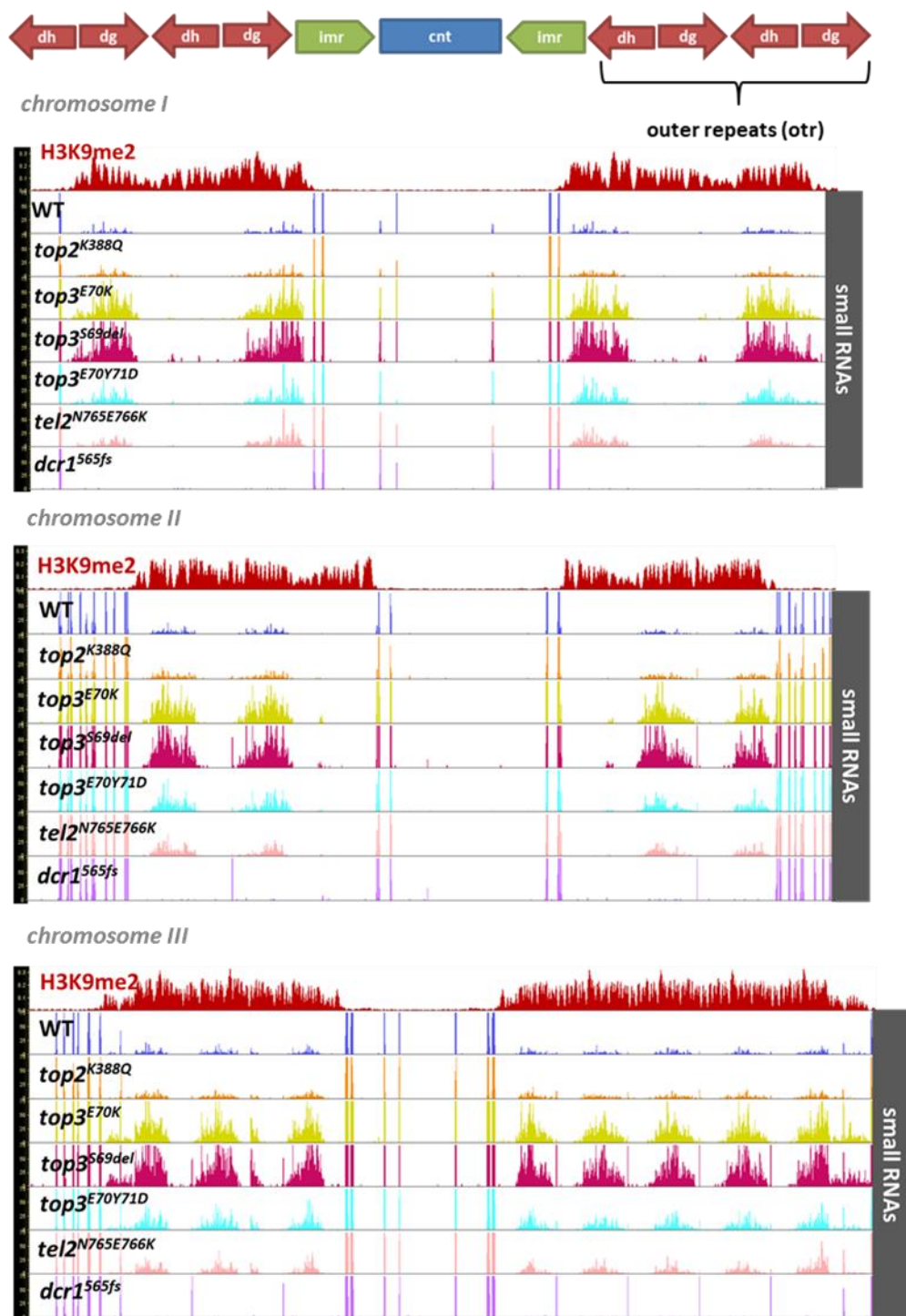
Figure 2.10. siRNA levels are increased in *top3* and *tel2* mutants at pericentromeres. A. (top) Schematic showing the organization of centromeres in *S. pombe*. siRNA production is robust at the *dg* and *dh* repeats in wild type cells due to RNAi activity in this region; H3K9me2 is also enriched. (lower panels) siRNA sequencing reads normalized per million mappable reads per sequencing run and plotted for each mutant. The wild type parent strain (ZB2116) and *dcr*^{565fs} are included as controls. Shown are the centromeres of chromosomes I, II, and III superimposed with H3K9me2 ChIP-seq enrichment.
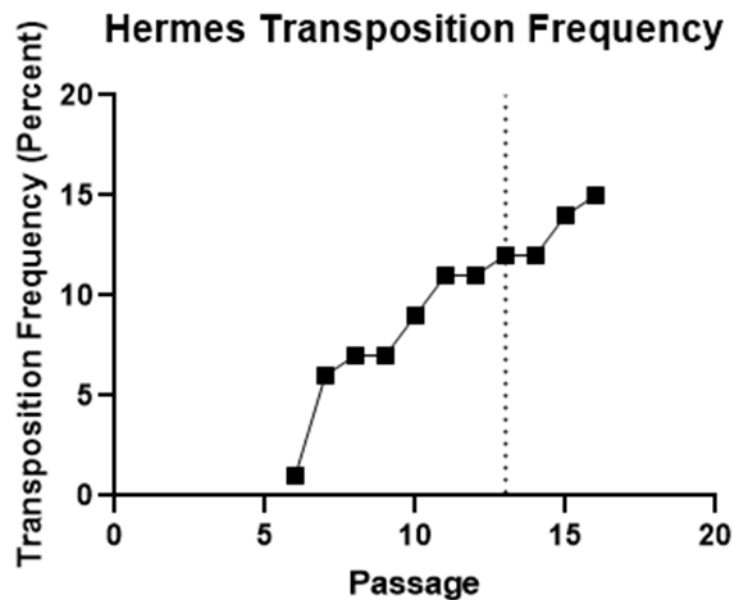
Figure 2.11. Hermes integration frequency. A. Line graph showing Hermes transposition frequency as a percentage ($FOA^R G418^R$ colonies/ total colony count) after each daily passage. Dashed line at P13 is the day the culture was harvested to proceed with selection for Hermes integration events. Transposition frequency was monitored for several passages after harvesting, however subsequent cultures were not included in the post-selection libraries.
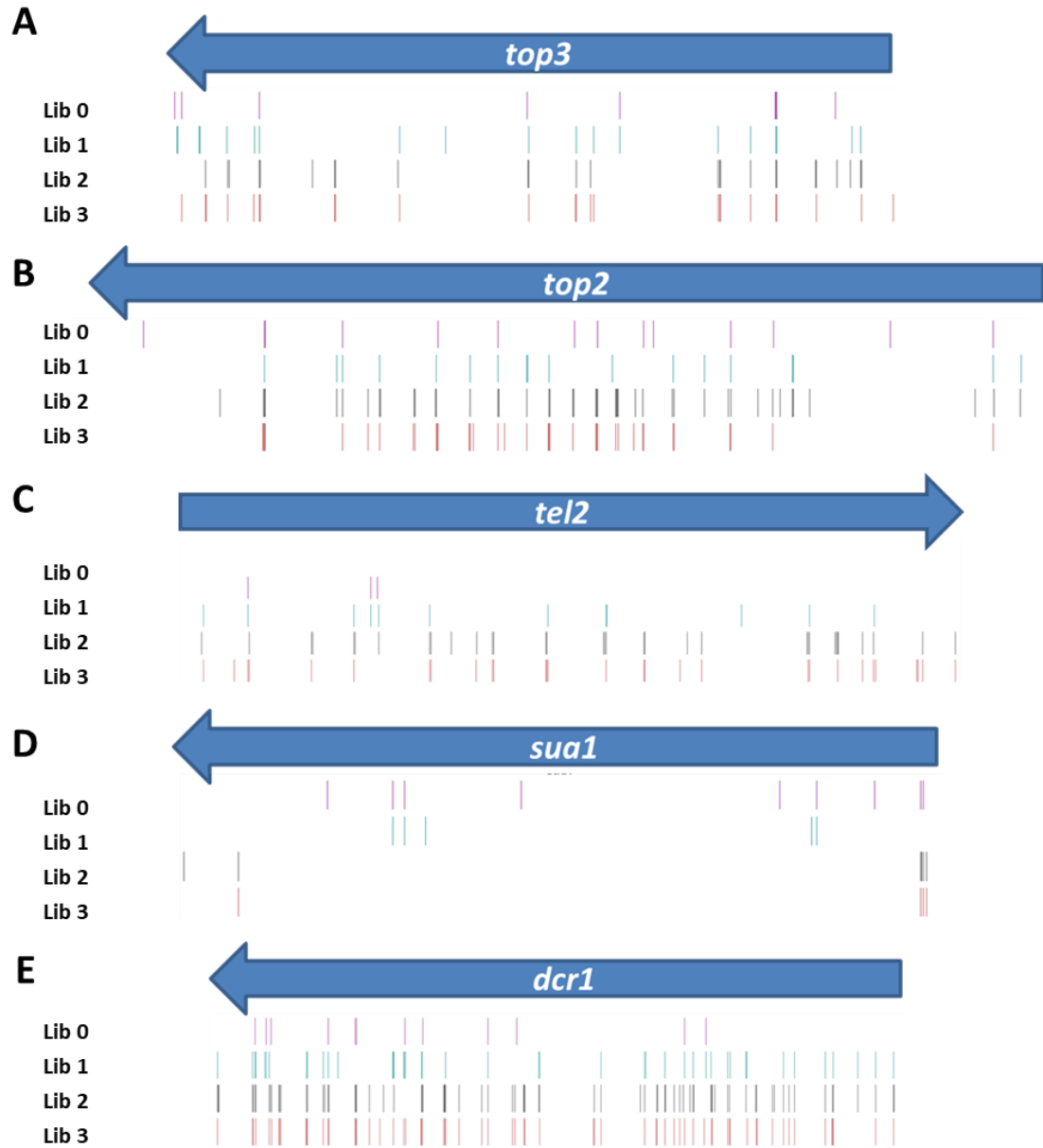
Figure 2.12. Collapsed integration profiles. Representative image showing *Hermes* insertion enrichment with each successive round of selection for loss of *ade6+* reporter silencing within the coding sequence of a gene with no known role in PEV (*sua1*, 2d); a gene with a well described role in PEV (*dcr1*, 2e); and novel genes which became enriched in the screen (*top3*, 2a; *top2*; 2b, *tel2*; 2c). Tick marks represent collapsed insertion position in either the pre-selection library (Lib 0) or after one of three rounds of selection for loss of silencing (Lib 1, 2, and 3).

A

B
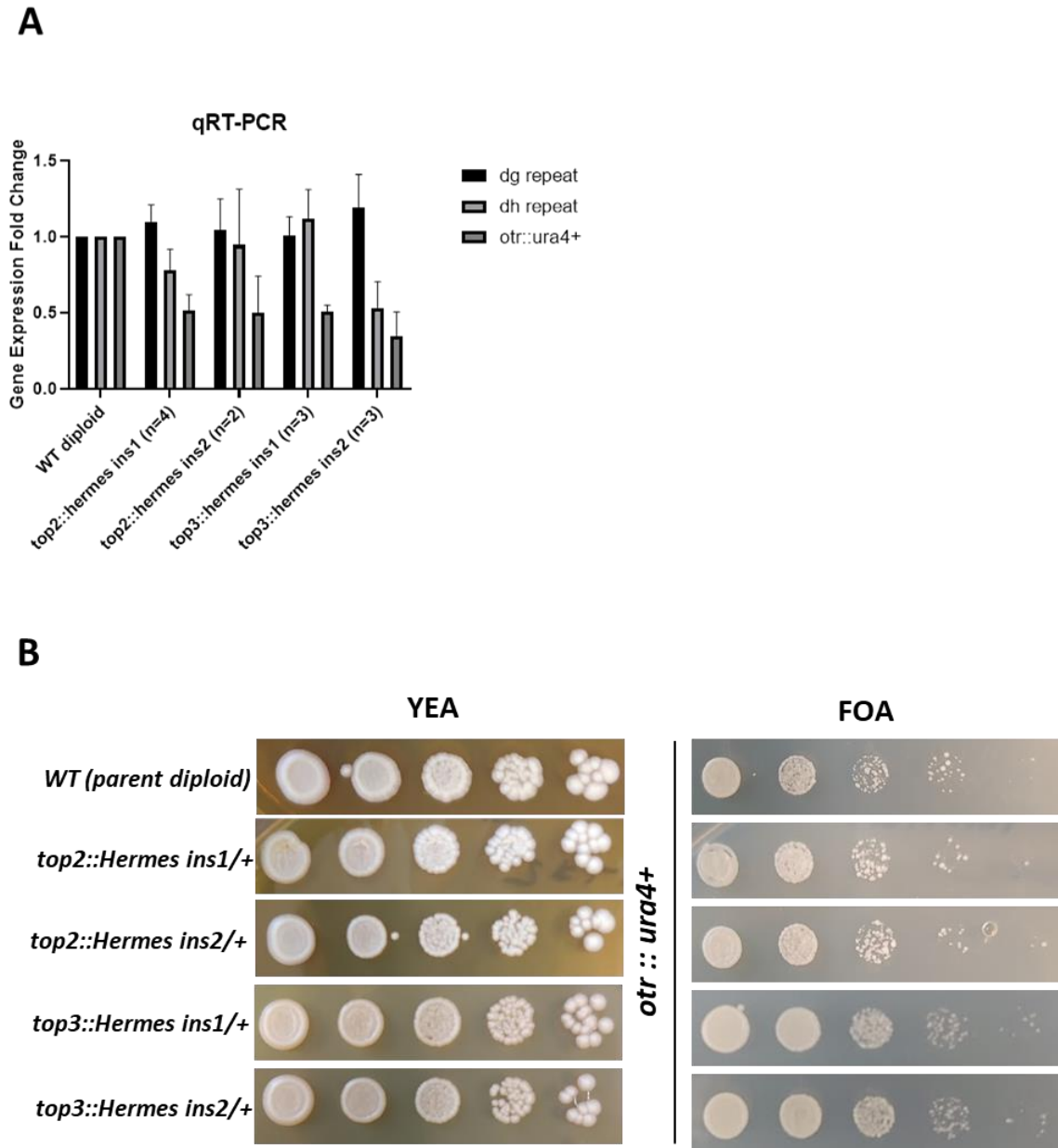
Figure 2.13. Diploids carrying heterozygous *top2::Hermes* or *top3::Hermes* alleles do not exhibit a pericentromeric silencing defect. A. qRT-PCR showing *dg*, *dh*, and *ura4+* reporter expression from multiple transformants of the indicated insertion. B. Spotting assays of diploids carrying the indicated insertions grown on YEA and FOA to select against expression of the ura4+ reporter showed no change from the control. Multiple transformants carrying each Hermes insertion were tested, shown are representative images.
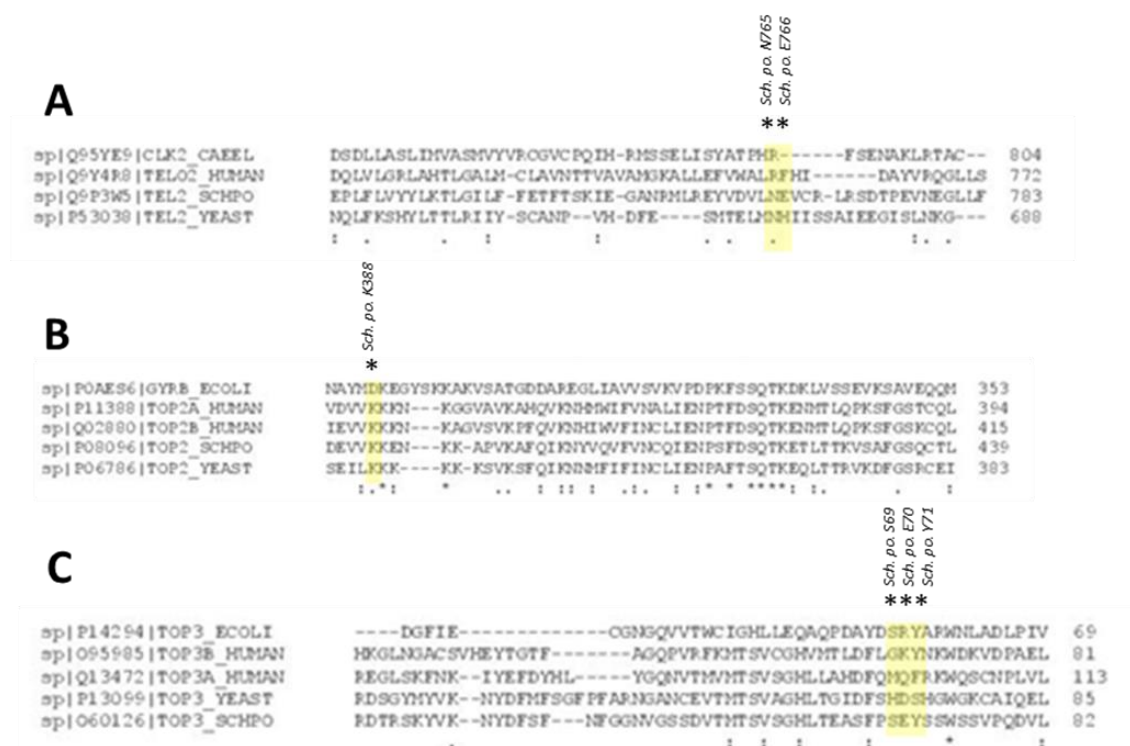
Figure 2.14. Multiple sequence alignments. A. Multiple sequence alignments showing the affected region in *tel2*[N765E766K] and its homologs in humans (*telo2*), *C. elegans* (*clk2*}, and *S. cerevisiae* (*tel2*). Protein sequences were obtained from UniProt; sequence ID is indicated. B. Multiple sequence alignments showing the affected region in *top2*[K388Q] and its homologs in humans (*top2 alpha* and *beta*), *S. cerevisiae* (*top2*), and *E. coli (gyrB).* Protein sequences were obtained from UniProt; sequence ID is indicated. C. Multiple sequence alignments showing the affected regions in *top3*[S69del], *top3*[E70K], and *top3*[E70Y71D] and their homologs in humans *(top3 alpha* and *beta), E. coli (top3),* and *S. cerevisiae (top3)*. Protein sequences were obtained from UniProt; sequence ID is indicated. All sequence alignments were generated using Clustal Omega on the default settings.
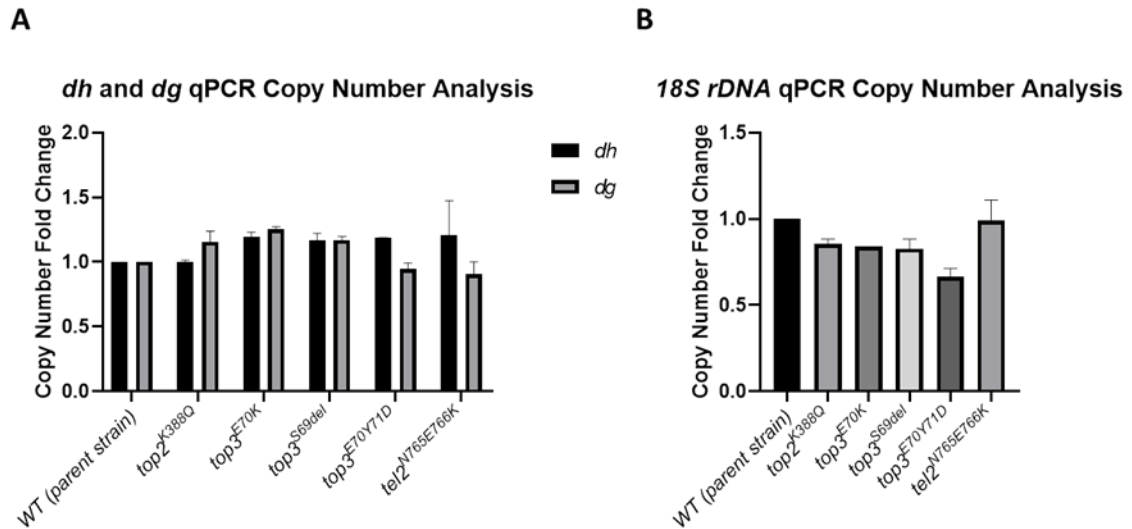
Figure 2.15. Repetitive loci in CRISPR mutants show mild variations in copy number. A. *dh* and *dg* copy number was analyzed in all CRISPR mutants relative to wild type by qPCR quantification of target and reference concentrations in genomic DNA. Relative copy number was determined by double delta Ct analysis; delta Ct= the difference in Ct values between the target locus and the euchromatic *act1* locus. qPCR reactions were performed in triplicate.
B. *18S rDNA* copy number was analyzed in all CRISPR mutants relative to wild type by qPCR quantification of target and reference concentrations in genomic DNA. Relative copy number was determined by double delta Ct analysis; delta Ct= the difference in Ct values between the target locus and the euchromatic *act1* locus. qPCR reactions were performed in triplicate.

TABLE 2.1 Genes identified as significantly enriched (p < .05) in the Hermes PEV screen. Essential genes are indicated in boldface type.

ID	Gene Name	Description	P-value
SPAC664.01c	swi6	heterochromatin (HP1) family chromodomain protein Swi6	0.001
SPAC3A11.09	sod22	plasma membrane sodium ion/proton antiporter Sod22	0.004
SPBC21B10.09	0	endomembrane system acetyl-CoA transmembrane transporter (predicted)	0.004
SPCC970.07c	raf2	CLRC ubiquitin ligase complex subunit Raf2	0.006
SPCC613.12c	raf1	CLRC ubiquitin ligase complex WD repeat subunit Raf1/Dos1	0.006
SPAPB24D3.02c	0	amino acid transmembrane transporter (predicted)	0.007
SPBC19F5.03	**sac11**	**inositol polyphosphate phosphatase (predicted)**	**0.007**
SPAC1952.17c	tbc13	GTPase activating protein, involved in vesicle-mediated transport (predicted)	0.007
SPAC29A4.03c	**mrps9**	mitochondrial ribosomal protein subunit Mrps9 (predicted)	0.008
SPCC622.16c	epe1	Jmjc domain chromatin associated protein Epe1	0.009
SPBC119.17	**cym1**	**mitochondrial metalloendopeptidase (predicted)**	**0.010**
SPBC25B2.11	pof2	F-box protein Pof2	0.010
SPBC577.02	rpl3801	60S ribosomal protein L38 (predicted)	0.011
SPBC725.07	pex5	peroxisomal targeting signal receptor Pex5 (predicted)	0.011
SPBC337.05c	**cct8**	**chaperonin-containing T-complex theta subunit Cct8**	**0.011**
SPBC1734.15	rsc4	RSC complex subunit Rsc4	0.012
SPBC30D10.09c	0	ER membrane organization protein, HVA22/TB2/DP1 family protein	0.012
SPCC965.03	**vma8**	**V-type ATPase V1 subunit D (predicted)**	**0.012**
SPAC6F12.03c	fsv1	SNARE Fsv1	0.013
SPBC4C3.08	otg2	alpha-1,3-galactosyltransferase	0.014
SPCC338.13	**cog4**	**Golgi transport complex subunit Cog4 (predicted)**	**0.014**
SPBC1711.09c	0	SNARE associated Golgi protein (predicted)	0.015
SPBC1347.09	0	hexaprenyldihydroxybenzoate methyltransferase, Coq3 variant (predicted)	0.015
SPBC36.03c	mfs3	plasma membrane spermidine transmembrane transporter Mfs3	0.015
SPAC1952.06c	0	spliceosomal complex subunit (predicted)	0.016
SPAC8E11.04c	0	palmitoyl-(protein) hydrolase (predicted)	0.016
SPAC5H10.04	0	NADPH dehydrogenase, (Old yellow enzyme) involved in small alpha,beta-unsaturated carbonyl compounds (predicted)	0.017
SPAC1565.04c	ste4	adaptor protein Ste4	0.017
SPAC13G7.08c	**crb3**	**Rix1 complex WD repeat subunit Crb3**	**0.017**
SPAC823.04	**rrp36**	**rRNA processing protein Rrp36 (predicted)**	**0.017**
SPAC16A10.03c	0	ubiquitin-protein ligase E3 involved in vesicle docking Pep5/Vps11-like (predicted)	0.017
SPAC23A1.20	new11	Schizosaccharomyces specific protein New11	0.017
SPAC4F10.04	ypa1	protein phosphatase type 2A regulator, PTPA family Ypa1	0.017
SPAC1952.03	otu2	ubiquitin specific cysteine protease, OTU family, Otu2	0.017
SPAC22E12.02	**0**	**splicing factor, WW domain -binding Rbm42 (predicted)**	**0.017**

SPBC30B4.08	eri1	double-strand siRNA ribonuclease Eri1	0.017
SPBC19C2.11c	**mdm34**	**ERMES complex subunit Mdm34 (predicted)**	**0.017**
SPBC18E5.03c	**sim4**	**CENP-K ortholog Sim4**	**0.017**
SPCC757.10	**vph2**	**endoplasmic reticulum membrane protein involved in assembly of the V-ATPase (predicted)**	**0.017**
SPCC11E10.08	rik1	CLRC ubiquitin ligase complex WD repeat protein Rik1	0.017
SPCC4F11.03c	0	Schizosaccharomyces specific protein	0.017
SPCC1183.01	**sec15**	**exocyst complex subunit Sec15**	**0.019**
SPAC1782.05	ypa2	protein phosphatase type 2A regulator, PTPA family Ypa2	0.019
SPBC15D4.10c	amo1	nuclear rim protein Amo1	0.019
SPCC1393.07c	mug4	Schizosaccharomyces specific protein, DNAJ domain	0.019
SPBC4C3.05c	**nuc1**	**DNA-directed RNA polymerase I complex large subunit Nuc1**	**0.020**
SPBC1198.03c	0	DUF4646 family conserved fungal protein	0.020
SPCC18.13	trm82	tRNA (guanine-N7-)-methyltransferase WD repeat subunit Trm82 (predicted)	0.020
SPBC18E5.10	0	mitochondrial iron-sulfur cluster protein (predicted)	0.020
SPBC146.10	mug57	cell surface fasciclin domain protein, implicated in adhesion Mug57	0.020
SPAC57A10.07	0	conserved membrane protein with Rossmann-like alpha/beta/alpha sandwich fold, conserved in fungi and protozoa	0.021
SPAC19B12.05c	**fcp1**	**CTD phosphatase Fcp1**	**0.021**
SPBC16C6.01c	0	lysine methyltransferase, human SETD6 ortholog (predicted)	0.021
SPCC1223.04c	set11	ribosomal protein lysine methyltransferase Set11	0.021
SPBC2F12.02c	**mrpl7**	**mitochondrial ribosomal protein subunit L7 (predicted)**	**0.021**
SPCC1620.12c	0	GTPase activating protein (predicted)	0.021
SPAC3G6.05	0	mitochondrial Mpv17/PMP22 family protein 1 (predicted)	0.022
SPBC336.10c	tif512	translation elongation and termination factor eIF5A (predicted)	0.022
SPAC25B8.06c	**dia4**	**mitochondrial serine-tRNA ligase (predicted)**	**0.022**
SPAC29E6.04	**nnf1**	**NMS complex subunit Nnf1**	**0.022**
SPBP23A10.12	frg1	FRG1 family protein, involved in mRNA splicing (predicted)	0.022
SPBC23G7.06c	nvj2	nucleus-vacuole junction protein Nvj2	0.022
SPBC21C3.02c	dep1	Sds3-like family protein Dep1	0.022
SPBC16A3.07c	nrm1	MBF complex corepressor Nrm1	0.022
SPCC622.19	jmj4	peptidyl-lysine 3-dioxygenase activity jmj4 (predicted)	0.022
SPCC1753.04	**tol1**	**3'(2'),5'-bisphosphate nucleotidase/inositol-1,4- bisphosphate 1-phosphatase**	**0.022**
SPCC1223.02	nmt1	4-amino-5-hydroxymethyl-2-methylpyrimidine phosphate synthase Nmt1	0.022
SPCC1739.07	**cti1**	**exosome C1D family subunit Cti1**	**0.022**
SPBC2G5.07c	**rpc25**	**DNA-directed RNA polymerase III complex subunit Rpc25**	**0.022**
SPAC31A2.15c	dcc1	Ctf18 RFC-like complex subunit Dcc1	0.023
SPAC16C9.03	**nmd3**	**export adaptor Nmd3 (predicted)**	**0.023**
SPAC6F6.05	**ost2**	**oligosaccharyltransferase epsilon subunit Ost2 (predicted)**	**0.023**
SPBP23A10.15c	**qcr1**	**mitochondrial processing peptidase (MPP) complex beta subunit Mas1 (predicted)**	**0.023**
SPBC1289.07c	**rpc40**	**DNA-directed RNA polymerase I and III subunit Rpc40**	**0.023**

SPCP31B10.04		0	DUF4448 family conserved fungal membrane protein, similar to cell surface proteins	0.023
SPBC16D10.04c	**dna2**		**DNA replication endonuclease-helicase Dna2**	**0.024**
SPAC823.13c	she9		mitochondrial inner membrane protein She9 (predicted)	0.025
SPBC12C2.12c	glo1		glyoxalase I	0.025
SPCC162.03		0	short chain dehydrogenase (predicted)	0.025
SPCC126.06	twf1		twinfilin (predicted)	0.025
SPAC2F3.01	imt1		mannosyltransferase Imt1	0.026
SPAC25B8.09		0	trans-aconitate 3-methyltransferase (predicted)	0.026
SPAC24H6.02c	tim15		TIM23 translocase complex subunit Tim15 (predicted)	0.027
SPBC18E5.05c	elp5		elongator complex subunit Elp5 (predicted)	0.027
SPAC20H4.01	**utp5**		**U3 snoRNP-associated protein Utp5 (predicted)**	**0.028**
SPBC713.03	dld2		mitochondrial D-lactate dehydrogenase, cytochrome Dld2 (predicted)	0.029
SPAC6C3.08	nas6		proteasome assembly chaperone, gankyrin	0.030
SPAC6G9.05	pcd1		coenzyme A diphosphatase (predicted)	0.030
SPBC1734.08	hse1		STAM like protein Hse1	0.030
SPCC1393.05	ers1		RNA-silencing factor Ers1	0.030
SPCC18.19c	ost5		oligosaccharyltransferase complex zeta subunit Ost5 (predicted)	0.030
SPAC15F9.01c	glm1		Glomulin, ubiquitin-protein transferase inhibitor Glm1 (predicted)	0.030
SPAC12B10.04	pby1		tubulin-tyrosine ligase Pby1 (predicted)	0.030
SPAC869.04		0	formamidase-like protein, implicated in cellular detoxification (predicted)	0.030
SPBC1198.08	dug1		dipeptidase Dug1 (predicted)	0.030
SPBC646.14c	**orc5**		**origin recognition complex subunit Orc5**	**0.030**
SPBC1215.01	shy1		cytochrome c oxidase assembly protein Shy1 (predicted)	0.030
SPBC15C4.01c	oca3		TPR repeat protein Oca3/ ER membrane protein complex Ecm2 (predicted)	0.030
SPCC5E4.10c		0	human leukocyte receptor 1 ortholog	0.030
SPAC664.08c	**bfr2**		**traub family protein involved in ribosome biogenesis (predicted)**	**0.030**
SPAC21E11.05c	cyp8		cyclophilin family peptidyl-prolyl cis-trans isomerase Cyp8	0.030
SPAC27D7.03c	mei2		RNA-binding protein involved in meiosis Mei2	0.030
SPBC337.06c	**cwf15**		**Prp19 complex subunit Cwf15**	**0.030**
SPCC126.02c	pku70		Ku domain protein Pku70	0.030
SPCC970.01	rad16		DNA repair endonuclease XPF	0.031
SPCC4B3.01	tum1		thiosulfate sulfurtransferase, involved in tRNA wobble position thiolation Tum1 (predicted)	0.031
SPAC23H4.12	alp13		MRG family Clr6 histone deacetylase complex subunit Alp13	0.031
SPBC776.03		0	homoserine dehydrogenase (predicted)	0.031
SPCC1442.11c		0	Schizosaccharomyces pombe specific protein	0.031
SPAC1834.05	alg9		mannosyltransferase complex subunit Alg9 (predicted)	0.032
SPAC1093.04c	**cca1**		**CTP 3'-tRNA nucleotidyltransferase Cca1**	**0.032**
SPAC22E12.06c	gmh3		alpha-1,2-galactosyltransferase Gmh3	0.032
SPBC1604.06c	**noc4**		**CBF/Mak21 family Noc4 (predicted)**	**0.032**

SPAC1952.11c	ure2	nickel-dependent urease Ure2	0.032
SPAC2F7.14c	rrp4	exosome subunit Rrp4	0.033
SPAC57A10.12c	ura3	mitochondrial dihydroorotate dehydrogenase Ura3	0.033
SPAC17A5.12	ucp7	UBA/TPR/DNAJ domain protein Ucp7	0.033
SPAPB1A10.16	dpc13	mitochondrial conserved protein Dpc13 (predicted)	0.033
SPAC1556.07	pmm1	phosphomannomutase Pmm1	0.033
SPBC337.13c	gtr1	Gtr1/RagA G protein Gtr1	0.033
SPBC27B12.01c	mmm1	ERMES complex subunit Mmm1 (predicted)	0.033
SPBC8D2.12c	tac1	mitochondrial Cox1 translational activator Tac1 (predicted)	0.033
SPBC1347.05c	0	DNAJ domain protein Scj1 (predicted)	0.033
SPCC569.08c	ade5	phosphoribosylglycinamide formyltransferase	0.033
SPAC12G12.02	efg1	rRNA processing protein Efg1 (predicted)	0.033
SPAC1486.02c	dsc2	Golgi Dsc E3 ligase complex subunit Dsc2	0.033
SPCC1795.03	gms1	Golgi UDP-galactose transmembrane transporter Gms1	0.033
SPAC4F8.05c	mrpl28	mitochondrial ribosomal protein subunit L28 (predicted)	0.033
SPAC2E1P5.04c	cwg2	geranylgeranyltransferase I beta subunit Cwg2	0.033
SPAC17C9.14	pex19	Pex19 protein (predicted)	0.033
SPBC1709.14	ngl1	peptide N-glycanase Ngl1	0.033
SPBC36.11	0	Schizosaccharomyces specific protein	0.034
SPBC15C4.04c	0	amino acid transmembrane transporter (predicted)	0.034
SPAC22G7.05	kri1	ribosome biogenesis protein Kri1 (predicted)	0.034
SPAC21E11.04	aca1	L-azetidine-2-carboxylic acid acetyltransferase Aca1	0.034
SPCC1020.03	mmt1	mitochondrial iron ion transmembrane transporter Mmt1 (predicted)	0.034
SPCC188.11	prp45	Prp19 complex subunit Prp45	0.034
SPCC1442.01	ste6	guanyl-nucleotide exchange factor Ste6	0.034
SPCC74.09	mug24	RNA-binding protein, rrm type	0.034
SPCC1672.04c	cox19	mitochondrial copper chaperone for cytochrome c oxidase Cox19 (predicted)	0.034
SPCC645.03c	isa1	mitochondrial [4Fe-4S] cluster asssembly and transfer protein Isa1	0.035
SPAC823.16c	atg1802	autophagy associated WD repeat protein Atg18b	0.035
SPCC74.01	sly1	SNARE binding protein Sly1 (predicted)	0.036
SPAC959.04c	omh6	alpha-1,2-mannosyltransferase Omh6 (predicted)	0.036
SPCC584.03c	0	GTPase regulator (predicted)	0.036
SPAC4F8.11	sea2	SEA complex WD repeat subunit Sea2 (predicted)	0.036
SPAC652.01	0	BC10 family small membrane protein, unknown biological role, human BLCAP ortholog	0.036
SPAC26A3.02	myh1	adenine DNA glycosylase Myh1	0.036
SPAC16E8.10c	rsm7	mitochondrial ribosomal protein subunit S7, Rsm7(predicted)	0.036
SPBC428.08c	clr4	histone lysine H3 methyltransferase Clr4	0.036
SPBC25H2.18	cox20	cytochrome c oxidase assembly protein Cox20 (predicted)	0.036
SPCC663.14c	trp663	plasma membrane TRP-like ion channel (predicted)	0.036

SPAC25B8.04c	mss51	mitochondrial Cox1 translation regulator Mss51 (predicted)	0.037
SPAC458.03	**tel2**	**Tel2/Rad-5/Clk-2 family protein Tel2**	**0.037**
SPBC1773.13	0	aromatic aminotransferase (predicted)	0.037
SPBC1734.16c	**pst3**	SIN3 family co-repressor Pst3	0.037
SPCC736.11	ago1	argonaute	0.037
SPCC576.14	dph5	diphthine synthase Dph5 (predicted)	0.037
SPAC23C11.13c	hpt1	guanine/xanthine/hypoxanthine phosphoribosyltransferase Hpt1	0.037
SPAC3F10.03	**grs1**	**mitochondrial and cytoplasmic glycine-tRNA ligase Grs1**	**0.038**
SPCC1739.06c	met1	uroporphyrin methyltransferase Met1	0.038
SPAC20G4.01	caf16	CCR4-Not complex subunit Caf16 (predicted)	0.039
SPBC29B5.01	atf1	transcription factor, Atf-CREB family Atf1	0.039
SPBC9B6.06	**mrpl10**	**mitochondrial ribosomal protein subunit L15 (predicted)**	**0.039**
SPBP4H10.18c	0	Schizosaccharomyces specific protein	0.039
SPAC222.15	meu13	Tat binding protein 1(TBP-1)-interacting protein (TBPIP) homolog (predicted)	0.039
SPAC105.03c	0	transcription factor (predicted)	0.039
SPAC328.02	dbl4	ubiquitin-protein ligase E3 involved in sporulation Dbl4	0.039
SPAC4F10.10c	**mnn9**	**mannosyltransferase complex subunit, Anp family Mnn9 (predicted)**	**0.039**
SPAC4F10.14c	btf3	nascent polypeptide-associated complex beta subunit	0.039
SPAC186.08c	0	L-lactate dehydrogenase (predicted)	0.039
SPBC428.20c	**alp6**	**gamma tubulin complex Spc98/GCP3 subunit Alp6**	**0.039**
SPBP35G2.06c	nup131	nucleoporin, WD repeat Nup131	0.039
SPBC29A3.03c	gid2	GID complex ubiquitin-protein ligase E3 subunit Gid2/Rmd5 (predicted)	0.039
SPBC29A3.10c	atp14	F1-FO ATP synthase subunit H (predicted)	0.039
SPBC1711.08	aha1	chaperone activator Aha1	0.039
SPBC11C11.05	**0**	**cell wall 1,6-beta-glucan biosynthesis protein, KRE9 family (predicted)**	**0.039**
SPBPB2B2.01	0	amino acid transmembrane transporter (predicted)	0.039
SPCC31H12.06	mug111	major facilitator family transmembrane transporter Mug111 (predicted)	0.039
SPCP1E11.10	dhm1	ankyrin repeat protein, unknown biological role	0.039
SPCC4F11.02	ptc1	MAP kinase threonine phosphatase Ptc1	0.039
SPAC144.06	apl5	AP-3 adaptor complex subunit Apl5 (predicted)	0.039
SPBC359.01	0	amino acid transmembrane transporter (predicted)	0.040
SPBC651.03c	gyp10	GTPase activating protein Gyp10	0.040
SPCC18.17c	0	proteasome assembly chaperone (predicted)	0.041
SPBC119.12	rud3	Golgi matrix protein Rud3 (predicted)	0.041
SPBC1778.03c	0	NADH pyrophosphatase (predicted)	0.041
SPBC725.16	**res1**	**MBF transcription factor complex subunit Res1**	**0.041**
SPAC31G5.06	**rrg8**	**mitochondrial conserved fungal protein Rrg8 (predicted)**	**0.042**
SPAC17G6.13	slt1	Schizosaccharomyces specific protein Slt1	0.042
SPAC19G12.13c	poz1	shelterin complex subunit Poz1	0.042

SPAC1952.01	gab1	Pig-U, Gab1 (predicted)	0.042
SPBC651.07	0	Schizosaccharomyces specific protein	0.042
SPBC30B4.06c	ips1	mitochondrial GIDA family tRNA uridine 5-carboxymethylaminomethyl modification enzyme Ips1 (predicted)	0.042
SPAC6C3.04	cit1	citrate synthase Cit1	0.042
SPBC83.15	**wdr74**	**ribosome assembly factor, WD repeat protein Nsa1/Wdr74 (predicted)**	**0.042**
SPAC2F3.16	0	ubiquitin-protein ligase E3, implicated in DNA repair (predicted)	0.042
SPAC890.02c	alp7	TACC protein Alp7	0.043
SPAC869.03c	0	plasma membrane urea transmembrane transporter (predicted)	0.044
SPBC713.09	0	Schizosaccharomyces specific protein	0.044
SPCC1442.07c	wss2	ubiquitin/metalloprotease fusion protein Udp7	0.044
SPBC1734.09	yea4	ER UDP-N-acetylglucosamine transmembrane transporter (predicted)	0.044
SPBC32H8.09	wdr8	mitosis-specific spindle pole body WD repeat protein Wdr8	0.044
SPBC23G7.08c	rga7	RhoGAP, GTPase activating protein Rga7	0.044
SPCC18.09c	hnt3	aprataxin Hnt3	0.044
SPAC2G11.09	0	calcium ion transmembrane transporter (predicted)	0.044
SPAPB1E7.10	**rpc17**	**DNA-directed RNA polymerase III complex subunit Rpc17**	**0.044**
SPAC19D5.03	cid1	terminal uridylyltransferase Cid1	0.046
SPBC106.06	**cct4**	**chaperonin-containing T-complex delta subunit Cct4**	**0.046**
SPBC1347.08c	0	ribonuclease H2 complex subunit (predicted)	0.046
SPAC12B10.09	pet801	mitochondrial carrier, S-adenosylmethionine (predicted)	0.046
SPAC11H11.01	sst6	ESCRT I complex subunit Vps23	0.046
SPBC29A3.09c	gcn20	AAA family ATPase Gcn20 (predicted)	0.046
SPBC19G7.04	0	HMG box protein	0.046
SPBC1778.10c	ppk21	serine/threonine protein kinase Ppk21 (predicted)	0.046
SPBC21.03c	0	EVE domain (PUA-related) protein, implicated in tRNA metabolism (possible RNA binding domain associated with tRNA methyltransferases)	0.046
SPBC3B9.09	vps36	ESCRT II complex subunit Vps36	0.046
SPAC24C9.05c	mug70	CBS and PB1 domain protein, conserved in fungi and plants, implicated in signalling Mug70	0.046
SPBC887.18c	hfi1	SAGA complex subunit Hfi1/Ada1	0.046
SPAC1486.07c	**mrpl19**	**mitochondrial ribosomal protein subunit L19 (predicted)**	**0.046**
SPAC17C9.02c	**lys7**	**alpha-aminoadipate reductase phosphopantetheinyl transferase Lys7**	**0.046**
SPAC20G8.10c	atg6	autophagy associated beclin family protein Atg6	0.046
SPAC11H11.03c	0	ATP-dependent polydeoxyribonucleotide 5'-hydroxyl-kinase activity implicated in DNA repair (predicted)	0.046
SPAC3G6.06c	rad2	FEN-1 endonuclease Rad2	0.046
SPBC19F8.03c	yap18	ENTH/VHS domain protein (predicted)	0.046
SPCC777.08c	bit61	Protor homolog, Bit61	0.046
SPBC16C6.10	chp2	heterochromatin (HP1) family chromodomain protein Chp2	0.047
SPAC27F1.05c	0	aminotransferase class-III, unknown specificty	0.047
SPBC342.04	rpn1301	19S proteasome regulatory subunit Rpn13a	0.047

SPAC1F3.10c	43739	mitochondrial intermediate peptidase Oct1 (predicted)	0.047
SPAC3F10.05c	mug113	GIY-YIGT nuclease superfamily protein	0.047
SPCC285.03	**dbp6**	**ATP-dependent RNA helicase Dbp6 (predicted)**	**0.047**
SPAC8C9.05	dtd1	D-Tyr-tRNA deacylase Dtd1 (predicted)	0.047
SPAC11H11.04	mam2	pheromone p-factor receptor	0.047
SPAC16E8.15	**tif45**	**translation initiation factor eIF4E, 4F complex subunit**	**0.047**
SPAC29A4.08c	**prp19**	**Prp19 complex subunit, ubiquitin-protein ligase E4 Prp19**	**0.047**
SPBC31E1.02c	pmr1	plasma membrane P-type ATPase, calcium transporting Pmr1	0.047
SPBC20F10.02c	0	DUF1741 family protein, human C10orf76 ortholog	0.047
SPBC56F2.10c	alg5	dolichyl-phosphate beta-glucosyltransferase Alg5	0.047
SPBC14F5.01	0	DUF4504 family protein, human C1orf74 ortholog	0.047
SPAC6G9.02c	**nop9**	**pumilio family RNA-binding protein Nop9 (predicted)**	**0.048**
SPAC6B12.03c	bit2	HbrB family protein involved in TOR signaling Bit2 (predicted)	0.048
SPAC8F11.08c	0	ER membrane associated esterase/lipase (predicted)	0.049
SPAC589.11	pth4	mitochondrial translation release factor	0.049
SPAC22F8.10c	**sap145**	**U2 snRNP-associated protein Sap145**	**0.049**
SPAC1250.02	mug95	Schizosaccharomyces specific protein Mug95	0.049
SPBC18E5.11c	edc3	enhancer of mRNA decapping Edc3	0.049
SPBC12D12.09	rev7	DNA polymerase zeta Rev7 (predicted)	0.049
SPBC13G1.13	tfb2	transcription factor TFIIH complex subunit Tfb2	0.049
SPBC3B9.06c	atg3	autophagy associated protein Atg3	0.049
SPAC23H4.18c	**rbx1**	**SCF complex, Cul4-RING and CLRC ubiquitin ligase ligase E3 subunit Rbx1**	**0.049**
SPAC19B12.10	sst2	human AMSH/STAMBP protein homolog, ubiquitin specific-protease	0.049
SPBC16E9.07	mug100	Schizosaccharomyces pombe specific protein Mug100	0.049
SPAC11E3.09	pyp3	protein-tyrosine phosphatase Pyp3	0.049
SPBC16A3.13	meu7	alpha-amylase homolog Aah4	0.049
SPCC16A11.03c	0	DUF2009 family protein, conserved in yeast and apicomplexa	0.049
SPAC1687.13c	csn5	COP9/signalosome complex protease subunit Csn5	0.049
SPBC29A10.11c	vps902	guanyl-nucleotide exchange factor, CUE domain absent Vps902	0.050
SPAC6F6.11c	0	pyridoxine-pyridoxal-pyridoxamine kinase (predicted)	0.050
SPAC4F8.03	sdo1	SBDS family ribosome assembly protein Sdo1 (predicted)	0.050
SPAC144.14	klp8	kinesin-like protein Klp8	0.050
SPBC56F2.02	rpl1901	60S ribosomal protein L19	0.050
SPAC17G6.04c	cpp1	protein farnesyltransferase beta subunit Cpp1	0.050

TABLE 2.2. GO analysis of significantly enriched genes within the Hermes PEV screen.

GO biological process complete	Genes passing filter	Genes p<0.05	Expected	Fold Enrichment	P-value
chromatin silencing at telomere (GO:0006348)	18	6	1.25	4.78	3.57E-03
negative regulation of chromatin organization (GO:1905268)	18	6	1.25	4.78	3.57E-03
chromatin silencing at centromere (GO:0030702)	41	9	2.86	3.15	4.33E-03
chromatin silencing by small RNA (GO:0031048)	28	7	1.95	3.59	6.37E-03
gene silencing by RNA (GO:0031047)	29	7	2.02	3.46	7.47E-03
negative regulation of histone H3-K4 methylation (GO:0051572)	4	3	0.28	10.77	7.85E-03
negative regulation of histone methylation (GO:0031061)	4	3	0.28	10.77	7.85E-03
removal of RNA primer involved in mitotic DNA replication (GO:1903469)	4	3	0.28	10.77	7.85E-03
protein N-linked glycosylation (GO:0006487)	48	9	3.34	2.69	1.04E-02
regulation of histone H3-K9 methylation (GO:0051570)	10	4	0.7	5.74	1.05E-02
DNA replication, removal of RNA primer (GO:0043137)	5	3	0.35	8.61	1.20E-02
membrane docking (GO:0022406)	41	8	2.86	2.8	1.27E-02
organelle localization by membrane tethering (GO:0140056)	41	8	2.86	2.8	1.27E-02
regulation of histone methylation (GO:0031060)	18	5	1.25	3.99	1.44E-02
negative regulation of histone modification (GO:0031057)	6	3	0.42	7.18	1.71E-02
protein processing involved in protein targeting to mitochondrion (GO:0006627)	6	3	0.42	7.18	1.71E-02
regulation of mitotic cell cycle phase transition (GO:1901990)	150	3	10.45	0.29	1.77E-02
chromatin silencing at silent mating-type cassette (GO:0030466)	27	6	1.88	3.19	1.80E-02
regulation of cell cycle process (GO:0010564)	227	7	15.81	0.44	2.00E-02
lactate metabolic process (GO:0006089)	7	3	0.49	6.15	2.33E-02
regulation of cell cycle (GO:0051726)	245	8	17.07	0.47	2.44E-02
regulation of chromatin organization (GO:1902275)	47	8	3.27	2.44	2.45E-02
negative regulation of chromosome organization (GO:2001251)	48	8	3.34	2.39	2.70E-02
regulation of histone modification (GO:0031056)	22	5	1.53	3.26	2.79E-02
glycoprotein metabolic process (GO:0009100)	65	10	4.53	2.21	2.84E-02
cellular protein metabolic process (GO:0044267)	787	70	54.82	1.28	2.90E-02
mitochondrial protein processing (GO:0034982)	8	3	0.56	5.38	3.05E-02
telomere localization (GO:0034397)	15	4	1.04	3.83	3.13E-02
mitochondrial translation (GO:0032543)	67	10	4.67	2.14	3.16E-02
cleavage involved in rRNA processing (GO:0000469)	23	5	1.6	3.12	3.22E-02
regulation of cell cycle phase transition (GO:1901987)	154	4	10.73	0.37	3.25E-02

negative regulation of cell cycle process (GO:0010948)	114	2	7.94	0.25	3.31E-02
donor selection (GO:0007535)	3	2	0.21	9.57	3.71E-02
positive regulation of histone H3-K9 methylation (GO:0051574)	3	2	0.21	9.57	3.71E-02
positive regulation of histone methylation (GO:0031062)	3	2	0.21	9.57	3.71E-02
proteasome regulatory particle assembly (GO:0070682)	3	2	0.21	9.57	3.71E-02
regulation of gene silencing by RNA (GO:0060966)	3	2	0.21	9.57	3.71E-02
mitochondrion-endoplasmic reticulum membrane tethering (GO:1990456)	9	3	0.63	4.78	3.87E-02
pheromone-dependent signal transduction involved in conjugation with cellular fusion (GO:0000750)	9	3	0.63	4.78	3.87E-02
mating type switching (GO:0007533)	17	4	1.18	3.38	4.37E-02
protein transport to vacuole involved in ubiquitin-dependent protein catabolic process via the multivesicular body sorting pathway (GO:0043328)	17	4	1.18	3.38	4.37E-02
cell division (GO:0051301)	87	1	6.06	0.16	4.44E-02
protein metabolic process (GO:0019538)	814	71	56.71	1.25	4.47E-02
cellular protein modification process (GO:0006464)	476	45	33.16	1.36	4.50E-02
protein modification process (GO:0036211)	476	45	33.16	1.36	4.50E-02
glycosylation (GO:0070085)	62	9	4.32	2.08	4.72E-02
macromolecule glycosylation (GO:0043413)	62	9	4.32	2.08	4.72E-02
protein glycosylation (GO:0006486)	62	9	4.32	2.08	4.72E-02
regulation of histone H3-K4 methylation (GO:0051569)	10	3	0.7	4.31	4.80E-02
regulation of translational elongation (GO:0006448)	10	3	0.7	4.31	4.80E-02
vesicle docking involved in exocytosis (GO:0006904)	10	3	0.7	4.31	4.80E-02
glycoprotein biosynthetic process (GO:0009101)	63	9	4.39	2.05	4.98E-02

TABLE 2.3. Genes targeted for CRISPR-Cas9 mediated mutagenesis. Genes are listed with their corresponding coding sequence cleavage site position(s) and the gRNA sequence used for targeting/construction of their respective sgRNA expressing plasmid.

Gene	Cleavage site (CDS nucleotide position)	gRNA sequence
rik1	nt 32	TCATTCCTTCTGGGCAACGG
dcr1	nt 917	GAAGCAGTTGTCAGATGACG
dcr1	nt 1696	CAATACCAACCTGAAAGACA
dcr1	nt 3619	TCAATTTCAAACCAGAACCA
top3	nt 60	TCGGTAGCAAGCATTCTAGG
top3	nt 208	CTCCAACTAGAATATTCAGA
top2	nt 1000	ACATGTTCATAAATTACCCT
top2	nt 1163	TATAGATGAAGTCGTCAAGA
top2	nt 1610	AGGAAAACTACTGAATGTAC
top2	nt 1755	ATGACAGATCAAGATCATGA
top2	nt 1805	CCTATCATTAAGTGCACTCG
top2	nt 1869	TTGCAAAAGAGAAGGATACG
tel2	nt 49	TTAAGGATTTCTTTTAAACG
tel2	nt 788	TGTTATACGATCATCTCTTG
tel2	nt 2294	ATATGTTGACGTTTTAAATG

TABLE 2.4. Strains used in this study

Strain ID	Genotype	Used for
TV312	otr1R(SphI)::ade6+, ura4-DS/E, ade6-210, leu1-32	Used in Hermes PEV screen
ZB2116	otr1R(SphI)::ade6+, ade6-M210, ura4-D18, ?	CRISPR mutagenesis parent strain
DG14	otr1R(SphI)::ura4, ura4-DS/E, ade6-210, his7-366, leu1-32	Used to obtain diploids for transformation
DG21	otr1R(SphI)::ura4, ura4-DS/E, ade6-216, his7-366, leu1-32	Used to obtain diploids for transformation
FY18409	rqh1::kanMX6, leu1-32, ura4-D18	Used for rqh1 nat/kan marker swap to generate rqh1::natmx4 transforming fragment
ZB2124	otr1R(SphI)::ade6+, ade6-M210, ura4-D18, top2 1163-6 (K388Q)	CRISPR mutant
ZB2157	otr1R(SphI)::ade6+, ade6-M210, ura4-D18, top3 208 C1 (E70K)	CRISPR mutant
ZB2159	otr1R(SphI)::ade6+, ade6-M210, ura4-D18, top3 208 t1 (S69del)	CRISPR mutant
ZB2162	otr1R(SphI)::ade6+, ade6-M210, ura4-D18, top3 208 s (E70Y71->D70 conversion)	CRISPR mutant
ZB2163	otr1R(SphI)::ade6+, ade6-M210, ura4-D18, tel2 2294 a1 (N765E766->K765 conversion)	CRISPR mutant
ZB2518	rqh1::natmx4, leu1-32, ura4-D18	used to amplify rqh::nat transforming fragment for transformation into top3::Hermes diploids
ZB2140	dcr1-1696 (dcr565 fs), ura4-D18, otr1R(SphI)::ade6+, ade6-M210	CRISPR mutant
ZB2601	otr1R(SphI)::ura4, ura4-DS/E, ade6-(210 or 216), his7-366, leu1-32. top3::hermes kanMX ins1, rqh::nat (1)	Double KO, analyzed by qPCR
ZB2602	otr1R(SphI)::ura4, ura4-DS/E, ade6-(210 or 216), his7-366, leu1-32. top3::hermes kanMX ins1, rqh::nat (3)	Double KO, analyzed by qPCR
ZB2603	otr1R(SphI)::ura4, ura4-DS/E, ade6-(210 or 216), his7-366, leu1-32. top3::hermes kanMX ins1, rqh::nat (5)	Double KO, analyzed by qPCR
ZB2713	otr1R(SphI)::ura4, ura4-DS/E, ade6-(210 or 216), his7-366, leu1-32. top3::hermes kanMX ins2, rqh::nat ©	Double KO, analyzed by qPCR
ZB2714	otr1R(SphI)::ura4, ura4-DS/E, ade6-(210 or 216), his7-366, leu1-32. top3::hermes kanMX ins2, rqh::nat (H)	Double KO, analyzed by qPCR
ZB2715	otr1R(SphI)::ura4, ura4-DS/E, ade6-(210 or 216), his7-366, leu1-32. top3::hermes kanMX ins2, rqh::nat (D)	Double KO, analyzed by qPCR
ZB2716	otr1R(SphI)::ura4, ura4-DS/E, ade6-(210 or 216), his7-366, leu1-32. top3::hermes kanMX ins2, rqh::nat €	Double KO, analyzed by qPCR
ZB2742	leu1-32 ura4-D18 T2R1-4137::ura4+ top2 1163-6 (K388Q) ade6-? otr-?	CRISPR mutant with subtelomeric reporter, used in spotting assay (not shown)
ZB2743	leu1-32 ura4-D18 T2R1-30292::ura4+ top2 1163-6 (K388Q) ade6-? otr-?	CRISPR mutant with subtelomeric reporter, used in spotting assay (not shown)
ZB2744	leu1-32 ura4-D18 T2R1-4137::ura4+ top3 208 C1 (E70K) ade6-? otr-?	CRISPR mutant with subtelomeric reporter, used in spotting assay (not shown)
ZB2745	leu1-32 ura4-D18 T2R1-7921::ura4+ top3 208 C1 (E70K) ade6-? otr-?	CRISPR mutant with subtelomeric reporter, used in spotting assay (not shown)
ZB2746	leu1-32 ura4-D18 T2R1-4137::ura4+ top3 208 t1 (S69del) ade6-? otr-?	CRISPR mutant with subtelomeric reporter, used in spotting assay (not shown)
ZB2747	leu1-32 ura4-D18 T2R1-4137::ura4+ top3 208 t1 (S69del) ade6-? otr-?	CRISPR mutant with subtelomeric reporter, used in spotting assay (not shown)
ZB2748	leu1-32 ura4-D18 T2R1-30292::ura4+ top3 208 t1 (S69del) ade6-? otr-?	CRISPR mutant with subtelomeric reporter, used in spotting assay (not shown)
ZB2749	leu1-32 ura4-D18 T2R1-4137::ura4+ top3 208 s (E70Y71->D70 conversion) ade6-? otr-?	CRISPR mutant with subtelomeric reporter, used in spotting assay (not shown)
ZB2750	leu1-32 ura4-D18 T2R1-4137::ura4+ top3 208 s (E70Y71->D70 conversion) ade6-? otr-?	CRISPR mutant with subtelomeric reporter, used in spotting assay (not shown)
ZB2751	leu1-32 ura4-D18 T2R1-4137::ura4+ top3 208 s (E70Y71->D70 conversion) ade6-? otr-?	CRISPR mutant with subtelomeric reporter, used in spotting assay (not shown)
ZB2752	leu1-32 ura4-D18 T2R1-7921::ura4+ top3 208 s (E70Y71->D70 conversion) ade6-? otr-?	CRISPR mutant with subtelomeric reporter, used in spotting assay (not shown)
ZB2753	leu1-32 ura4-D18 T2R1-7921::ura4+ top3 208 s (E70Y71->D70	CRISPR mutant with subtelomeric reporter, used

	conversion) ade6-? otr-?	in spotting assay (not shown)
ZB2754	leu1-32 ura4-D18 T2R1-30292::ura4+ top3 208 s (E70Y71->D70 conversion) ade6-? otr-?	CRISPR mutant with subtelomeric reporter, used in spotting assay (not shown)
ZB2755	leu1-32 ura4-D18 T2R1-4137::ura4+ tel2 2294 a1 (N765E766->K765 conversion) ade6-? otr-?	CRISPR mutant with subtelomeric reporter, used in spotting assay (not shown)
ZB2756	leu1-32 ura4-D18 T2R1-7921::ura4+ tel2 2294 a1 (N765E766->K765 conversion) ade6-? otr-?	CRISPR mutant with subtelomeric reporter, used in spotting assay (not shown)
ZB2757	leu1-32 ura4-D18 T2R1-7921::ura4+ tel2 2294 a1 (N765E766->K765 conversion) ade6-? otr-?	CRISPR mutant with subtelomeric reporter, used in spotting assay (not shown)
zb2575	leu1-32? ura4-D18 T2R1-4137::ura4+ (#2)	subtelomeric reporter control strain, used in spotting assay (not shown)
zb2577	leu1-32 ura4-D18 T2R1-7921::ura4+ (#1)	subtelomeric reporter control strain, used in spotting assay (not shown)
zb2579	leu1-32 ura4-D18 T2R1-30292::ura4+ (#3)	subtelomeric reporter control strain, used in spotting assay (not shown)
zb2521	otr1R(SphI)::ade6+, ade6-M210, ura4-D18, top3 208 C1 (E70K), rqh1::kanmx6 (#2)	Double KO, analyzed by qPCR
zb2522	otr1R(SphI)::ade6+, ade6-M210, ura4-D18, top3 208 C1 (E70K), rqh1::kanmx6 (#3)	Double KO, analyzed by qPCR
zb2523	otr1R(SphI)::ade6+, ade6-M210, ura4-D18,top3 208 t1 (S69del), rqh1::kanmx6 (#1)	Double KO, analyzed by qPCR
zb2524	otr1R(SphI)::ade6+, ade6-M210, ura4-D18, top3 208 t1 (S69del), rqh1::kanmx6 (#2)	Double KO, analyzed by qPCR
zb2525	otr1R(SphI)::ade6+, ade6-M210, ura4-D18, top3 208 s (E70Y71->D70 conversion), rqh1::kanmx6 (#1)	Double KO, analyzed by qPCR
zb2526	otr1R(SphI)::ade6+, ade6-M210, ura4-D18, top3 208 s (E70Y71->D70 conversion), rqh1::kanmx6 (#2)	Double KO, analyzed by qPCR
zb2527	otr1R(SphI)::ade6+, ade6-M210, ura4-D18, tel2 2294 a1 (N765E766->K765 conversion), rqh1::kanmx6 (#1)	Double KO, analyzed by qPCR
zb2528	otr1R(SphI)::ade6+, ade6-M210, ura4-D18, tel2 2294 a1 (N765E766->K765 conversion), rqh1::kanmx6 (#2)	Double KO, analyzed by qPCR
zb2529	otr1R(SphI)::ade6+, ade6-M210, ura4-D18, rqh1::kanMX6 (#1)	Rqh1 KO control, analyzed by qPCR

TABLE 2.5. Oligonucleotides used in this study

Primer ID	Primer name	Sequence	Used for
om1567	CFp75ura4R	CATCTGGTGTGTACAAAATTG	used to amplify CF CRISPR gRNA backbone
top2 1000	top2 1000	ATAGTTGCTGTTGCCAAAAAACATAACCTGTACCGAAGAAACATGTTCATAAATTACCCTgttttagagctagaaatagcaag	Used to amplify sgRNA fragment for CRISPR-Cas9 mutagenesis
top2 1163	top2 1163	ATAGTTGCTGTTGCCAAAAAACATAACCTGTACCGAAGAATATAGATGAAGTCGTCAAGAgttttagagctagaaatagcaag	Used to amplify sgRNA fragment for CRISPR-Cas9 mutagenesis
top2 1610	top2 1610	ATAGTTGCTGTTGCCAAAAAACATAACCTGTACCGAAGAAAGGAAAACTACTGAATGTACgttttagagctagaaatagcaag	Used to amplify sgRNA fragment for CRISPR-Cas9 mutagenesis
top2 1755	top2 1755	ATAGTTGCTGTTGCCAAAAAACATAACCTGTACCGAAGAAATGACAGATCAAGATCATGAgttttagagctagaaatagcaag	Used to amplify sgRNA fragment for CRISPR-Cas9 mutagenesis
top2 1869	top2 1869	ATAGTTGCTGTTGCCAAAAAACATAACCTGTACCGAAGAACCTATCATTAAGTGCACTCGgttttagagctagaaatagcaag	Used to amplify sgRNA fragment for CRISPR-Cas9 mutagenesis
top2 1805	top2 1805	ATAGTTGCTGTTGCCAAAAAACATAACCTGTACCGAAGAATTGCAAAAGAGAAGGATACGgttttagagctagaaatagcaag	Used to amplify sgRNA fragment for CRISPR-Cas9 mutagenesis
tel2 49	tel2 49	ATAGTTGCTGTTGCCAAAAAACATAACCTGTACCGAAGAATTAAGGATTTCTTTTAAACGgttttagagctagaaatagcaag	Used to amplify sgRNA fragment for CRISPR-Cas9 mutagenesis
tel2 788	tel2 788	ATAGTTGCTGTTGCCAAAAAACATAACCTGTACCGAAGAATGTTATACGATCATCTCTTGgttttagagctagaaatagcaag	Used to amplify sgRNA fragment for CRISPR-Cas9 mutagenesis
tel2 2294	tel2 2294	ATAGTTGCTGTTGCCAAAAAACATAACCTGTACCGAAGAAATATGTTGACGTTTTAAATGgttttagagctagaaatagcaag	Used to amplify sgRNA fragment for CRISPR-Cas9 mutagenesis
tel2 968	tel2 968	ATAGTTGCTGTTGCCAAAAAACATAACCTGTACCGAAGAAAAAGGAGCTAGAAAAAACAGgttttagagctagaaatagcaag	Used to amplify sgRNA fragment for CRISPR-Cas9 mutagenesis
tel2 2310	tel2 2310	ATAGTTGCTGTTGCCAAAAAACATAACCTGTACCGAAGAACTGGAGTGTCTGATCGAAGTgttttagagctagaaatagcaag	Used to amplify sgRNA fragment for CRISPR-Cas9 mutagenesis
tel2 848	tel2 848	ATAGTTGCTGTTGCCAAAAAACATAACCTGTACCGAAGAAAATTAATCGAAGGAAGTGAGgttttagagctagaaatagcaag	Used to amplify sgRNA fragment for CRISPR-Cas9 mutagenesis
top3 208	top3 208	ATAGTTGCTGTTGCCAAAAAACATAACCTGTACCGAAGAACTCCAACTAGAATATTCAGAgttttagagctagaaatagcaag	Used to amplify sgRNA fragment for CRISPR-Cas9 mutagenesis
top3 60	top3 60	ATAGTTGCTGTTGCCAAAAAACATAACCTGTACCGAAGAATCGGTAGCAAGCATTCTAGGgttttagagctagaaatagcaag	Used to amplify sgRNA fragment for CRISPR-Cas9 mutagenesis
rik1 32	rik1 32	ATAGTTGCTGTTGCCAAAAAACATAACCTGTACCGAAGAATCATTCCTTCTGGGCAACGGgttttagagctagaaatagcaag	Used to amplify sgRNA fragment for CRISPR-Cas9 mutagenesis
dcr1 917	dcr1 917	ATAGTTGCTGTTGCCAAAAAACATAACCTGTACCGAAGAAGAAGCAGTTGTCAGATGACGgttttagagctagaaatagcaag	Used to amplify sgRNA fragment for CRISPR-Cas9 mutagenesis
dcr1 1696	dcr1 1696	ATAGTTGCTGTTGCCAAAAAACATAACCTGTACCGAAGAACAATACCAACCTGAAAGACAgttttagagctagaaatagcaag	Used to amplify sgRNA fragment for CRISPR-Cas9 mutagenesis
dcr1 3619	dcr1 3619	ATAGTTGCTGTTGCCAAAAAACATAACCTGTACCGAAGAATCAATTTCAAACCAGAACCAgttttagagctagaaatagcaag	Used to amplify sgRNA fragment for CRISPR-Cas9 mutagenesis
om1807	top2 f nt905	acctgaacaatgaacgcatc	used to amplify top2 coding sequence for genotyping by Sanger sequencing
om1808	top2 r nt1922	TTCCAGTATTCGTACTCGGG	used to amplify top2 coding sequence for genotyping by Sanger sequencing
om1809	tel2 f 5utr -50	ATCCACCGAAGGTTACTGTC	used to amplify tel2 coding sequence for genotyping by Sanger sequencing
om1810	tel2 r 1102	TGGAGAACATTAGGGATTTGGA	used to amplify tel2 coding sequence for genotyping by Sanger sequencing
om1811	tel2 f 1918	CACGATCAGTTTTATTCACCCA	used to amplify tel2 coding sequence for genotyping by Sanger sequencing
om1812	tel2 r 2573	AAAGGAGCTGAGTCATCCAG	used to amplify tel2 coding sequence for genotyping by Sanger sequencing
om1813	top3 f 5utr	GACCTTAACACCTTACACGC	used to amplify top3 coding sequence for genotyping by Sanger sequencing
om1814	top3 r	GAAGTCTGCTCGGATAACCT	used to amplify top3 coding sequence for genotyping by Sanger sequencing
om2061	rqh1 F	aatttgtaagtcgcgcagtc	used to amplify Rqh1 KO frag
om2063	rqh1 R	ggagaccaaacaatgcatggac	used to amplify Rqh1 KO frag

oM988	p33_F_qPCR	tatcctgcgtctcggtatcc	used to amplify dg repeats (qPCR)
oM989	p33_R_qPCR	ctgttcgtgaatgctgagaaag	used to amplify dg repeats (qPCR)
oM984	p30_F_qPCR	ccatatcaatttcccatgttcc	used to amplify dh repeats (qPCR)
oM985	p30_R_qPCR	catcaagcgagtcgagatga	used to amplify dh repeats (qPCR)
oM4	act1qPCRF	TGCACCTGCCTTTTATGTTG	used to amplify actin (qPCR)
oM5	act1qPCRR	TGGGAACAGTGTGGGTAACA	used to amplify actin (qPCR)
om1946	hermes TIR R new	cag aga act tca aca agc ca	used to amplify Hermes TIR/KanMX6 for Gibson assembly
om1947	hermes TIR L new	caa caa caa gtg gct tat ttt	used to amplify Hermes TIR/KanMX6 for Gibson assembly
om1948	top2 ins1 USF F	CGAGGTTTCGATGGAGCAAACT	used to amplify *top2* CDS homology fragment for generation of *top2::Hermes ins1* transforming fragment by Gibson assembly
om1949	top2 ins1 USF R	AAAATAAGCCACTTGTTGTTGGTCTTAAATTAGCAGTTATATCC	used to amplify *top2* CDS homology fragment for generation of *top2::Hermes ins1* transforming fragment by Gibson assembly
om1950	top2 ins1 DSF F	TGGCTTGTTGAAGTTCTCTGTTTAAGACATATGCTTAATGGCGAGCCTTTG	used to amplify *top2* CDS homology fragment for generation of *top2::Hermes ins1* transforming fragment by Gibson assembly
om1951	top2 ins1 DSF R	CGTTGCTTGAGTACGCGACAGTT	used to amplify *top2* CDS homology fragment for generation of *top2::Hermes ins1* transforming fragment by Gibson assembly
om1952	top2 ins2 USF F	AACTTGGTATGACAATATGTC	used to amplify *top2* CDS homology fragment for generation of *top2::Hermes ins2* transforming fragment by Gibson assembly
om1953	top2 ins2 USF R	AAAATAAGCCACTTGTTGTTGGTCATTAACATGTTCATAAATTACCCTAGGAGG	used to amplify *top2* CDS homology fragment for generation of *top2::Hermes ins2* transforming fragment by Gibson assembly
om1954	top2 ins2 DSF F	TGGCTTGTTGAAGTTCTCTGTTAATGACCGTTGGGACGTGGCCTTTGCTGTTTC	used to amplify *top2* CDS homology fragment for generation of *top2::Hermes ins2* transforming fragment by Gibson assembly
om1955	top2 ins2 DSF R	ACCTCCTCCACTACAGAAGAT	used to amplify *top2* CDS homology fragment for generation of *top2::Hermes ins2* transforming fragment by Gibson assembly
om1956	top3 ins1 USF F	ATGCGCGTCCTATGTGTTGC	used to amplify *top3* CDS homology fragment for generation of *top3::Hermes ins1* transforming fragment by Gibson assembly
om1957	top3 ins1 USF R	TGGCTTGTTGAAGTTCTCTGCTGTTAAGTGACCGGATACAGAAGTCATTG	used to amplify *top3* CDS homology fragment for generation of *top3::Hermes ins1* transforming fragment by Gibson assembly
om1958	top3 ins1 DSF F	AAAATAAGCCACTTGTTGTTGCTTAACAGAAGCTTCTTTTCCTTCTGAA	used to amplify *top3* CDS homology fragment for generation of *top3::Hermes ins1* transforming fragment by Gibson assembly
om1959	top3 ins1 DSF R	TATAACTTACGACCGTTCCA	used to amplify *top3* CDS homology fragment for generation of *top3::Hermes ins1* transforming fragment by Gibson assembly
om1960	top3 ins2 USF F	ACCGACCAATTTGACTCTTC	used to amplify *top3* CDS homology fragment for generation of *top3::Hermes ins2* transforming fragment by Gibson assembly
om1961	top3 ins2 USF R	TGGCTTGTTGAAGTTCTCTGCTTCCATTTTAACCTGCACCAACGTTTCGGCT	used to amplify *top3* CDS homology fragment for generation of *top3::Hermes ins2* transforming fragment by Gibson assembly
om1962	top3 ins2 DSF F	AAAATAAGCCACTTGTTGTTGAATGGAAGAAGAGCTTTTTTCTAAAAAGG	used to amplify *top3* CDS homology fragment for generation of *top3::Hermes ins2* transforming fragment by Gibson assembly
om1963	top3 ins2 DSF R	ACAAATTCAGTTACACCTTGGC	used to amplify *top3* CDS homology fragment for generation of *top3::Hermes ins2* transforming fragment by Gibson assembly
om1968	top2 ins1 USF	gaattcggagctcggtacccatcgccgaggtttcgatggagcaaact	used to introduce plasmid backbone

	F GA		homology for Gibson assembly of *top2::Hermes ins1* transforming fragment
om1969	top2 ins1 DSF R GA	gactctagaggatccccgatccgttgcttgagtacgcgacagtt	used to introduce plasmid backbone homology for Gibson assembly of *top2::Hermes ins1* transforming fragment
om1970	top2 ins2 USF F GA	gaattcgagctcggtacccatcgcaacttggtatgacaatatgtc	used to introduce plasmid backbone homology for Gibson assembly of *top2::Hermes ins2* transforming fragment
om1971	top2 ins2 DSF R GA	gactctagaggatccccgatcacctcctccactacagaagat	used to introduce plasmid backbone homology for Gibson assembly of *top2::Hermes ins2* transforming fragment
om1972	top3 ins1 USF F GA	gaattcgagctcggtacccatcgcatgcgcgtcctatgtgttgc	used to introduce plasmid backbone homology for Gibson assembly of *top3::Hermes ins1* transforming fragment
om1973	top3 ins1 DSF R GA	gactctagaggatccccgatctataacttacgaccgttcca	used to introduce plasmid backbone homology for Gibson assembly of *top3::Hermes ins1* transforming fragment
om1974	top3 ins2 USF F GA	gaattcgagctcggtacccatcgcaccgaccaatttgactcttc	used to introduce plasmid backbone homology for Gibson assembly of *top3::Hermes ins2* transforming fragment
om1975	top3 ins2 DSF R GA	gactctagaggatccccgatcacaaattcagttacaccttggc	used to introduce plasmid backbone homology for Gibson assembly of *top3::Hermes ins2* transforming fragment
om2089	rDNA_18S_qPCR F	ccctgcattgttatttcttg	used to amplify 18S rDNA repeats (qPCR)
om2090	rDNA_18S_qPCR R	tcaactttcgatggtaggat	used to amplify 18S rDNA repeats (qPCR)
om1567	CFp75ura4R	CATCTGGTGTGTACAAAATTG	used to amplify CF CRISPR gRNA backbone
oM894	ura4#3	CGAGGATTTCGACCAGGATA	used to amplify ura4 (qPCR)
oM895	ura4#4	GAGACCACGTCCCAAAGGTA	used to amplify ura4 (qPCR)
	p7bc1LinkV2	CAAGCAGAAGACGGCATACGAGATATCACGGTAATACGACTCACTATAGGGC	Hermes library prep linker
	p7bc8LinkV2	CAAGCAGAAGACGGCATACGAGATACTTGAGTAATACGACTCACTATAGGGC	Hermes library prep linker
	p7bc10LinkV2	CAAGCAGAAGACGGCATACGAGATTAGCTTGTAATACGACTCACTATAGGGC	Hermes library prep linker
	p7bc11LinkV2	CAAGCAGAAGACGGCATACGAGATGGCTACGTAATACGACTCACTATAGGGC	Hermes library prep linker
	HERbc05	AATGATACGGCGACCACCGAGATCTACACTCTTTCCCTACACGACGCTCTTCCGATCTACAGTGCTATGTGGCTTACGTTTGCCTG	Hermes library prep barcode primer
	HERbc06	AATGATACGGCGACCACCGAGATCTACACTCTTTCCCTACACGACGCTCTTCCGATCTGCCAATCTATGTGGCTTACGTTTGCCTG	Hermes library prep barcode primer
	HERbc12	AATGATACGGCGACCACCGAGATCTACACTCTTTCCCTACACGACGCTCTTCCGATCTCTTGTACTATGTGGCTTACGTTTGCCTG	Hermes library prep barcode primer
	HERbc09	AATGATACGGCGACCACCGAGATCTACACTCTTTCCCTACACGACGCTCTTCCGATCTGATCAGCTATGTGGCTTACGTTTGCCTG	Hermes library prep barcode primer

TABLE 2.6. Plasmids used in this study

Plasmid ID		Used for
pMZ241	pHL2578	Hermes transposase-expressing plasmid
pMZ242	pHL2577	Hermes transposon donor plasmid
pMZ639	pDB4280	Cloning-free CRISPR ura4 plasmid (linearize to generate backbone)
pMZ641	pDB4282	Cloning-free CRISPR ura4 plasmid (linearize to generate fragment for sgRNA amplification)
pmz771	top2::hermes ins1	Contains assembled top2::Hermes ins1 transformation fragment
pmz773	top2::hermes ins2	Contains assembled top2::Hermes ins2 transformation fragment
pmz774	top3::hermes ins1	Contains assembled top3::Hermes ins1 transformation fragment
pmz777	top3::hermes ins2	Contains assembled top3::Hermes ins2 transformation fragment
pMZ160	pTfURA4	XhoI digested to remove insert; backbone used in Gibson Assembly of Hermes transforming fragments
pMZ54	p4339	Digested w/ EcoRI to generate nat fragment for nat/kan marker swap in FY18409

CHAPTER III: INVESTIGATION OF VARIABLES AFFECTING TF2 TRANSPOSABLE ELEMENT INTEGRATION IN *S. POMBE*

3.1 Introduction

Transposable elements, also known as "jumping genes", are mobile genetic elements which possess the ability to "jump" or mobilize and integrate into discrete locations throughout host genomes. Eukaryotic transposable elements are divided into two classes depending on whether their mobilization occurs via a transcribed RNA intermediate that is subsequently reverse-transcribed into cDNA and then inserted, thereby creating a new copy of the transposon (Class I retroelements, also referred to as retrotransposons) or a DNA intermediate that is excised followed by insertion into a new locus (Class II transposable elements) (Wessler, 2006). Many transposable elements exhibit distinct integration targeting preferences; some of the best-described examples include the targeting of Ty1 and Ty3 upstream of RNA Pol III-transcribed promoters, the preference of Ty5 for heterochromatic regions, and the sequence specificity of ZAM retroelements in *Drosophila*. (Brodeur, Sandmeyer, & Olson, 1983; Faye et al., 2008; Guo & Levin, 2010; Zou et al., 1996). In many instances, such as those described above, the targeting preferences exhibited by transposons are mediated by their accompanying integrase protein, which facilitates target site selection, tethering, and integration (Gai & Voytas, 1998; Sultana et al., 2017; Xie et al., 2001).

Previously, our lab has shown that Tf1 retrotransposon integration in fission yeast is guided by an interaction between Tf1 integrase and the host DNA binding protein Sap1 and that this targeting depends on Sap1's efficiency as a replication fork barrier (Jacobs et al., 2015). The fission yeast *Schizosaccharomyces pombe* is colonized by the Tf family

of retrotransposons which includes Tf1 and closely related Tf2 elements. Laboratory

strains *of S. pombe* contain 13 full-length Tf2 elements while Tf1 transposons can be

found in some wild yeast isolates (Esnault & Levin, 2015). There is a high degree of

sequence similarity between Tf1 and Tf2; while their respective Gag sequences are

divergent, the coding sequence for reverse transcriptase (RT) and integrase (IN) are

nearly identical. Despite their apparent sequence similarity, Tf1 and Tf2 have

significantly different mobilization efficiencies and integration modalities (Esnault &

Levin, 2015; Weaver, Shpakovski, Caputo, Levin, & Boeke, 1993). Tf1 predominantly

mobilizes via an integrase-dependent mechanism while Tf2 mobilizes by homologous

recombination (HR) with pre-existing full-length Tf2 elements independent of integrase

approximately 70% of the time (Hoff et al., 1998). Despite the marked difference in

mobilization efficiency and preference, domain swapping experiments have revealed that

Tf2 integrase retains full activity (Esnault & Levin, 2015).

Due to the high degree of similarity between Tf1 and Tf2 integrase, we generated

a yeast strain in which all 13 Tf2 elements have been removed using CRISPR-Cas9

facilitated inter-LTR recombination (hereafter referred to as Tf-0) to test whether Tf2

integrase could compensate in the absence of full length transposable elements via

integrase-mediated transposition. We also set out to characterize the integration site

preference of Tf2 integrase, since standard methods for integration site analysis such as

high throughput sequencing of *de novo* insertions are technically challenging due to the

transposable element's propensity for mobilization via HR. We found that Tf2 integration

site preference is remarkably divergent from Tf1; while *de novo* Tf2 integrations show a

bias towards gene promoters and H2A.z-enriched regions similar to Tf1, Sap1 binding

has no predictive value in determining the location of Tf2 insertions. Despite this uncoupling, Sap1's RFB activity is still required for efficient Tf2 mobilization by HR. In this work we explore several possible mechanisms behind this requirement, including the possibility that Sap1's RFB activity may lead to generation of fragile sites at Tf2 elements by forcing replication-transcription collisions. Interestingly, we find that loss of Sap1's RFB activity stabilizes heterochromatin at Tf2 elements, which may in turn influence the recombinogenicity of these regions.

3.2 Materials and Methods

Strains

Strains used in this study are listed in Table 3.1.

Mobilization assays

The mobilization assays were performed as previously described (Hoff et al., 1998) with some modification. Plasmids carrying either a full-length Tf2 transposon (pHL1631), a Tf2 transposon with a frameshift in the Gag coding sequence (Tf2 Gag FS, pHL1632), or a Tf2 transposon with a frameshift affecting the Integrase coding sequence (Tf2 IN FS, pHL1633) under the control of an *nmt1* promoter were independently transformed into each strain to be tested and plated on EMMG+DO-URA+15 uM B1 to select for successful plasmid transformation. For each time point (4 and 6 day induction periods) two transformants from each strain and plasmid combination were patched onto EMMG+DO-URA+15 uM B1 as independent biological replicates and incubated for 2 days at 32° C before replica plating onto non-repressive plates (EMMG+DO-URA). After the appropriate induction period patches were replica plated onto YEA+ 1g/L FOA

to select against Tf2-expressing plasmids and incubated for an additional two days at 32°

C. To quantify Tf2 mobilization frequency each patch was scraped off of the YEA+FOA

counterselective plates and resuspended in 1 mL of water. 100 uL of each crude cell

suspension was removed and added to 900 uL of sterile water in a spectrophotometer

cuvette to measure the optical density at 595 nm (OD_{600}). The adjusted optical density

was then used to calculate the volume of cells required to prepare a 1 mL cell suspension

with an OD_{600} of 0.8. The cell suspension at OD_{600} 0.8 was then diluted five fold by

removing 300 uL and transferring it to a fresh 2 mL eppendorf tube with 1.2 mL of sterile

water for a final OD_{600} of 0.16. The diluted (OD_{600} .16) cell suspension was then further

diluted 200X by adding 7.5 uL of the OD_{600} .16 cell suspension to 1492.5 uL of sterile

water in a 2 mL eppendorf tube. 1 mL of the OD_{600} .16 cell suspension was plated on 4

YEA+FOA plates supplemented with 200 mg/L G418 (KSE Scientific) while 1 mL of the

corresponding 200 mL dilution was plated on 4 YEA plates (250 uL per plate) to quantify

the number of viable colony forming units in each suspension. All strains were incubated

at 32° C for approximately 2.5 days with the exception of *sap1-c* containing strains. Due

to the delayed growth phenotype exhibited by *sap1-c* mutants, all *sap1-c* containing

strains were incubated for 4 days at 32° C to allow for an approximately equivalent

generation time as their wild type counterparts. To quantify the mobilization frequency in

each genetic background the number of colonies which grew on selective

(YEA+FOA+G418) plates was counted for each strain replicate in addition to the number

of colonies which grew on the corresponding non-selective (YEA) plates. The percent

mobilization frequencies for each strain analyzed were obtained using the following

equation: [(# of FOA^{R}G418^R colonies) / (# of viable colonies on YEA x 200)]

RNA preparation, Reverse Transcription, and qPCR

5 mL yeast cultures were grown overnight, washed, and harvested. Bulk RNA was

isolated for reverse transcription and analysis using a Direct-Zol Miniprep RNA

purification kit (Zymo Research) or by hot acid phenol RNA extraction following the

protocol outlined in (Bahler & Wise, 2017). For RNA purifications performed using the

Direct-Zol Miniprep kit cell pellets were resuspended in 300 mL of the provided TRI

reagent and dispensed into 2 mL screw cap tubes with approximately 500 uL of glass

beads. Cells were lysed in TRI Reagent by bead beating (4 cycles of 2.5 minutes each

carried out at 4° C, followed by a 2 minute rest on ice in between cycles). The remaining

steps were carried out according to the manufacturer's instructions. Reverse transcription

was subsequently performed using SuperScript VILO Master Mix (Invitrogen) according

to the manufacturer's instructions. qPCR reactions were set up using KAPA SYBR FAST

qPCR Master Mix (2x) according to the manufacturer's instructions and run on a

Mastercycler ep realplex Real-time PCR System (Eppendorf) for analysis. Cell cycle Tf2

expression was analyzed as described in the Cell Cycle Analysis of Tf2 Expression

Methods section; plasmid Tf2 expression levels were quantified by extracting RNA from

all plasmid-transformed strains in media lacking thiamine to induce Tf2 expression prior

to RNA extraction, cDNA preparation, and quantification of plasmid Tf2 expression

levels by using primers directed against the *neo* cassette (om175,176) to ensure

specificity for plasmid-expressed *Tf2* and normalizing to *act1* (om4,5).

ChIP-qPCR

Chromatin immunoprecipitation was performed as previously described with some modifications (H. P. W. Cam, Simon, 2016). 100 mL of cells were grown overnight at 32° C to an OD_{600} of .5-.8 and fixed with freshly prepared 1% formaldehyde for 10 minutes. Cells were lysed by bead beating in lysis buffer (4 cycles of 2.5 minutes each carried out at 4° C, followed by a 2 minute rest on ice in between cycles). Immunoprecipitations were carried out with approximately 15-25 ug of input chromatin in a total reaction volume of 250 ul with 2 ug of ChIP Grade Anti-Histone H3 (di methyl K9) antibody (ab1220, Abcam) or 1.8 ug of Recombinant Biotinylated H3K9me3 Antibody (C15500003, Diagenode) with 2 IP replicates per strain/antibody combination. Chromatin from each strain was prepared, solubilized, and pooled prior to splitting the corresponding sample from each strain in half for subsequent H3K9me2 and H3K9me3 immunoprecipitation performed in parallel. from The H3K9me3 ChIPs were performed using a modified protocol according to the manufacturer's recommendations; briefly, 73 uL of M-280 Streptavidin Dynabeads (Invitrogen) per ChIP reaction were prepared by washing with TBS/BSA before addition of 1.8 ug of H3K9me3 antibody diluted in 100 uL of TBS/BSA, followed by a 1 hour long incubation at 4° C to allow for antibody-bead binding. The antibody-conjugated beads were subsequently blocked by washing twice with 200 uL of 5 uM biotin to prevent binding of endogenous biotinylated proteins to the beads before proceeding with immunoprecipitation. Antibody incubation and washing steps were all carried out in Eppendorf Protein LoBind microcentrifuge tubes; after elution of cross-linked chromatin from Dynabeads Protein G (Invitrogen) or Dynabeads M-280 Streptavidin (Invitrogen), reverse cross-linking and all subsequent steps were carried out using Eppendorf DNA LoBind microcentrifuge tubes.

After immunoprecipitation, samples were analyzed by qPCR as described in the previous

section. Fold enrichment was determined by calculating target region enrichment relative

to a mock ChIP reaction in which no antibody was added and normalizing to *act1*

enrichment (H3K9me2 ChIP-qPCR) or enrichment relative to a mock ChIP reaction in

which a biotinylated anti-IgG antibody (provided as part of a set with the anti-H3K9me3

antibody) was added as a negative control before normalizing to *act1* enrichment

(H3K9me3 ChIP-qPCR).

Generation of ectopic promoter-RFB modified Tf2-3 *strains*

Fragments carrying the desired *Tf2-3* modifications were prepared by Gibson assembly.

Upstream and downstream homology fragments were generated by amplifying flanking

DNA directly from the parent strain ZB1923. Several kilobases of DNA are missing from

ZB1923 as a result of inter-LTR recombination in the process of generating the final Tf-0

strain, and so upstream sequence was taken from the sequence immediately adjacent to

the breakpoint of the Tf2 LTR involved in the recombination event while downstream

sequence was amplified from the *Tf2-3* CDS. The eno1 promoter fragment was

generated by amplification from plasmid pMZ371 ; Ter2 S and AS sequences were

introduced by generating primers incorporating the desired sequence; and the natMX4

cassette was amplified from pMZ371 in the presence of 5% DMSO . After plasmids

containing the desired sequences for transformation were prepared and verified by Sanger

sequencing, the assembled fragment was amplified in its entirety from each plasmid as a

complete transforming fragment (including target site homology and a selectable

marker), gel purified, and transformed into ZB1923 by electroporation. Transformants

were selected by plating electroporated cells on YEA for 24 hours before replica plating

to YEA supplemented with 200 ug/mL clonNAT (Werner BioAgents). The transforming

fragment was subsequently re-amplified from genomic DNA by colony PCR (Phire Plant

Direct PCR Master Mix, Thermo Scientific), gel extracted, and sent for Sanger

sequencing to confirm that all of the active sequences (*eno1* promoter, Ter2, Tf2 CDS)

were intact. A fragment was amplified across the breakpoint closest to the natMX4

cassette by colony PCR to further confirm integration in the correct genomic location. All

strains were subsequently transformed with pHL1633 (Tf2 IN FS) to assay

retrotransposition in each strain.

Colony PCR

Colony PCR was performed by preparing 10 uL colony PCR reactions using Phire Plant

Direct PCR Master Mix (Thermo Scientific) according to the manufacturer's instructions.

Genotyping Tf2 recombination events in wild type cells was performed by picking

colonies with a retrotransposition event and resuspending them in 20 uL of sterile water

and adding 1 uL of cell suspension to 9 uL of PCR master mix. 13 reactions were

prepared per colony; 12 reactions for Tf2 transposon genotyping using individual primers

specific to each of the 12 transposons and an internal primer directed against the spliced

neo junction within retrotransposed Tf2 and one reaction containing primers directed

against an external region as a PCR control. PCR reactions were subsequently amplified

in an ABI 2720 Thermal Cycler and the presence and location of Tf2 recombination

events were recorded. Genotyping *Tf2-3* recombination events in the ectopic promoter-

RFB retrotransposition assay was performed using a primer directed against the spliced

neo junction in retrotransposed Tf2 elements and a primer immediately downstream of

Tf2-3 to identify plasmid Tf2- *Tf2-3* recombination events. A pinhead-sized amount of

cells were removed from each colony and added directly into each PCR reaction prior to amplification on an ABI 2720 Thermal Cycler.

Library preparation of Tf2 insertions for high-throughput sequencing

Insertion libraries were prepared as previously described (Guo & Levin, 2010) with some modification. The mobilization assay plasmids expressing WT Tf2 and Tf2 IN FS were modified for preparation of Tf2 insertion libraries for high-throughput sequencing by addition of a unique tag of substituted nucleotides in the U5 sequence of Tf2 and introduction of a SpeI site to prohibit PCR amplification of the internal transposon sequence, as outlined in (Guo & Levin, 2010). Plasmids compatible with high-throughput sequencing library preparation were generated by Gibson assembly of a ~700 bp synthesized gene fragment (Invitrogen) for introduction of the desired modifications and a fragment obtained by amplifying the entirety of the WT Tf2 or Tf2 IN FS mobilization assay plasmids with the exclusion of the region to be replaced by the synthesized gene fragment. The modified plasmids were then transformed into the desired yeast strains by electroporation and plated on EMMG+DO-URA+15 uM B1 to select for transformants while maintaining plasmid Tf2 repression.

Twenty-eight plates containing 16 independent patches were prepared for each replicate/strain by patching transformants onto EMMG+DO-URA + 15 uM B1 and incubating for 2 days at 32° C followed by a 4 day induction period on EMMG+DO-URA. After the transposition period all plates were scraped and the cells obtained were resuspended in liquid YEA+ 1g/L FOA+15 uM B1 to a starting OD_{600} of .25 and grown to an OD of 6.0 to select against Tf2-expressing plasmids. Cells were then passaged to

YEA+FOA+G418+B1 at a starting density of .5 and incubated at 32° C before reaching a final OD_{600} of 8.0 to select for cells carrying de novo Tf2 integrations. The final cultures were harvested followed by extraction of genomic DNA by potassium acetate precipitation and phenol-chloroform extraction (J. M. Murray, Watson, & Carr, 2016). Illumina MiSeq samples were prepared as previously described (Guo & Levin, 2010); briefly, genomic DNA was digested with MseI (NEB) overnight followed by column purification to obtain digested genomic DNA. Linker oligonucleotides were annealed and ligated to MseI-digested DNA (T4 DNA Ligase, Invitrogen) followed by an additional column purification step. The purified ligation reaction products were then digested with SpeI (NEB) overnight followed by PCR amplification of the SpeI-cut product (Titanium Taq DNA Polymerase, Clontech) using primers om538 and the desired barcoding primer (bc02 [om544] or bc07 [om543]). Sequencing libraries were column purified and amplicons between 200-600 bp were isolated by Pippin Prep. Sequencing runs were subsequently performed on an Illumina miSeq (RUCDR).

Cell cycle analysis of Tf2 expression

Cell cycle analysis of Tf2 expression was conducted using strain DG704 which contains the temperature sensitive *cdc25-22* mutant, which at the restrictive temperature arrests the cell cycle in the G2-M transition. Cultures were grown overnight at permissive temperature (26° C) to a starting OD_{600} of .45 before shifting to the restrictive temperature (36° C) for 4.5 hours. G2 arrest was confirmed by microscopy prior to release at the permissive temperature (26° C). Samples were then taken every 15 minutes for ~2.5 hours with 10 mL of culture harvested, washed, and pelleted before resuspending in Trizol reagent for RNA extraction using the Direct-zol RNA Miniprep Purification Kit

(Zymo Research) as described in the RNA extraction Methods section. Several uL of cells were placed on a slide for analysis by microscopy after ethanol fixation; the proportion of septated cells was quantified and recorded for each time point. qRT-PCR was subsequently performed for relative quantification of Tf2 expression at all time points as described in the RNA Extraction, Reverse Transcription, and qPCR Methods section using primers directed against *Tf2* LTR (om16,17) or *Tf2* CDS (om18,19) and normalized to *act1* (om4,5).

S9.6 DNA-RNA Hybrid Immunoprecipitation (DRIP)

DRIP was performed as previously described, with some modification (Taneja et al.). Briefly, 100 mL cultures were grown at 32° C to an OD_{600} of .5-.8, washed, and harvested. Harvested cells were then speroplasted using Zymolyase 100T, pelleted, and resuspended in 1X TE supplemented with 1% SDS before incubation at 65 C for 10 minutes. All subsequent steps were conducted using Eppendorf DNA LoBind tubes. Chromatin was isolated by adding 350 uL of 5 M potassium acetate, incubating samples on ice for 5 minutes, and centrifuging the samples at 16k x g for 10 minutes at 4 C. Chromatin was then precipitated by addition of 490 uL isopropanol before centrifugation for 5 minutes at 16k x g for 5 minutes. Pelleted chromatin was washed with cold 70% ethanol before being resuspended in 20 uL of TE. All samples were treated with 2 ug of RnaseA for 30 minutes at 42 C followed by 100 ug of Proteinase K for 30 minutes at 65 C. DNA was subsequently purified by phenol chloroform extraction followed by ethanol precipitation in the presence of sodium acetate at -80 C. Purified DNA was then resuspended in TE and each sample was split in half, with one portion reserved for S9.6 experimental immunoprecipitation while the other half was retained as a negative control

after RnaseH treatment. All samples were digested with 50 U each of the restriction enzymes EcoRV, SalI, XhoI, BglII, and HincII in NEB Buffer 3.1 at 37° C overnight; each of the negative controls had an additional 3 uL of Thermostable RnaseH (NEB, M0523S) added simultaneously. After all digestions had gone to completion DNA was again purified by ethanol precipitation. 1 uL was reserved from each sample and diluted in 19 uL of TE as "input" DNA. All samples were subsequently immunoprecipitated with 6 ug of S9.6 antibody (Millipore, MABE1095) overnight at 4 C in 500 uL of binding buffer (10 mM Na2HPO4, 140 mM NaCl, 0.05% Triton X-100). Immunoprecipitated DNA was recovered by adding 20 uL of Protein A conjugated Dynabeads and incubating for 1 hour at 4 C. Protein A Dynabeads were subsequently washed 3 times with 1 mL of binding buffer and eluted in 50 uL of elution buffer (50 mM Tris HCl, pH 8, 10 mM EDTA, .5% SDS) at 65° C for 10 minutes. The supernatant was removed and transferred to fresh Eppendorf DNA LoBind tubes and the elution step was repeated once more before treating all samples with 100 ug of Proteinase K for 1 hour at 55° C. Immunoprecipitated DNA was purified by phenol-chloroform extraction followed by ethanol precipitation and samples were subsequently analyzed by qPCR.

3.3 Results

3.3.1 Tf2 mobilization is reduced in Tf-0

Tf2 transposable elements have previously been shown to mobilize via an integrase-independent mechanism reliant on host HR machinery approximately 70% of the time despite their similarity to Tf1 transposable elements which utilize integrase-mediated transposition (Esnault & Levin, 2015; Faye et al., 2008; Sehgal, Lee, &

Espenshade, 2007). Further, Tf2 have been observed to preferentially recombine with pre-existing transposable elements in a phenomenon known as integration site recycling (Esnault & Levin, 2015; Hoff et al., 1998; Sehgal et al., 2007). We set out to analyze whether the mobilization preferences and integration efficiency of Tf2 transposons are impacted by the absence of pre-existing full-length transposable elements as substrates for HR. We performed a series of retrotransposition assays to quantify bulk Tf2 mobilization events by transforming cells with a plasmid expressing a full-length Tf2 transposon under the control of the thiamine-repressible promoter nmt1 (as described in (Hoff et al., 1998; Mallet, Larochelle, & Bachand, 2017; Sehgal et al., 2007) (Figure 3.1a). In this system the sequence upstream of the 5' LTR transcription start site has been removed from the encoded transposon to ensure production of a functional in-frame Tf2 transcript; additionally, the transposable element carries an intron-containing neomycin resistance gene inserted into the 3' UTR of the transposon in the reverse orientation with respect to the Tf2 coding sequence. In this arrangement only those cells in which at least one transposition event has occurred will exhibit G418 resistance (Mallet et al., 2017; Sehgal et al., 2007). To quantify mobilization events the cells were plated on media lacking thiamine to allow for plasmid Tf2 expression throughout a defined induction period (4 or 6 days), and after counter-selecting against the Tf2 expressing plasmid at the conclusion of the induction period cells were plated on G418 and FOA containing media to select for cells in which a genomic transposition event had occurred. The same cell suspension was simultaneously plated on non-selective YEA media to normalize transposition events based on the number of viable colony forming units present. The transposition events which occurred in strains transformed with the WT Tf2-expressing

plasmid served as a baseline for retrotransposition frequency. Integrase-mediated transposition is precluded in Tf2 IN FS due to a frameshift in the integrase coding sequence, allowing for determination of the proportion of mobilization events which occur via HR with respect to overall retrotransposition rates given that endogenous Tf2 proteins are insufficient to complement plasmid-expressed Tf2 in *trans* (Hoff et al., 1998). The frameshift occurring in Gag in Tf2 Gag FS prevents production of a functional polyprotein, therefore reverse transcription and retrotransposition of plasmid-expressed Tf2 should be prohibited; as expected we were unable to recover any $FOA^R G418^R$ colonies from Tf2 Gag FS expressing strains indicating an absence of background colony growth. Tf2 Gag FS results are not shown here because they were all negative for retrotransposition; strains transformed with Tf2 Gag FS-expressing plasmid were included as a negative control.

Assaying Tf2 mobilization rates in the transposon-free strain Tf-0 revealed that gross mobilizations decreased in the absence of full-length Tf2 elements; after 4 and 6 days of plasmid Tf2 expression Tf-0 had 85% and 88% fewer insertions than its wild type counterpart, respectively (Figure 3.1b). The proportion of integrase-independent mobilizations which occurred in Tf-0, assessed by determining the ratio of Tf2 IN fs insertions to WT Tf2 insertions, was only slightly affected by the lack of full-length transposons as HR substrates (Day 4, .73 [PB1] and .60 [Tf-0]; Day 6, .86 and .49). These results suggest that even in the absence of full length transposable elements as HR substrates de novo Tf2 mobilizations still occur predominantly via an integrase-independent mechanism, albeit at a much lower frequency and with integrase-mediated transpositions comprising a slightly larger portion of all retroransposition events.

Tf2 elements have previously been demonstrated to preferentially recombine with pre-existing full-length genomic Tf2 transposons in a phenomenon known as integration site recycling (Hoff et al., 1998). Colonies with a wild type genetic background containing all 13 endogenous Tf2 elements with de novo WT Tf2 integrations were genotyped with primers directed against the spliced neo-AI junction (present within all newly mobilized transposable elements) and primers unique to the region immediately downstream of the 3' end of all 13 existing genomic Tf2 transposons to identify colonies bearing Tf2 integrase-independent insertions which were the products of HR between plasmid Tf2 cDNA and existing transposons. Consistent with previous studies 19/22 colonies tested positive for at least one genomic Tf2 recombination events, with the remainder presumably bearing the products of integrase-dependent mobilization into regions outside of existing Tf2 elements (data not shown). Given the abundance of solo LTRs throughout the genome, mobilizations via HR in Tf-0 are presumably the products of recombination with Tf2 LTRs given that they are the only remaining homologous genomic elements. The significantly reduced mobilization frequency in Tf-0 also suggests, however, that overall Tf2 LTRs are weak substrates for HR, possibly due to reduced sequence homology or the absence of another targeting feature associated with full length transposable elements.

3.3.2 Tf2 mobilization is reduced in sap1-c and becomes integrase-dependent

Sap1 is a DNA binding protein which serves as a polar replication fork barrier (RFB); Sap1 binds within the ribosomal DNA (rDNA) repeats where its polar RFB activity ensures replication proceeds only in the sense direction with respect to ribosomal RNA transcription to prevent mitotic recombination (Krings & Bastia, 2005; Mejía-

Ramírez, Sánchez-Gorostiaga, Krimer, Schvartzman, & Hernández, 2005; Noguchi &
Noguchi, 2007). Sap1 also binds to Tf1 and Tf2 LTRs where it exerts the opposite effect
by promoting regional instability (Zaratiegui, Vaughn, et al., 2011). Previous work from
our lab has shown that Sap1-dependent replication fork barriers guide Tf1 integrations
and that Sap1 interacts with Tf1 integrase to facilitate retrotransposition (Jacobs et al.,
2015). Given the significant degree of similarity between Tf1 and Tf2 elements we
wondered whether Tf2 exhibited a similar dependence on Sap1's replication fork barrier
activity, as their respective integrases are nearly identical at the sequence level yet they
exhibit significant differences in mobilization method and frequency. *sap1-c* is an allele
of Sap1 which retains the ability to bind DNA but loses its RFB activity, and so the
retrotransposition assay was performed in a *sap1-c* mutant background to assess whether
loss of Sap1's RFB activity affected Tf2 retrotransposition (Zaratiegui, Vaughn, et al.,
2011). Similar to Tf1 we saw a substantial reduction in Tf2 mobilizations in *sap1-c*, with
overall mobilizations decreasing by approximately 95% by both Day 4 and Day 6 in
sap1-c compared to the wild type strain (Figure 3.1b). There was also a complete loss of
mobilizations in the Tf2 IN FS strain, indicating that in the absence of Sap1's RFB
activity Tf2 mobilization reverted to an almost entirely integrase-dependent mechanism.
To rule out the possibility that retrotransposition rates may reflect transcriptional
differences in each strain we quantified plasmid Tf2 expression levels and found that
expression levels were fairly consistent between strains (Figure 3.1d). Together, these
results suggest that Sap1 RFB activity is necessary for Tf2 IN and HR mediated
mobilization.

3.3.3 High-throughput sequencing of de novo Tf2 mobilizations

High-throughput sequencing of de novo transposable element integrations has often been used to identify host factors influencing transposon integration site preference. Construction of sequencing libraries for de novo Tf2 integrations is technically challenging given its preference for recombination with pre-existing Tf2 elements, since these mobilization events grossly outnumber all other retrotransposition events. The lack of transposons in Tf-0 provides a unique opportunity to assess the de novo integration preferences of Tf2 in a "naïve" host lacking pre-existing transposons as recombination substrates. To this end the plasmids previously used in the Tf2 mobilization assays were modified to include a unique sequence for PCR amplification and construction of Tf2 insertion libraries based on the strategy developed previously by (Guo & Levin, 2010) for high-throughput sequencing of Tf1 integrations.

Analysis of de novo Tf2 integrations revealed some similarity to Tf1 integration site preferences. Like the related Tf1 transposon, Tf2 transposable elements show a slight bias towards insertion in gene promoters (Figure 3.2a). We noted that this preference also accounts for the observation that Tf2 insertions tend to occur in regions enriched for the histone variant H2Az (Figure 3.2b); when insertions which overlap with promoters are excluded from analysis, the apparent enrichment disappears (not shown). Tf1 insertions have been previously demonstrated to exhibit a strong bias for regions bound by the DNA binding protein Sap1, which physically interacts with Tf1 integrase to tether cDNA to integration sites (Hickey et al., 2015; Jacobs et al., 2015). We found that although Tf2 insertions were slightly enriched around Sap1 binding sites and exhibited the same periodicity characteristic of integrase-mediated Tf1 transpositions (Figure 3.2c), unlike Tf1 Sap1 binding was a poor predictor of Tf2 integration (Figure 3.2d). Therefore the

insertions which are targeted to Sap1 binding sites are presumably the products of integrase-mediated mobilizations, which overall make up only a very small portion of Tf2 transposition events. We analyzed the genomic sequences surrounding Tf2 integration sites (15 bp upstream and downstream of the point of insertion) to determine whether transposon integrations exhibited any sequence specificity, given that Tf2 elements preferentially mobilize via sequence-directed HR; however, we did not find any significantly enriched DNA motifs at insertion sites.

3.3.4 The homologous recombination pathway is preserved in sap1-c

The observation that Tf2 insertions decrease so dramatically in *sap1-c* and yet Sap1 binding has little predictive value for determining Tf2 integration presented a paradox, but also raised the possibility that the *sap1-c* allele may be associated with a more general defect in homologous recombination, as the transposable element is reliant on host HR machinery for integrase-independent mobilization via HR (Murton, Grady, Chan, Cam, & Whitehall, 2016; Sehgal et al., 2007). To assay the competence of DNA integration via HR in *sap1-c* and a wild type strain both were transformed with either a Tf2 fragment marked with *ura4* or a fragment containing the *leu1* coding sequence to alleviate the prototrophy for uracil and leucine present in both strains and provide a read-out for HR efficiency. In this arrangement the frequency of fragment integration via HR is not subject to other potentially limiting factors within the retrotransposon lifecycle, such as the presence of retrotransposon capsid protein which limits Tf2 integration levels relative to Tf1 due to sequence differences between the two transposon-encoded factors (Esnault & Levin, 2015). In an independent experiment all three strains were transformed with a ura4-marked plasmid, which confirmed that transformation efficiency was

comparable among all three strains (roughly 2 transformants per 200 ng of DNA per

10,000 colony forming units [CFUs]). In *sap1-c* the efficiency of *leu1-32* correction by

leu1 fragment was nearly 18 times higher than in wild type, while the efficiency of

Tf2::ura4 integration was approximately 30% lower but not entirely absent as in the

retrotransposition assay (Figure 3.1c). We concluded that the HR pathway is still present

and functional in both strains yet there appear to be site-specific differences in HR

efficiency between Tf2 elements and other genomic locations; proper retrotransposition

seems to further restrict and augment target site availability as substrates for integrase-

independent mobilization.

3.3.5 RNA-DNA hybrids (R loops) occur at Tf2 LTRs

Similar to Tf1, Tf2 elements exhibit a striking reliance on Sap1's RFB activity yet

in the case of the former it promotes integrase-dependent mobilization while it facilitates

retrotransposition through an integrase-independent pathway in the latter. This raised the

possibility that while Sap1 itself may not be sufficient to recruit Tf2 cDNA, its RFB

activity may create favorable conditions for Tf2 retransposition via HR; indeed,

replication fork barrier activity has been demonstrated to stimulate homologous

recombination in an effort to restart the stalled replication fork (B. Michel et al., 2001;

Osman & Whitby, 2009; Rothstein, Michel, & Gangloff, 2000). We also noted that

Sap1's polar RFB activity forces DNA replication to occur in the antisense direction with

respect to transcription through the Tf2 coding sequence (Figure 3.3a), in stark contrast to

Sap1's role in coordinating replication within the rDNA repeats and preventing head-on

collisions between the DNA replication and RNA transcription machineries, as these

collisions can often be deleterious to genome stability (Krings & Bastia, 2005; Mejía-

Ramírez et al., 2005). Replication-transcription collisions are also known to stimulate recombination and induce the formation of RNA-DNA hybrids known as R loops, which can act as further impediments to the replication fork or degenerate to recombinogenic double-strand breaks as a consequence of unpaired stretches of single-stranded DNA (Ponnari Gottipati et al., 2008; Sankar, Wastuwidyaningtyas, Dong, Lewis, & Wang, 2016; Skourti-Stathaki & Proudfoot, 2014). The endoribonuclease Dicer (Dcr1), a component of the core RNAi machinery, is also involved in promoting RNA Pol II release at sites of replication-transcription collisions independently of its role in RNAi-mediated silencing; Dicer localizes to Tf2 elements despite the absence of RNAi activity at Tf2 retrotransposons, suggesting its presence may be a consequence of its role in promoting the former (Castel et al., 2014; Hansen et al., 2005; Lorenz et al., 2012). Additionally, previous studies have found that the body of Tf2 elements is significantly enriched in Histone H2A phosphorylated at Serine 139, also known as gamma-H2A, a marker of replicative stress and DNA damage(Rozenzhak et al., 2010). We hypothesized that replicative stress occurring in the body of transposable elements may be the result of Sap1's polar RFB activity at the 5' end of the gene and DNA-replication transcription conflicts occurring within the gene body as a result; further, the presence of two stalled replication forks in close proximity to one another may lead to the generation of recombinogenic fragile sites within Tf2 elements.

To test this model, we first asked whether transcription and DNA replication occur contemporaneously. Cell-cycle analysis of Tf2 expression in cultures synchronized by *cdc25-22* G2 arrest revealed that transcription of Tf2 elements increases slightly during S phase, thus generating favorable conditions for such encounters to occur (Figure

3.3b). Our results agree with data obtained from expression microarray experiments performed on cultures synchronized by elutriation (Figure 3.3c) (Rustici et al., 2004).We then assayed whether we could detect RNA:DNA hybrids, the hallmark of replication-transcription collisions, at Tf2 LTRs in Tf-0. Using the S9.6 antibody which nonspecifically recognizes RNA-DNA hybrids for DNA-RNA immunoprecipitation we were able to detect low levels of R loops at Tf2 LTRs in Tf-0, which produce low levels of spurious abortive transcripts even in the absence of an associated coding sequence (Figure 3.3d). Since R loops are a naturally occurring part of the Tf2 retrotransposon life cycle during reverse transcription of Tf2 cDNA, assaying for their presence in the transposon free strain Tf-0 which lacks all sources of transposon-derived RT allowed us to pinpoint the R loop signal as originating from endogenous genomic Tf2 LTRs. The difference in signal between the wild type and Tf-0 strain, therefore, can be attributed to the loss of reverse transcription-derived R loop signal.

3.3.6 Generation of an ectopic promoter-RFB system

In the model proposed above, increasing transcription at Tf2 target sites should increase the occurrence of replication-transcription collisions thus generating a concomitant increase in Tf2 retrotransposition; conversely, loss of fork barrier activity should decrease retrotransposition events. To minimize the potential for off-target or pleiotropic effects which can occur as a result of genetic manipulation of these variables we generated an ectopic promoter-RFB system to assay the effect of increasing transcription, RFB activity, or both simultaneously at a single Tf2 target site.

Given Tf2 elements' strong preference for recombination with endogenous full-length transposons, we reasoned that in a retrotransposition assay performed in a strain missing all but one full-length transposon "target" the majority of transposition events would result from recombinations between Tf2 cDNA and the target transposon. The Tf-0 strain was initially generated in an iterative process involving multiple rounds of inter-LTR recombination to promote transposon loss stimulated by CRISPR-Cas9 cleavage inside the Tf2 coding sequence; we used a Tf-0 precursor strain which retained only *Tf2-3* and lost all other transposons to generate a series of modified strains for use in a retrotransposition assay (Figure 3.4a). In the first modified strain the entire 5' LTR was removed from the transposon; in the second the 5' LTR was removed and replaced with the constitutively active *eno1* promoter; in the third and fourth strains the 5' LTR was removed and replaced with the Ter2 Reb1-dependent (and Sap1-independent) polar RFB in the sense and antisense direction, respectively (Ter2 S and Ter2 AS). When bound by the polar DNA binding factor Reb1, Ter2 S and Ter2 AS block replication forks approaching in the antisense and sense direction, respectively, with respect to Tf2 transcription. In this arrangement Ter 2 AS provided the closest approximation of our proposed model of replication-transcription collisions as a result of Sap1's RFB activity. Finally, the fifth and sixth strains had the 5' LTR removed and replaced with only Ter2 S and Ter2 AS, respectively. We then repeated the retrotransposition assays in all six modified strains as well as the original parent strain; for the purposes of this assay we only used the plasmid expressing the IN FS transposon to ensure all transpositions are the product of HR and thus more representative of *Tf2-3-* cDNA recombinations. At both timepoints the frequency of transpositions was slightly lower in the Δ5' LTR strain than

in the parent strain (ZB1923), indicating that the LTR or an associated factor promotes mobilization via HR (Figure 3.4c). The modified transposon in all strains still retained the 3' LTR, however, which could potentially present a RFB due to Sap1 binding. The results were otherwise difficult to interpret due to the variation in retrotransposition frequency between the 4 and 6 day timepoints and/or the finding that differences between them were so subtle as to preclude formation of any definitive conclusions. We confirmed that the majority of retrotranspositions in all strains were the product of recombination between plasmid borne cDNA and *Tf2-3* by genotyping all FOA^{R}G418^R colonies by colony PCR using primers specific to the spliced intron junction in the neo cassette and primers specific to the region adjacent to the 3' end of *Tf2-3* (Figure 3.4b). At a minimum we concluded that the combination of an ectopic RFB with an ectopic promoter in this system did not generate a sustained increase in retrotranspositions over the RFB alone. We noted, however, that activation of Tf2 expression by the *eno1* promoter in the absence of an RFB promoter seemed to decrease overall retrotranpositions yet addition of the Ter2 RFB 'recovered' the frequency of transposition by Day 6.

Going forward, the utility of this assay may be improved with some modification: first, extensive genotyping by PCR could be used to 'normalize' the raw retrotransposition rates to produce more informative data. Given that retrotransposition rates are relatively low, even minor variability in the proportion of *Tf2-3* recombinations vs. external retrotransposition events may obscure analysis of assay outcomes. Second, assembling the same ectopic system in a transposon with a stronger replication bias may improve the ability to differentiate between strains. Unpublished Okazaki fragment

sequencing data from our lab suggests that there is a moderately strong replication origin near the 3' end of *Tf2-3* which replicates through the transposon in the antisense direction. In this arrangement, because the transposon is already being preferentially replicated in the antisense direction, Sap1's RFB activity would not be engaged. Thus, assembling the same ectopic system in a transposon which shows evidence of RFB activity at the 5' LTR may provide a truer test of the proposed model. Finally, we elected to use Ter2 to promote polar RFB activity to assess whether nonspecific fork barrier activity would produce the same effect as Sap1; indeed, by Day 6 the unmodified *Tf2-3* and the Ter2-AS construct exhibited similar retrotransposition frequency, which may suggest that this is the case. The possibility remains that Sap1 could influence Tf2 element retrotransposition outside of its effect on the replication fork, therefore substitution of Ter2 with Ter1, the sequence associated with Sap1 binding, may further elucidate and separate the role of Sap1 within the proposed model. Further investigation is needed, therefore, to determine whether replication-transcription collisions influence Tf2 mobilization. Here we have described an ectopic system which, with some optimization, may provide a platform for dissecting the relative contributions of each component within the model set forth in this study.

3.3.7 Increased H3K9 trimethylation at Tf2 elements in sap1-*c*

The HR efficiency assay described previously revealed a site-specific decrease in HR at Tf2 elements in *sap1-c* despite having operational HR machinery. We explored the possibility that recombinations at Tf2 elements could be suppressed in *sap1-c* by altered chromatin status, as an unrelated experiment revealed that *sap1-c* exhibits increased heterochromatin at the normally repressed subtelomeric region of chromosome II (data

not shown). Tf2 elements typically exhibit low levels of heterochromatic silencing, as they are largely silenced by CENP-B homologs and histone deacetylases through an RNAi-independent mechanism (Hugh P Cam et al., 2008; H. P. Cam et al., 2005). Interestingly, while *sap1-c* exhibited a mild reduction in di-methylated H3K9 (H3K9me2), we found an approximately three fold enrichment in tri-methylated H3K9 (H3K9me3) (Figure 3.5a, 3.5b). H3K9me2 has been shown to exhibit faster recovery kinetics than H3K9me3 and to be more permissive to transcription, while H3K9me3 is required for stable (RNAi-independent) inheritance of epigenetic domains in *S. pombe* (Jih et al., 2017).

Since Tf2 silencing is not dependent on RNAi, Tf2-derived siRNAs are often undetectable or only present at very low levels in cycling cells; siRNA levels were not significantly increased in *sap1-c*, ruling out the possibility that RNAi may be ectopically activated in this mutant (Figure 3.5c). Taken together, these results suggest that heterochromatin may be stabilized in *sap1-c* as opposed to generally increased at transposons. Increased stability of heterochromatin at Tf2 elements may consequently generate a reduction in integrations at heterochromatinized transposons, as recombination is typically suppressed in heterochromatic domains (Peng & Karpen, 2008). Going forward, more work is needed to verify the causality of the relationship between increased heterochromatin in *sap1-c* and reduced transposition; repeating the retrotransposition assay in a Δ*clr4 sap1-c* double mutant, for example, may shed light on the relationship between the observed phenomena.

3.4 Discussion

Tf2 retrotransposons are unique in their preference for integrase-independent mobilization and exhibit a strong predisposition for recombination with endogenous full-length Tf2 elements. In this study we analyzed Tf2 retrotransposition in the absence of full-length Tf2 transposons and asked whether removing their preferred HR substrates would influence their mobilization preferences or the efficiency of retrotransposition. We found that although Tf2 retrotransposition still occurred via a primarily integrase-independent mechanism in Tf-0 overall retrotransposition frequency was significantly reduced, indicating that Tf2 LTRs are not suitable substrates for efficient integration via HR and that integration site recycling is restricted to full-length retrotransposons. Using a novel transposon-free strain we were able to generate insertion profiles of de novo Tf2 retrotransposition to investigate Tf2 integration site preferences. We found that Tf2 elements exhibited some shared similarity with Tf1, including a bias towards insertion in gene promoters. Strikingly, we found that Sap1 binding was not strongly associated with Tf2 integrations, despite the dramatic reduction in retrotransposition efficiency observed in Sap1 mutants lacking RFB activity and the requirement of Sap1 RFB activity for Tf2 mobilization via HR. Thus, both Tf1 and Tf2 exhibit a shared dependence on a single host factor for efficient retrotransposition which materializes through divergent mechanisms.

In this study we propose a model in which Sap1's RFB activity generates fragile sites at Tf2 elements which in turn may increase the recombinogenicity of Tf2 target sites, thus improving their suitability as target sites for HR-mediated mobilization. Tf2 expression occurs at low levels and increases slightly at S phase, indicating that transcription and replication occur simultaneously. Further, we were able to

unambiguously detect the presence of R loops at endogenous Tf2 LTRs, which are hallmarks of replication-transcription collisions. We then asked whether we could treat the two components of this model- transcription and directional replication- as separable components by generating an ectopic promoter-RFB system to directly test this hypothesis; however, we were unable to make meaningful conclusions from the assay without further optimization.

Interestingly, we found that levels of H3K9me3 increase in *sap1-c*, indicating that heterochromatin may be stabilized in the absence of Sap1's RFB activity. Homologous recombination is often repressed in heterochromatin, therefore increased stability and epigenetic inheritance of heterochromatin at Tf2 elements may generate a corresponding reduction in target site recombinogenicity. Replication fork perturbation is accompanied by subsequent loss of heterochromatic markings in some contexts and increased epigenetic plasticity, thus in addition to promoting genetic instability at Tf2 elements Sap1's RFB activity may shield Tf2 transposons from heterochromatic silencing.

This model is not mutually exclusive with the former hypothesis- in previous studies increased transcription of Tf2 elements is accompanied by increased H3K9 methylation (Chalamcharla et al., 2015; Lorenzi et al., 2015). The finding that transcription can stimulate recombination (transcription-associated recombination, TAR), particularly in actively replicating cells, has been well documented; accordingly, a number of strategies have evolved to attenuate the recombinogenicity of encounters between the transcription and replication machinery given the potential for illicit recombination events that can contribute to genomic instability (Aguilera & García-Muse, 2012; Gavaldá et al., 2013; Mischo et al., 2011; Prado & Aguilera, 2005). One

such observation is the finding that R loop formation can promote chromatin condensation and compaction, a feature associated with heterochromatin (Castellano-Pozo et al., 2013). Thus, while R loop formation as a consequence of replication-transcription collisions in the body of Tf2 elements and/or increased transcription at Tf2s may trigger local silencing, the presence of a secondary stalled replication fork nearby may influence repair outcomes by promoting HR to restart the fork, thereby modulating the overall effect of these insults.

On an evolutionary time scale, recombination between Tf2 elements significantly contributes to shaping the fission yeast genome, as many of the breakpoints of structural variations which appear in wild fission yeast isolates are located in proximity to Tf2 LTRs (Jeffares et al., 2017). While these structural variations may simply be the product of chance occurrences of non-allelic homologous recombination (NAHR), we note that Tf2 LTRs have previously been demonstrated to serve as stress-activated promoters (Nakase & Matsumoto, 2018; Sehgal et al., 2007). In these instances, TAR may enhance the adaptive response of the host cell by focusing the power of structural evolution at the most critical loci in response to stressful environmental conditions. Going forward, understanding the factors modulating and influencing recombinogenicity at Tf2 elements is essential to understanding the forces shaping genomic architecture evolution in fission yeast.
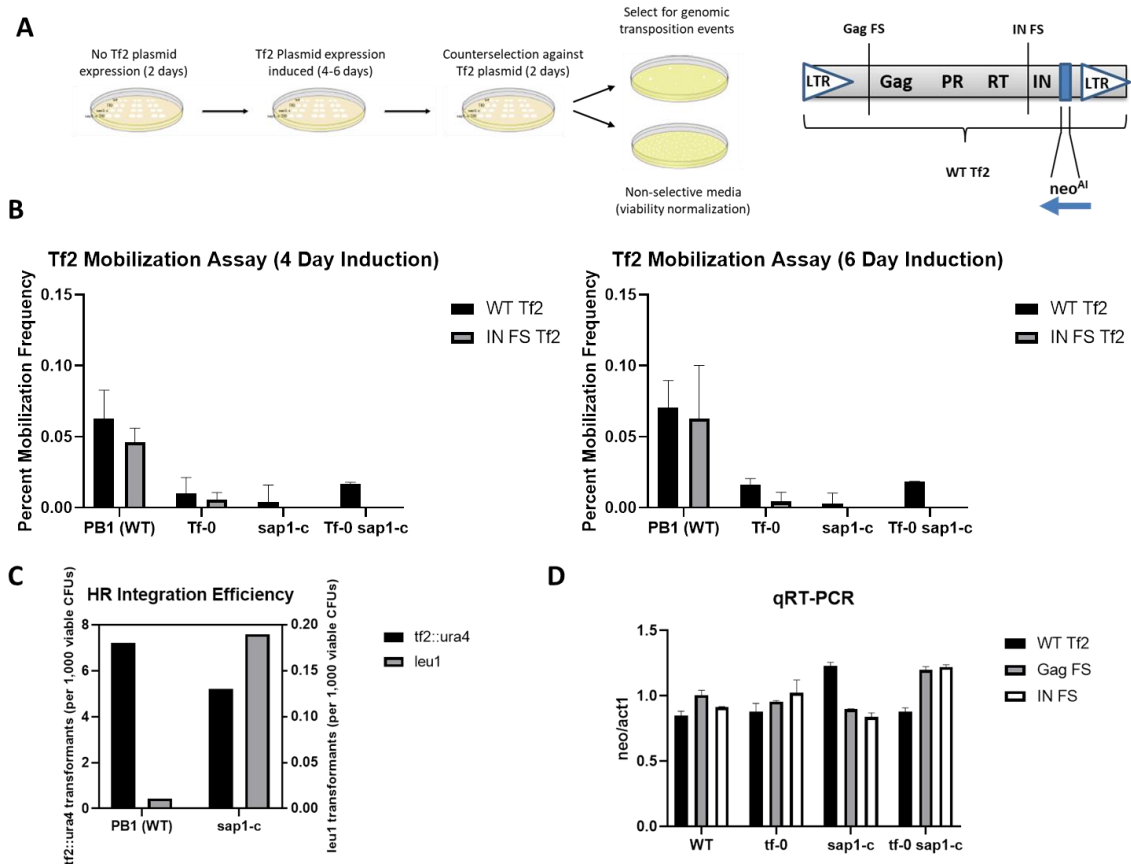
Figure 3.1. Tf2 shows reduced retrotransposition in the absence of full length transposons and Sap1 RFB activity. A. Retrotransposition assay overview (left), schematic of Tf2-expressing plasmids (right). Details of the assay are described in the Methods section of this chapter. *Figure adapted from N. Chalhoub*. B. Retrotransposition assays were performed after four and six day inductions of plasmid Tf2 expression. Each strain was transformed with a plasmid expressing wild type Tf2 (WT Tf2), Tf2 with a frameshift in the Gag coding sequence (Gag FS Tf2), or Tf2 with a frameshift in the Integrase coding sequence (IN FS Tf2). Retrotransposition was reduced in a strain lacking full-length transposons (Tf-0) as well as in a *sap1-c* mutant background. Data represent the results from at least two independent experiments with each strain assayed in duplicate. Error bars= sample ranges. C. Tf2 elements exhibit a site-specific decrease in HR integration efficiency in *sap1*-c. Graph shows the HR integration efficiency of a wild type strain (PB1) and *sap1-c* transformed with a ura4-marked *Tf2* fragment and a *leu1* fragment (left axis= *tf2::ura4* transformants per 1,000 viable CFUs; right axis= *leu1*+ transformants per 1,000 viable CFUs). Integration efficiency of *tf2::ura4* is 30% lower in *sap1*-c compared to wild type while *leu1* correction is approximately 17 times higher. d. qRT-PCR results quantifying relative plasmid Tf2 expression levels in retrotransposition assay strains. Transcript levels were quantified using primers directed against *neo* and normalized to *act1* expression. Plasmid Tf2 expression is consistent in all four strains used in the retrotransposition assay. Error bars=SEM.
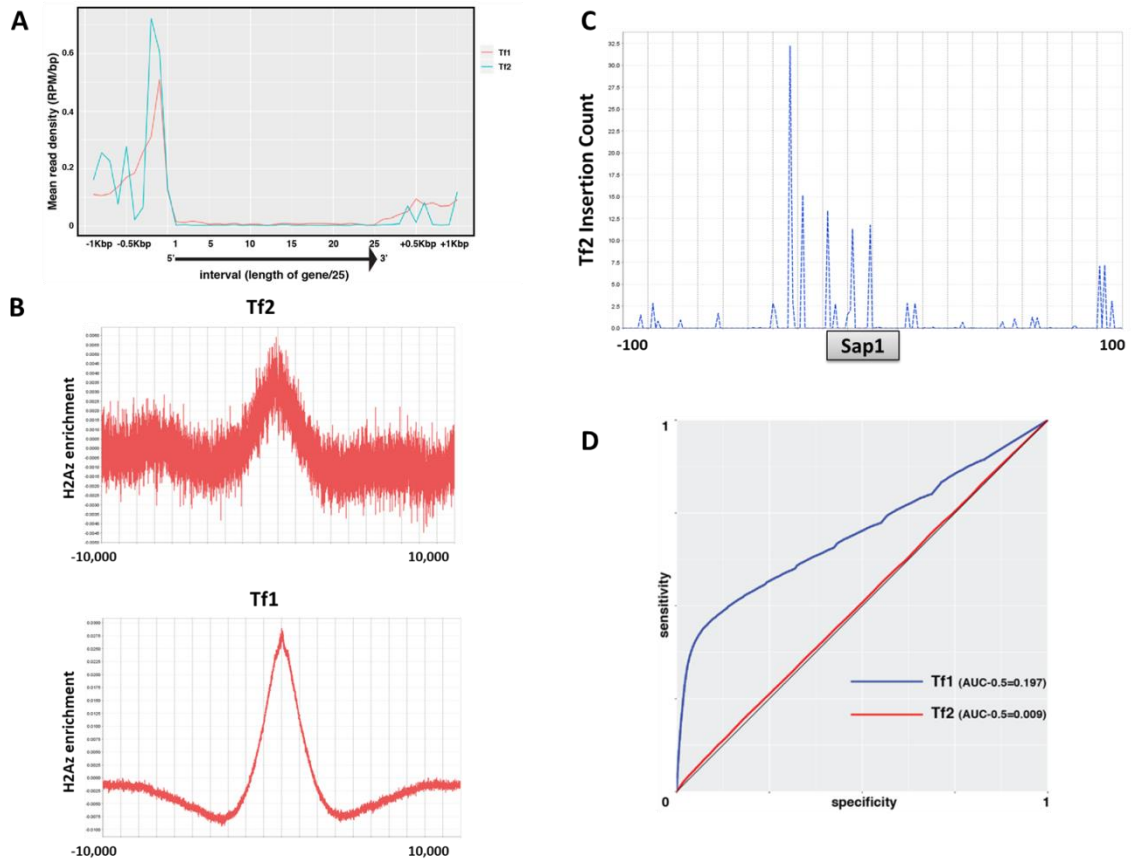
Figure 3.2. Integration site preferences of Tf2 retrotransposons. A. Mean read density distribution of Tf1 and Tf2 insertions over all protein coding genes (n=5,823). Similar to Tf1, Tf2 shows a preference for gene promoters. B. Anchor plot showing H2A.z enrichment with respect to Tf2 insertions (upper panel) and Tf1 insertions (lower panel). Similar to Tf1, Tf2 shows a slight bias towards insertion in H2A.z-enriched regions in accordance with its preference for gene promoters; the enrichment is lost when Tf2 insertions overlapping with promoters are excluded from the analysis. c) Tf2 insertions are slightly enriched at Sap1 binding sites and exhibit the same periodicity associated with integrase-dependent mobilization in Tf1. These insertions likely represent the relatively small population of integrase-dependent retrotransposition events. D. ROC curves from a representative Tf2 insertion library (red) and Tf1 insertion library (blue). Unlike Tf1, Sap1 binding is a poor predictor of Tf2 integration.
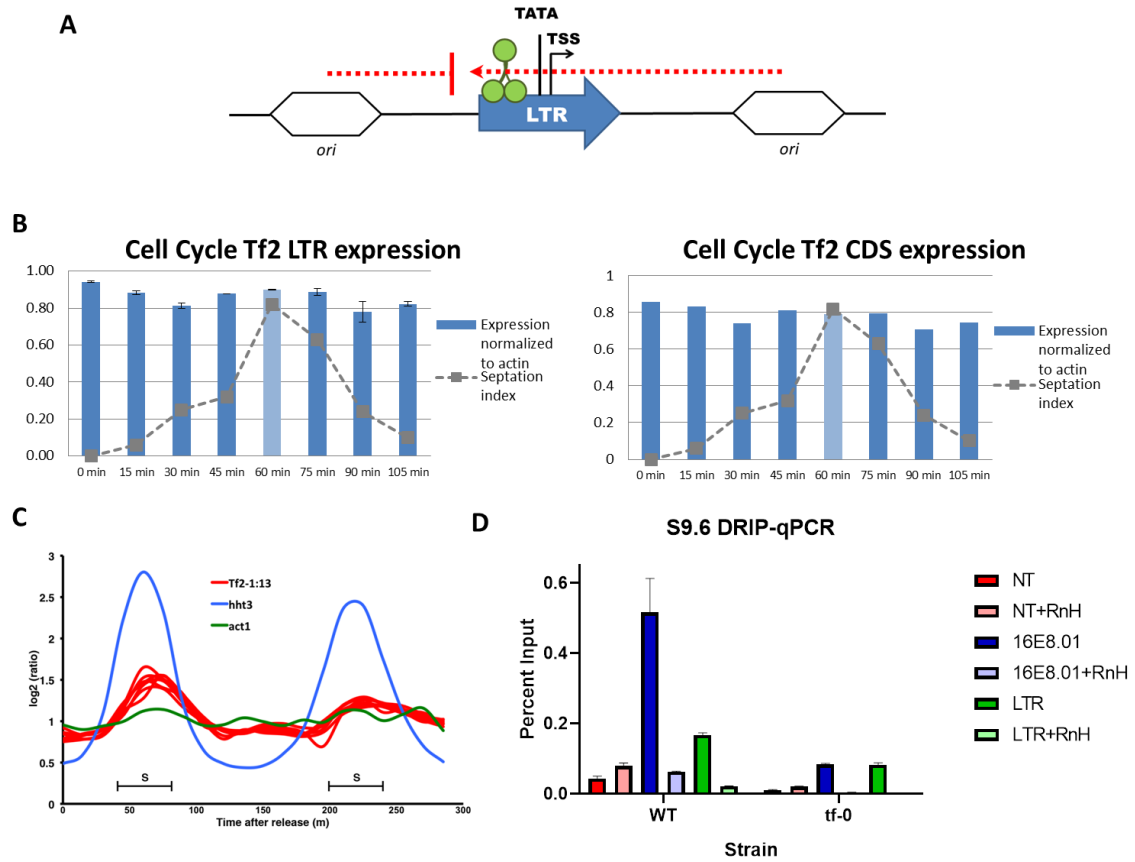
Figure 3.3. Sap1 RFB activity may promote replication-transcription collisions at Tf2 elements. A. Cartoon showing the orientation of Tf2 transcription with respect to Sap1's RFB activity. Sap1's polar RFB activity permits replication in a direction that is antisense to transcription at Tf2 LTRs. B. Cell cycle analysis of Tf2 LTR and CDS expression. Tf2 expression shows a slight peak at S phase; low level expression occurs throughout the cell cycle. *cdc25-22* ts mutant cells were grown at 26° C before shifting to the restrictive temperature (36° C) for 4 hours to induce cell cycle arrest in G2. Samples were then taken every 15 minutes after release at the permissive temperature to analyze the septation index by microscopy and resuspended in Trizol for RNA extraction followed by qRT-PCR to analyze Tf2 expression levels using primers directed against the Tf2 LTR (left panel) or Tf2 CDS (right panel). Target expression is normalized to *act1* expression; all qPCR reactions were set up in quadruplicate. C. Microarray expression data obtained from Rustici et. al., *Nature* (2004). Synchronized cells were obtained by centrifugal elutriation and gene expression was monitored throughout the cell cycle. Shown is expression data for *act1* (actin), *hht3* (Histone H3), and *tf2-1-13*. D. R loop formation occurs at endogenous genomic Tf2 LTRs. DNA-RNA Immunoprecipitation (DRIP) was performed to probe for R loop formation at genomic Tf2 LTRs; R loop signal accumulates as a result of naturally occurring RT intermediates in the wild type strain but is still detectable in the absence of RT intermediates in Tf-0. NT= not transcribed, 16E8.01= positive control, error bars=SEM.
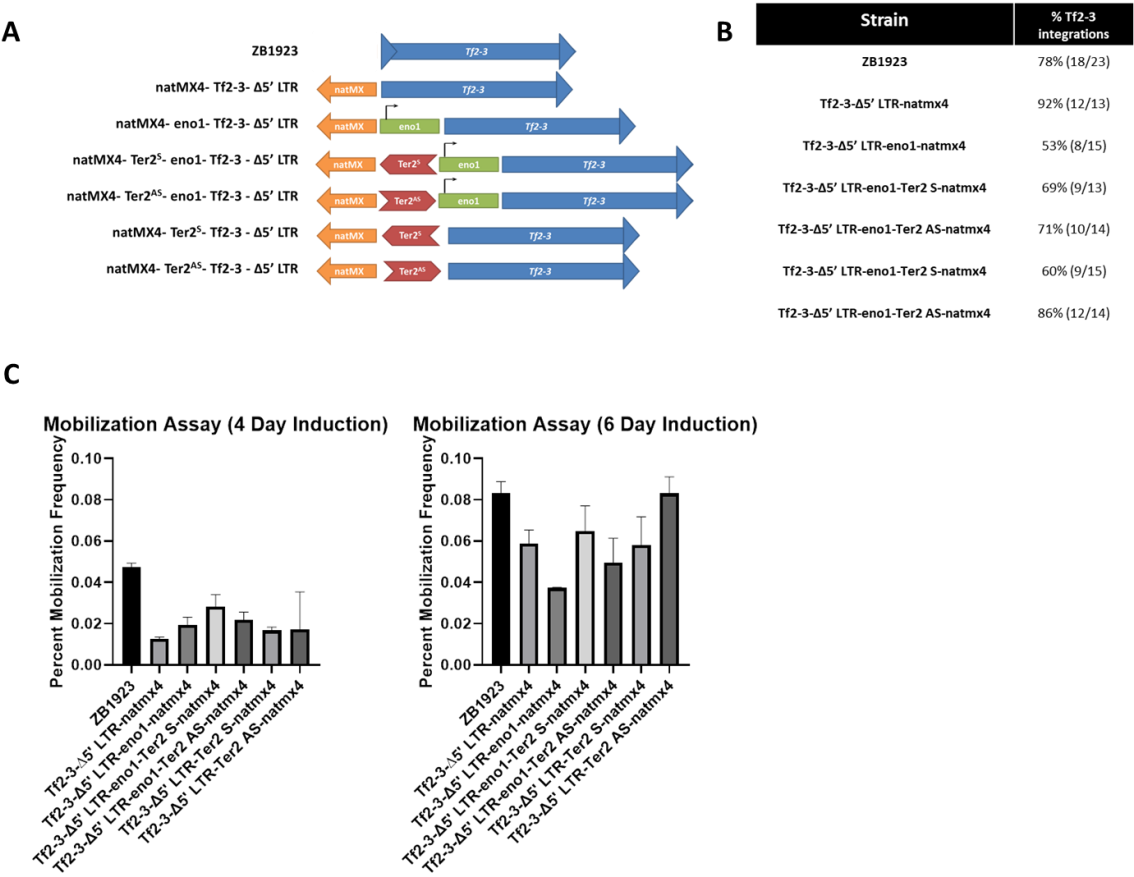
Figure 3.4. Generation of an ectopic promoter-RFB system to probe the contributions of transcription and RFB activity at Tf2 target sites and their influence on retrotransposition into Tf2 targets. A. Overview of the modified strains generated for use in the Tf2 retrotransposition assay. The 5' LTR was removed from all strains (with the exception of the parent strain ZB1923) and subsequently modified to include the constitutive *eno1* promoter to promote *Tf2* transcription and/or polar RFB Reb1-binding Ter2 sequence in the sense or antisense orientation in addition to the selectable marker *natmx4*. B. Colonies in which a retrotransposition event had occurred were genotyped by colony PCR to determine the proportion of recombination events occurring between plasmid-derivedTf2 cDNA and *Tf2-3*. In all strains the majority of insertions were the result of recombination with *Tf2-3*. C. Results of the retrotransposition assay. All strains were transformed with an Tf2 IN FS-expressing plasmid to increase the proportion of HR-mediated retrotransposition events. Results represent the outcome of one experiment; two independent transformants were analyzed for each strain. Tf2 expression was induced for 4 and 6 days before quantifying retrotransposition frequency. Error bars= ranges.

A

H3K9me2 ChIP-qPCR

B

H3K9me3 ChIP-qPCR

C
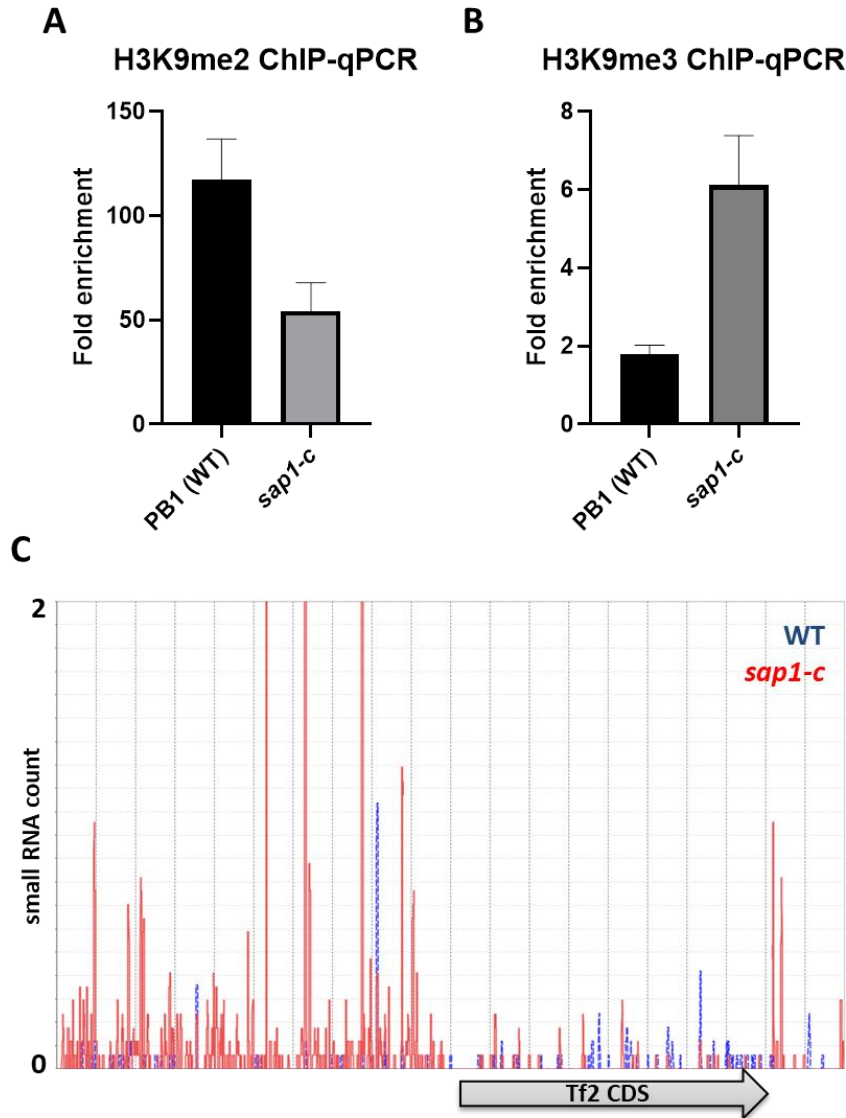
Figure 3.5. *sap1-c* **promotes stable heterochromatin formation at Tf2 elements.** A. H3K9me2 ChIP-qPCR in a wild type strain and *sap1*-c. H3K9me2 levels decrease by approximately 30% in *sap1*-c. Data represents the results of two IP replicates with each replicate assayed by qPCR in duplicate. Error bars=SEM. B. H3K9me3 ChIP-qPCR in a wild type strain and *sap1-c*. H3K9me3 levels increase approximately three fold in *sap1*-c. Data represents the results of two IP replicates with each replicate assayed by qPCR in duplicate. H3K9me2 and H3K9me3 ChIPs were performed in parallel, with a single pool of sonicated chromatin split before use in both subsequent IPs. Error bars=SEM. C. Tf2-derived small RNAs are comparable to wild type in *sap1-c*. Small RNA read counts in both strains are normalized per million reads produced by each sequencing run.

TABLE 3.1 Strains used in this study

Strain name	Genotype	Used for
PB1	leu1-32 ura4-D18	Retrotransposition assay/ChIP/DRIP/transformation efficiency assay
ZB1925	leu1-32, ura4-D18, pan-deltaTf2	Retrotransposition assay/ChIP/DRIP
ZB1947	sap1c, leu1-32, ura4-D18, pan-deltaTf2	Retrotransposition assay
ZB1069	sap1-c, ura4-D18	Retrotransposition assay/ChIP
DG704	cdc25-22 ts, leu1	Cell cycle Tf2 expression synchronization
ZB1923	leu1-32, ura4-D18, deltaTf2-1, deltaTf2-2,deltaTf2-4, deltaTf2-5, delta-Tf2-6, delta-Tf2-7, delta-Tf2-8, delta-Tf2-9, delta-Tf2-10, delta-Tf2-11, deltaTf2-12, delta-Tf2-13	Ectopic promoter-RFB retrotransposition assay
ZB1107	sap1c, leu1-32, ura4+, ade6+	sap1-c transformation efficiency assay
ZB2483	Tf2-3 A1 (#1) :: natmx4, leu1-32, ura4-D18, deltaTf2-1, deltaTf2-2,deltaTf2-4, deltaTf2-5, delta-Tf2-6, delta-Tf2-7, delta-Tf2-8, delta-Tf2-9, delta-Tf2-10, delta-Tf2-11, deltaTf2-12, delta-Tf2-13	Ectopic promoter-RFB retrotransposition assay
ZB2486	Tf2-3 B5 #1 :: eno1 natmx4, leu1-32, ura4-D18, deltaTf2-1, deltaTf2-2,deltaTf2-4, deltaTf2-5, delta-Tf2-6, delta-Tf2-7, delta-Tf2-8, delta-Tf2-9, delta-Tf2-10, delta-Tf2-11, deltaTf2-12, delta-Tf2-13	Ectopic promoter-RFB retrotransposition assay
ZB2488	Tf2-3 C2 #1 :: eno1 Ter2S natmx4, leu1-32, ura4-D18, deltaTf2-1, deltaTf2-2,deltaTf2-4, deltaTf2-5, delta-Tf2-6, delta-Tf2-7, delta-Tf2-8, delta-Tf2-9, delta-Tf2-10, delta-Tf2-11, deltaTf2-12, delta-Tf2-13	Ectopic promoter-RFB retrotransposition assay
ZB2491	Tf2-3 D1 #1 :: eno1 Ter2AS natmx4, leu1-32, ura4-D18, deltaTf2-1, deltaTf2-2,deltaTf2-4, deltaTf2-5, delta-Tf2-6, delta-Tf2-7, delta-Tf2-8, delta-Tf2-9, delta-Tf2-10, delta-Tf2-11, deltaTf2-12, delta-Tf2-13	Ectopic promoter-RFB retrotransposition assay
ZB2493	Tf2-3 E5 #4 :: Ter2S natmx4, leu1-32, ura4-D18, deltaTf2-1, deltaTf2-2,deltaTf2-4, deltaTf2-5, delta-Tf2-6, delta-Tf2-7, delta-Tf2-8, delta-Tf2-9, delta-Tf2-10, delta-Tf2-11, deltaTf2-12, delta-Tf2-13	Ectopic promoter-RFB retrotransposition assay
ZB2496	Tf2-3 F3 #3 :: Ter2AS natmx4, leu1-32, ura4-D18, deltaTf2-1, deltaTf2-2,deltaTf2-4, deltaTf2-5, delta-Tf2-6, delta-Tf2-7, delta-Tf2-8, delta-Tf2-9, delta-Tf2-10, delta-Tf2-11, deltaTf2-12, delta-Tf2-13	Ectopic promoter-RFB retrotransposition assay
zb2551	ura4-d18, leu1-32 +pHL1631	Retrotransposition assay
zb2552	ura4-d18, leu1-32 +pHL1631	Retrotransposition assay
zb2553	ura4-d18, leu1-32 +pHL1632	Retrotransposition assay
zb2554	ura4-d18, leu1-32 +pHL1632	Retrotransposition assay
zb2555	ura4-d18, leu1-32 +pHL1633	Retrotransposition assay
zb2556	ura4-d18, leu1-32 +pHL1633	Retrotransposition assay
zb2557	leu1-32, ura4-D18, pan-deltaTf2 +pHL1631	Retrotransposition assay
zb2558	leu1-32, ura4-D18, pan-deltaTf2 +pHL1631	Retrotransposition assay
zb2559	leu1-32, ura4-D18, pan-deltaTf2 +pHL1632	Retrotransposition assay
zb2560	leu1-32, ura4-D18, pan-deltaTf2 +pHL1632	Retrotransposition assay
zb2561	leu1-32, ura4-D18, pan-deltaTf2 +pHL1633	Retrotransposition assay
zb2562	leu1-32, ura4-D18, pan-deltaTf2 +pHL1633	Retrotransposition assay
zb2569	sap1-c, ura4-D18 +pHL1631	Retrotransposition assay

zb2570	sap1-c, ura4-D18 +pHL1631	Retrotransposition assay
zb2571	sap1-c, ura4-D18 +pHL1632	Retrotransposition assay
zb2572	sap1-c, ura4-D18 +pHL1632	Retrotransposition assay
zb2573	sap1-c, ura4-D18 +pHL1633	Retrotransposition assay
zb2574	sap1-c, ura4-D18 +pHL1633	Retrotransposition assay
ZB2539	sap1c, leu1-32, ura4-D18, pan-deltaTf2+pHL1631 transformant #1	Retrotransposition assay
ZB2540	sap1c, leu1-32, ura4-D18, pan-deltaTf2 +pHL1631 transformant #2	Retrotransposition assay
ZB2176	ZB1947-pHL1632 sap1-c, leu1-32, ura4-D18, pan-deltaTf2; GagFS	Retrotransposition assay
ZB2177	ZB1947-pHL1633 sap1-c, leu1-32, ura4-D18, pan-deltaTf2; INFS	Retrotransposition assay

TABLE 3.2 Oligonucleotides used in this study

Primer ID	Primer name	Sequence	Used for
oM4	act1qPCRF	TGCACCTGCCTTTTATGTTG	act1 primer for qPCR/ChIP/cell cycle expression normalization
oM5	act1qPCRR	TGGGAACAGTGTGGGTAACA	act1 primer for qPCR/ChIP/cell cycle expression normalization
om1535	16E8.01 drip ctrl F	Ctgccgatccatttcaatct	DRIP positive control for qPCR
om1536	16E8.01 drip ctrl R	Agtggcctgaacaggaattg	DRIP positive control for qPCR
om1992	primer #1 tf2_3 CDS F ABCDEF	gtgaattcgagctcggtacccatcgcgctcatttgggaataatgaagggtattc	Used in construction of ectopic promoter-RFB strains
om1993	primer #2 Tf2_3 DS R ABCDEF	cgactctagaggatcccccgatctcgaccagcctcattgggcataatgct	Used in construction of ectopic promoter-RFB strains
om1994	primer #3 Tf2_3 DS F ABCDEF	ggagggtattctgggcctccatgtccaaacaaagacagacgcgtttcaaaataag	Used in construction of ectopic promoter-RFB strains
om1995	primer #4 natmx4 R ABCDEF	Ggacatggaggcccagaatacc	Used in construction of ectopic promoter-RFB strains
om1996	primer #5 Tf2_3 CDS R BCD	tacagtaaacatcgctgcagcgggataactgaactcttgtgatctaca	Used in construction of ectopic promoter-RFB strains
om1997	primer #6 eno1 F BCD	Cccgctgcagcgatgtttactgt	Used in construction of ectopic promoter-RFB strains
om1998	primer #7 eno1 ter2S C	cgctatactgaggtaagggtaatgcacgcatgcaactgcagcatctcttgccc	Used in construction of ectopic promoter-RFB strains
om1999	primer #8 eno1 Ter2 AS D	ctatactggtgcattaccccttacctgcatgcaactgcagcatctcttgcccttc	Used in construction of ectopic promoter-RFB strains
om2000	primer #9 Ter2S natmx4 CE	gtgcattacccttacctcagtatagcgaccagcattcaca	Used in construction of ectopic promoter-RFB strains
om2001	primer #10 Ter2 AS DF	aggtaagggtaatgcaccagtatagcgaccagcattcaca	Used in construction of ectopic promoter-RFB strains
om2002	primer #11 natmx4 AB	Cagtatagcgaccagcattca	Used in construction of ectopic promoter-RFB strains
om2003	primer #12 Tf2_3 CDS R natmx4 A	aatcgtatgtgaatgctggtcatactgataactgaactcttgtgatctacaatta..	Used in construction of ectopic promoter-RFB strains
om2004	primer #13 eno1 natmx4 B	cgtatgtgaatgctggtcgctatactggcatgcaactgcagcatctcttgccc	Used in construction of ectopic promoter-RFB strains
om2005	primer #14 Tf2_3 CDS Ter2S R E	aggtaagggtaatgcacataactgaactcttgtgatc	Used in construction of ectopic promoter-RFB strains
om2006	primer #15 Tf2_3 CDS Ter2AS R F	gtccattacccttacctataactgaactcttgtgatctaca	Used in construction of ectopic promoter-RFB strains
om2022	Tf2-3 CDS amp F for transformation	Gctcatttgggaataatgaagggt	Used for amplification of modified Tf2-3 constructs

om2023	Tf2-3 DS amp R for transformation	Cgctgtaatggtgtaagtatcaa	Used for amplification of modified Tf2-3 constructs
om2024	primer 16 eno1 r	Gcatgcaactgcagcat	Used in construction of ectopic promoter-RFB strains
om2025	primer 17 CDS r	ataactgaactcttgtgatctacatgacgctcagtggaacga	Used in construction of ectopic promoter-RFB strains
om2026	primer 18 ColE1 OriF	Tgacgctcagtggaacga	Used in construction of ectopic promoter-RFB strains
om2027	primer 19 ColE1 OriR	Tcgttccactgagcgtca	Used in construction of ectopic promoter-RFB strains
om2067	neo jct F	Gacattatcgcgagcccatt	Neo junction primer for genotyping Tf2 insertions
om2085	leu2 F	Cttcttcaacaacatgtgtgc	Primer for amplification of leu1+ frag
om2087	leu2 R	Gttcttcaacaacagccttagt	Primer for amplification of leu1+ frag
oM16	TF2LTRqF	tgataggtaacattataacccagt	Tf2 LTR primer for qPCR/ChIP/DRIP/Tf2 expression
oM17	TF2LTRqR	Acgcagtttggtatctgatt	Tf2 LTR primer for qPCR/ChIP/DRIP/Tf2 expression
oM18	TF2CDSqF	Ggtaggcagtttatgtgctc	TF2 CDS primer for qPCR/ChIP/Tf2 expression
oM19	TF2CDSqR	Agaacagcctcgtatggtaa	TF2 CDS primer for qPCR/ChIP
OM1366	Tf2-1_MP_A	Aggactttctgatgtttgtacct	Tf2 genotyping primer
OM1367	Tf2-2_MP_A	Tggttgttcaatgccaaattagt	Tf2 genotyping primer
OM1368	Tf2-3_MP_B	Gaggataagtaaagaaagtctgtga	Tf2 genotyping primer
OM1369	Tf2-4_MP_A	Caagttgtcgcattccactcc	Tf2 genotyping primer
OM1370	Tf2-5_MP_A	Agcattgcataccctaaagca	Tf2 genotyping primer
om1371	Tf2-6_MP_B	Gccgtcaccaattagcatgac	Tf2 genotyping primer
OM1372	Tf2-7_MP_B	Accaggcgttacttcaatcttg	Tf2 genotyping primer
OM1373	Tf2-9_MP_C	Attcccgtaagtttcccgctt	Tf2 genotyping primer
OM1374	Tf2-10_MP_B	Tggcgttatcaagctacggaa	Tf2 genotyping primer
OM1375	Tf2-11_MP_C	Gattgccctcccttgatcaca	Tf2 genotyping primer
OM1376	Tf2-12_MP_C	Agagggttttgcggatcttgt	Tf2 genotyping primer
OM1377	Tf2-13_MP_C	Aaaaccttcaaacgtgctgcc	Tf2 genotyping primer
om1850	chrI NT region F	Caactttccttcaccaacc	DRIP NT control for qPCR
om1851	chrI NT region R	Aaaagacgctattcgaaggt	DRIP NT control for qPCR
oM538	p7 linker	caagcagaagacggcatacgagatgtaataacgactcactatagggc	Linker primer for Tf2 insertion high throughput sequencing library prep

oM543	TF1bc07	Aatgatacggcgaccaccgagatctacactctttccctacacgacgctcttccgatctcagatcgatgcat aggaatttagtttatgg	Barcoding primer for Tf2 insertion high throughput sequencing library prep
oM544	TF1bc02	Aatgatacggcgaccaccgagatctacactctttccctacacgacgctcttccgatctcgatgtgatgcata ggaatttagtttatgg	Barcoding primer for Tf2 insertion high throughput sequencing library prep
oM536	HL 1870	Gtaatacgactcactatagggctccgcttaagggac	Annealed to generate linker for Tf2 insertion high throughput sequencing library prep
oM537	HL 1871	5Phos/tagtcccttaaccggag/3AmMO	Annealed to generate linker for Tf2 insertion high throughput sequencing library prep
om1803	[5LTR] tf2 cds	caa aca ggg aaa gta caa gga tcc aac aaa ggt gat cgt tta ac	Used to generate high-throughput sequencing ready plasmid for Tf2 insertion profiling
om1804	[nmt1] 5LTR	cta ata tag ctc ata act gaa ctc gag gat atg cca gga ttc c	Used to generate high-throughput sequencing ready plasmid for Tf2 insertion profiling
oM175	neoProbeF1	TTATGCCTCTTCCGACCATC	neo primer for qPCR
oM176	neoProbeR1	GCCTGAGCGAGACGAAATAC	neo primer for qPCR

TABLE 3.3 Plasmids used in this study

Plasmid ID		Used for
pHL1631	pEH704-18, Tf2-neoAI	Retrotransposition assay
pHL1632	pEH705-15, Gag FS	Retrotransposition assay
pHL1633	pEH712-1, IN FS	Retrotransposition assay
pMZ160	pTF-Ura4	Digested with XhoI to obtain tf2::ura4 fragment for transformation efficiency assay
pmz684	pEH704-18, Tf2-neoAI hts ready	Generation of Tf2 insertions for high throughput sequencing
pmz685	pEH712-1, IN FS, hts ready	Generation of Tf2 insertions for high throughput sequencing
pmz788	Tf2-3 A1 (construct A, Tf2-3 CDS-natmx4-Tf2-3 DS)	Used to amplify transforming fragment for generation of modified Tf2-3
pmz789	Tf2-3 B5 (construct B, Tf2-3 CDS-eno1-natmx4-Tf2-3 DS)	Used to amplify transforming fragment for generation of modified Tf2-3
pmz790	Tf2-3 C2 (construct C, Tf2-3 CDS-eno1-Ter2 S-natmx4-Tf2-3 DS)	Used to amplify transforming fragment for generation of modified Tf2-3
pmz791	Tf2-3 C5 (construct C, Tf2-3 CDS-eno1-Ter2 S-natmx4-Tf2-3 DS)	Used to amplify transforming fragment for generation of modified Tf2-3
pmz792	Tf2-3 D1 (construct D, Tf2-3 CDS-eno1-Ter2 AS-natmx4-Tf2-3 DS)	Used to amplify transforming fragment for generation of modified Tf2-3
pmz793	Tf2-3 D3 (construct D, Tf2-3 CDS-eno1-Ter2 AS-natmx4-Tf2-3 DS)	Used to amplify transforming fragment for generation of modified Tf2-3
pmz794	Tf2-3 E5 (construct E, Tf2-3 CDS-Ter2 S-natmx4-Tf2-3 DS)	Used to amplify transforming fragment for generation of modified Tf2-3
pmz795	Tf2-3 F3 (construct F, Tf2-3 CDS-Ter2 AS-natmx4-Tf2-3 DS)	Used to amplify transforming fragment for generation of modified Tf2-3

REFERENCES

Aguilera, A., & Gaillard, H. (2014). Transcription and recombination: when RNA meets DNA. *Cold Spring Harbor perspectives in biology, 6*(8), a016543.

Aguilera, A., & García-Muse, T. (2012). R Loops: From Transcription Byproducts to Threats to Genome Stability. *Molecular Cell, 46*(2), 115-124. doi:https://doi.org/10.1016/j.molcel.2012.04.009

Alabert, C., & Groth, A. (2012). Chromatin replication and epigenome maintenance. *Nat Rev Mol Cell Biol, 13*(3), 153-167.

Allshire, R. C., & Ekwall, K. (2015). Epigenetic Regulation of Chromatin States in Schizosaccharomyces pombe. *Cold Spring Harb Perspect Biol, 7*(7), a018770. doi:10.1101/cshperspect.a018770

Allshire, R. C., & Madhani, H. D. (2017). Ten principles of heterochromatin formation and function. *Nature Reviews Molecular Cell Biology, 19*, 229. doi:10.1038/nrm.2017.119

Alper, B. J., Lowe, B. R., & Partridge, J. F. (2012). Centromeric heterochromatin assembly in fission yeast—balancing transcription, RNA interference and chromatin modification. *Chromosome research, 20*(5), 521-534.

Amaral, N., Ryu, T., Li, X., & Chiolo, I. (2017). Nuclear Dynamics of Heterochromatin Repair. *Trends Genet, 33*(2), 86-100. doi:10.1016/j.tig.2016.12.004

Aygün, O., Mehta, S., & Grewal, S. I. S. (2013). HDAC-mediated suppression of histone turnover promotes epigenetic stability of heterochromatin. *Nature Structural &Amp; Molecular Biology, 20*, 547. doi:10.1038/nsmb.2565

Bahler, J., & Wise, J. A. (2017). Preparation of Total RNA from Fission Yeast. *Cold Spring Harb Protoc, 2017*(4), pdb.prot091629. doi:10.1101/pdb.prot091629

Bayne, E. H., Bijos, D. A., White, S. A., Alves, F. d. L., Rappsilber, J., & Allshire, R. C. (2014). A systematic genetic screen identifies new factors influencing centromeric heterochromatin integrity in fission yeast. *Genome Biology, 15*(10), 481. doi:10.1186/s13059-014-0481-4

Bayne, E. H., White, S. A., Kagansky, A., Bijos, D. A., Sanchez-Pulido, L., Hoe, K. L., . . . Allshire, R. C. (2010). Stc1: a critical link between RNAi and chromatin modification required for heterochromatin integrity. *Cell, 140*(5), 666-677. doi:10.1016/j.cell.2010.01.038

Belancio, V. P., Deininger, P. L., & Roy-Engel, A. M. (2009). LINE dancing in the human genome: transposable elements and disease. *Genome Medicine, 1*(10), 97. doi:10.1186/gm97

Ben-Shahar, T. R., Heeger, S., Lehane, C., East, P., Flynn, H., Skehel, M., & Uhlmann, F. (2008). Eco1-dependent cohesin acetylation during establishment of sister chromatid cohesion. *Science, 321*(5888), 563-566.

Bernard, P., Maure, J. F., Partridge, J. F., Genier, S., Javerzat, J. P., & Allshire, R. C. (2001). Requirement of heterochromatin for cohesion at centromeres. *Science, 294*(5551), 2539-2542. doi:10.1126/science.1064027

Bertomeu, T., Coulombe-Huntington, J., Chatr-Aryamontri, A., Bourdages, K. G., Coyaud, E., Raught, B., . . . Tyers, M. (2018). A High-Resolution Genome-Wide CRISPR/Cas9 Viability Screen Reveals Structural Features and Contextual Diversity of the Human Cell-Essential Proteome. *Mol Cell Biol, 38*(1). doi:10.1128/mcb.00302-17

Blewitt, M., & Whitelaw, E. (2013). The use of mouse models to study epigenetics. *Cold Spring Harb Perspect Biol, 5*(11), a017939. doi:10.1101/cshperspect.a017939

Bourque, G. (2009). Transposable elements in gene regulation and in the evolution of vertebrate genomes. *Curr Opin Genet Dev, 19*(6), 607-612. doi:10.1016/j.gde.2009.10.013

Bourque, G., Burns, K. H., Gehring, M., Gorbunova, V., Seluanov, A., Hammell, M., . . . Feschotte, C. (2018). Ten things you should know about transposable elements. *Genome Biology, 19*(1), 199. doi:10.1186/s13059-018-1577-z

Bowen, N. J., Jordan, I. K., Epstein, J. A., Wood, V., & Levin, H. L. (2003). Retrotransposons and their recognition of pol II promoters: a comprehensive survey of the transposable elements from the complete genome sequence of Schizosaccharomyces pombe. *Genome Res, 13*(9), 1984-1997. doi:10.1101/gr.1191603

Brodeur, G. M., Sandmeyer, S. B., & Olson, M. V. (1983). Consistent association between sigma elements and tRNA genes in yeast. *Proc Natl Acad Sci U S A, 80*(11), 3292-3296. doi:10.1073/pnas.80.11.3292

Buchanan, L., Durand-Dubief, M., Roguev, A., Sakalar, C., Wilhelm, B., Strålfors, A., . . . Francis Stewart, A. (2009). The Schizosaccharomyces pombe JmjC-Protein, Msc1, Prevents H2A.Z Localization in Centromeric and Subtelomeric Chromatin Domains. *PLoS Genet, 5*(11), e1000726. doi:10.1371/journal.pgen.1000726

Buchon, N., & Vaury, C. (2006). RNAi: a defensive RNA-silencing against viruses and transposable elements. *Heredity, 96*(2), 195-202. doi:10.1038/sj.hdy.6800789

Bushman, F. D. (2003). Targeting Survival: Integration Site Selection by Retroviruses and LTR-Retrotransposons. *Cell, 115*(2), 135-138. doi:https://doi.org/10.1016/S0092-8674(03)00760-8

Bzymek, M., & Lovett, S. T. (2001). Instability of repetitive DNA sequences: The role of replication in multiple mechanisms. *Proceedings of the National Academy of Sciences, 98*(15), 8319-8325. doi:10.1073/pnas.111008398

Cam, H. P., Noma, K.-i., Ebina, H., Levin, H. L., & Grewal, S. I. (2008). Host genome surveillance for retrotransposons by transposon-derived proteins. *Nature, 451*(7177), 431.

Cam, H. P., Sugiyama, T., Chen, E. S., Chen, X., FitzGerald, P. C., & Grewal, S. I. (2005). Comprehensive analysis of heterochromatin- and RNAi-mediated epigenetic control of the fission yeast genome. *Nat Genet, 37*(8), 809-819. doi:10.1038/ng1602

Cam, H. P. W., Simon. (2016). Chromatin Immunoprecipitation (ChIP) in Schizosaccharomyces pombe. *Cold Spring Harbor Protocols*.

Castel, S. E., Ren, J., Bhattacharjee, S., Chang, A. Y., Sanchez, M., Valbuena, A., . . . Martienssen, R. A. (2014). Dicer promotes transcription termination at sites of replication stress to maintain genome stability. *Cell, 159*(3), 572-583. doi:10.1016/j.cell.2014.09.031

Castellano-Pozo, M., Santos-Pereira, J. M., Rondón, A. G., Barroso, S., Andújar, E., Pérez-Alegre, M., . . . Aguilera, A. (2013). R loops are linked to histone H3 S10 phosphorylation and chromatin condensation. *Molecular Cell, 52*(4), 583-590.

Chalamcharla, V. R., Folco, H. D., Dhakshnamoorthy, J., & Grewal, S. I. S. (2015). Conserved factor Dhp1/Rat1/Xrn2 triggers premature transcription termination and nucleates heterochromatin to promote gene silencing. *Proceedings of the National Academy of Sciences, 112*(51), 15548-15555. doi:10.1073/pnas.1522127112

Chao, M. C., Abel, S., Davis, B. M., & Waldor, M. K. (2016). The design and analysis of transposon insertion sequencing experiments. *Nature Reviews Microbiology, 14*(2), 119.

Chen, E. S., Zhang, K., Nicolas, E., Cam, H. P., Zofall, M., & Grewal, S. I. (2008). Cell cycle control of centromeric repeat transcription and heterochromatin assembly. *Nature, 451*(7179), 734-737. doi:10.1038/nature06561

Chen, E. S., Zhang, K., Nicolas, E., Cam, H. P., Zofall, M., & Grewal, S. I. S. (2008). Cell cycle control of centromeric repeat transcription and heterochromatin assembly. *Nature, 451*, 734. doi:10.1038/nature06561

Chikashige, Y., Kinoshita, N., Nakaseko, Y., Matsumoto, T., Murakami, S., Niwa, O., & Yanagida, M. (1989). Composite motifs and repeat symmetry in S. pombe centromeres: Direct analysis by integration of NotI restriction sites. *Cell, 57*(5), 739-751. doi:https://doi.org/10.1016/0092-8674(89)90789-7

Dai, J., Xie, W., Brady, T. L., Gao, J., & Voytas, D. F. (2007). Phosphorylation regulates integration of the yeast Ty5 retrotransposon into heterochromatin. *Molecular Cell, 27*(2), 289-299.

DeBeauchamp, J. L., Moses, A., Noffsinger, V. J., Ulrich, D. L., Job, G., Kosinski, A. M., & Partridge, J. F. (2008). Chp1-Tas3 interaction is required to recruit RITS to fission yeast centromeres and for maintenance of centromeric heterochromatin. *Mol Cell Biol, 28*(7), 2154-2166.

Dheur, S., Saupe, S. J., Genier, S., Vazquez, S., & Javerzat, J.-P. (2011). Role for cohesin in the formation of a heterochromatic domain at fission yeast subtelomeres. *Mol Cell Biol, 31*(5), 1088-1097.

Doench, J. G., Fusi, N., Sullender, M., Hegde, M., Vaimberg, E. W., Donovan, K. F., . . . Root, D. E. (2016). Optimized sgRNA design to maximize activity and minimize off-target effects of CRISPR-Cas9. *Nature Biotechnology, 34*, 184. doi:10.1038/nbt.3437

https://www.nature.com/articles/nbt.3437#supplementary-information

Du, L.-L., & Novick, P. (2002). Pag1p, a novel protein associated with protein kinase Cbk1p, is required for cell morphogenesis and proliferation in Saccharomyces cerevisiae. *Mol Biol Cell, 13*(2), 503-514.

Ekwall, K., Cranston, G., & Allshire, R. C. (1999). Fission Yeast Mutants That Alleviate Transcriptional Silencing in Centromeric Flanking Repeats and Disrupt Chromosome Segregation. *Genetics, 153*(3), 1153.

Ekwall, K., & Ruusala, T. (1994). Mutations in rik1, clr2, clr3 and clr4 genes asymmetrically derepress the silent mating-type loci in fission yeast. *Genetics, 136*(1), 53-64.

Elgin, S. C., & Reuter, G. (2013). Position-effect variegation, heterochromatin formation, and gene silencing in Drosophila. *Cold Spring Harb Perspect Biol, 5*(8), a017780. doi:10.1101/cshperspect.a017780

Esnault, C., & Levin, H. L. (2015). The Long Terminal Repeat Retrotransposons Tf1 and Tf2 of Schizosaccharomyces pombe. *Microbiol Spectr, 3*(4). doi:10.1128/microbiolspec.MDNA3-0040-2014

Evertts, A. G., Plymire, C., Craig, N. L., & Levin, H. L. (2007). The hermes transposon of Musca domestica is an efficient tool for the mutagenesis of Schizosaccharomyces pombe. *Genetics, 177*(4), 2519-2523. doi:10.1534/genetics.107.081075

Fabre, F., Chan, A., Heyer, W.-D., & Gangloff, S. (2002). Alternate pathways involving Sgs1/Top3, Mus81/ Mms4, and Srs2 prevent formation of toxic recombination intermediates from single-stranded gaps created by DNA replication. *Proceedings of the National Academy of Sciences, 99*(26), 16887-16892. doi:10.1073/pnas.252652399

Fasching, Clare L., Cejka, P., Kowalczykowski, Stephen C., & Heyer, W.-D. (2015). Top3-Rmi1 Dissolve Rad51-Mediated D Loops by a Topoisomerase-Based Mechanism. *Molecular Cell, 57*(4), 595-606. doi:https://doi.org/10.1016/j.molcel.2015.01.022

Faye, B., Arnaud, F., Peyretaillade, E., Brasset, E., Dastugue, B., & Vaury, C. (2008). Functional characteristics of a highly specific integrase encoded by an LTR-retrotransposon. *PLoS One, 3*(9), e3185.

Feschotte, C. (2008). Transposable elements and the evolution of regulatory networks. *Nature Reviews Genetics, 9*(5), 397.

Fischer, T., Cui, B., Dhakshnamoorthy, J., Zhou, M., Rubin, C., Zofall, M., . . . Grewal, S. I. S. (2009). Diverse roles of HP1 proteins in heterochromatin assembly and functions in fission yeast. *Proc Natl Acad Sci U S A, 106*(22), 8998-9003. doi:10.1073/pnas.0813063106

Forsburg, S. L. (2001). The art and design of genetic screens: yeast. *Nature Reviews Genetics, 2*, 659. doi:10.1038/35088500

Fournier, L.-A., Kumar, A., & Stirling, P. (2018). Chromatin as a Platform for Modulating the Replication Stress Response. *Genes (Basel), 9*(12), 622.

Gai, X., & Voytas, D. F. (1998). A single amino acid change in the yeast retrotransposon Ty5 abolishes targeting to silent chromatin. *Mol Cell, 1*(7), 1051-1055.

Gangloff, S., McDonald, J. P., Bendixen, C., Arthur, L., & Rothstein, R. (1994). The yeast type I topoisomerase Top3 interacts with Sgs1, a DNA helicase homolog: a potential eukaryotic reverse gyrase. *Mol Cell Biol, 14*(12), 8391-8398. doi:10.1128/mcb.14.12.8391

Gavaldá, S., Gallardo, M., Luna, R., & Aguilera, A. (2013). R-loop mediated transcription-associated recombination in trf4Δ mutants reveals new links between RNA surveillance and genome integrity. *PLoS One, 8*(6), e65541.

Goodwin, A., Wang, S.-W., Toda, T., Norbury, C., & Hickson, I. D. (1999). Topoisomerase III is essential for accurate nuclear division in Schizosaccharomyces pombe. *Nucleic Acids Research, 27*(20), 4050-4058. doi:10.1093/nar/27.20.4050

Goto, T., & Wang, J. C. (1984). Yeast DNA topoisomerase II is encoded by a single-copy, essential gene. *Cell, 36*(4), 1073-1080. doi:https://doi.org/10.1016/0092-8674(84)90057-6

Gottipati, P., Cassel, T. N., Savolainen, L., & Helleday, T. (2008). Transcription-Associated Recombination Is Dependent on Replication in Mammalian Cells. *Mol Cell Biol, 28*(1), 154-164. doi:10.1128/mcb.00816-07

Gottipati, P., & Helleday, T. (2009). Transcription-associated recombination in eukaryotes: link between transcription, replication and recombination. *Mutagenesis, 24*(3), 203-210. doi:10.1093/mutage/gen072

Grech, L., Jeffares, D., Sadée, C. Y., Rodriguez-Lopez, M., Bitton, D. A., Hoti, M., . . . Illingworth, C. J. (2019). Fitness Landscape of the Fission Yeast Genome. *Molecular biology and evolution*.

Grewal, S. I., & Elgin, S. C. (2007). Transcription and RNA interference in the formation of heterochromatin. *Nature, 447*(7143), 399-406. doi:10.1038/nature05914

Grewal, S. I. S., & Jia, S. (2007). Heterochromatin revisited. *Nature Reviews Genetics, 8*, 35. doi:10.1038/nrg2008

Griffiths, D., Uchiyama, M., Nurse, P., & Wang, T. S. (2000). A novel mutant allele of the chromatin-bound fission yeast checkpoint protein Rad17 separates the DNA structure checkpoints. *Journal of Cell Science, 113*(6), 1075-1088.

Groh, S., & Schotta, G. (2017). Silencing of endogenous retroviruses by heterochromatin. *Cell Mol Life Sci, 74*(11), 2055-2065. doi:10.1007/s00018-017-2454-8

Guo, Y., & Levin, H. L. (2010). High-throughput sequencing of retrotransposon integration provides a saturated profile of target activity in Schizosaccharomyces pombe. *Genome Res, 20*(2), 239-248. doi:10.1101/gr.099648.109

Guo, Y., Park, J. M., Cui, B., Humes, E., Gangadharan, S., Hung, S., . . . Levin, H. L. (2013). Integration profiling of gene function with dense maps of transposon integration. *Genetics, 195*(2), 599-609. doi:10.1534/genetics.113.152744

Guo, Y., Singh, P. K., & Levin, H. L. (2015). A long terminal repeat retrotransposon of Schizosaccharomyces japonicus integrates upstream of RNA pol III transcribed genes. *Mob DNA, 6*, 19. doi:10.1186/s13100-015-0048-2

Hagan, I. M. (2016). Chromatin and cell wall staining of Schizosaccharomyces pombe. *Cold Spring Harbor Protocols, 2016*(6), pdb. prot091025.

Hall, S. R., & Goralski, K. B. (2018). ZATT, TDP2, and SUMO2: breaking the tie that binds TOP2 to DNA. *Translational Cancer Research, 7*(4), S439-S444.

Hansen, K. R., Burns, G., Mata, J., Volpe, T. A., Martienssen, R. A., Bahler, J., & Thon, G. (2005). Global effects on gene expression in fission yeast by silencing and RNA interference machineries. *Mol Cell Biol, 25*(2), 590-601. doi:10.1128/mcb.25.2.590-601.2005

Hayashi, M. T., Takahashi, T. S., Nakagawa, T., Nakayama, J., & Masukata, H. (2009). The heterochromatin protein Swi6/HP1 activates replication origins at the pericentromeric region and silent mating-type locus. *Nat Cell Biol, 11*(3), 357-362. doi:10.1038/ncb1845

He, H., Gonzalez, M., Zhang, F., & Li, F. (2014). DNA replication components as regulators of epigenetic inheritance—lesson from fission yeast centromere. *Protein Cell, 5*(6), 411-419. doi:10.1007/s13238-014-0049-9

He, H., Li, Y., Dong, Q., Chang, A.-Y., Gao, F., Chi, Z., . . . Li, F. (2017). Coordinated regulation of heterochromatin inheritance by Dpb3–Dpb4 complex. *Proceedings of the National Academy of Sciences, 114*(47), 12524-12529. doi:10.1073/pnas.1712961114

Hedges, D. J., & Deininger, P. L. (2007). Inviting instability: Transposable elements, double-strand breaks, and the maintenance of genome integrity. *Mutation Research/Fundamental and Molecular Mechanisms of Mutagenesis, 616*(1), 46-59. doi:https://doi.org/10.1016/j.mrfmmm.2006.11.021

Heitz, E. (1929). *Heterochromatin, chromocentren, chromomeren*: Komm. Fischer.

Hickey, A., Esnault, C., Majumdar, A., Chatterjee, A. G., Iben, J. R., McQueen, P. G., . . . Levin, H. L. (2015). Single-Nucleotide-Specific Targeting of the Tf1 Retrotransposon Promoted by the DNA-Binding Protein Sap1 of Schizosaccharomyces pombe. *Genetics, 201*(3), 905-924. doi:10.1534/genetics.115.181602

Hoff, E. F., Levin, H. L., & Boeke, J. D. (1998). Schizosaccharomyces pombe retrotransposon Tf2 mobilizes primarily through homologous cDNA recombination. *Mol Cell Biol, 18*(11), 6839-6852.

Hsu, P. D., Scott, D. A., Weinstein, J. A., Ran, F. A., Konermann, S., Agarwala, V., . . . Zhang, F. (2013). DNA targeting specificity of RNA-guided Cas9 nucleases. *Nature Biotechnology, 31*, 827. doi:10.1038/nbt.2647

https://www.nature.com/articles/nbt.2647#supplementary-information

Huang, H., Stromme, C. B., Saredi, G., Hodl, M., Strandsby, A., Gonzalez-Aguilera, C., . . . Patel, D. J. (2015). A unique binding mode enables MCM2 to chaperone histones H3-H4 at replication forks. *Nat Struct Mol Biol, 22*(8), 618-626. doi:10.1038/nsmb.3055

Ira, G., Malkova, A., Liberi, G., Foiani, M., & Haber, J. E. (2003). Srs2 and Sgs1–Top3 suppress crossovers during double-strand break repair in yeast. *Cell, 115*(4), 401-411.

Irvine, D. V., Goto, D. B., Vaughn, M. W., Nakaseko, Y., McCombie, W. R., Yanagida, M., & Martienssen, R. (2009). Mapping epigenetic mutations in fission yeast using whole-genome next-generation sequencing. *Genome Res, 19*(6), 1077-1083. doi:10.1101/gr.089318.108

Jacobs, J. Z., Rosado-Lugo, J. D., Cranz-Mileva, S., Ciccaglione, K. M., Tournier, V., & Zaratiegui, M. (2015). Arrested replication forks guide retrotransposon integration. *Science, 349*(6255), 1549-1553. doi:10.1126/science.aaa3810

Jahn, L. J., Mason, B., Brøgger, P., Toteva, T., Nielsen, D. K., & Thon, G. (2018). Dependency of Heterochromatin Domains on Replication Factors. *G3 (Bethesda), 8*(2), 477-489. doi:10.1534/g3.117.300341

Janssen, A., Colmenares, S. U., & Karpen, G. H. (2018). Heterochromatin: Guardian of the Genome. *Annu Rev Cell Dev Biol, 34*, 265-288. doi:10.1146/annurev-cellbio-100617-062653

Jasencakova, Z., & Groth, A. (2010). Replication stress, a source of epigenetic aberrations in cancer? *Bioessays, 32*(10), 847-855.

Jasencakova, Z., Scharf, A. N. D., Ask, K., Corpet, A., Imhof, A., Almouzni, G., & Groth, A. Replication Stress Interferes with Histone Recycling and Predeposition Marking of New Histones. *Molecular Cell, 37*(5), 736-743. doi:10.1016/j.molcel.2010.01.033

Jeffares, D. C., Jolly, C., Hoti, M., Speed, D., Shaw, L., Rallis, C., . . . Sedlazeck, F. J. (2017). Transient structural variations have strong effects on quantitative traits and reproductive isolation in fission yeast. *Nat Commun, 8*, 14061. doi:10.1038/ncomms14061

https://www.nature.com/articles/ncomms14061#supplementary-information

Jih, G., Iglesias, N., Currie, M. A., Bhanu, N. V., Paulo, J. A., Gygi, S. P., . . . Moazed, D. (2017). Unique roles for histone H3K9me states in RNAi and heritable silencing of transcription. *Nature, 547*(7664), 463-467. doi:10.1038/nature23267

Kanoh, J., Sadaie, M., Urano, T., & Ishikawa, F. (2005). Telomere Binding Protein Taz1 Establishes Swi6 Heterochromatin Independently of RNAi at Telomeres. *Current Biology, 15*(20), 1808-1819. doi:https://doi.org/10.1016/j.cub.2005.09.041

Kaur, H., De Muyt, A., & Lichten, M. (2015). Top3-Rmi1 DNA single-strand decatenase is integral to the formation and resolution of meiotic recombination intermediates. *Mol Cell, 57*(4), 583-594. doi:10.1016/j.molcel.2015.01.020

Keller, C., Adaixo, R., Stunnenberg, R., Woolcock, K. J., Hiller, S., & Buhler, M. (2012). HP1(Swi6) mediates the recognition and destruction of heterochromatic RNA transcripts. *Mol Cell, 47*(2), 215-227. doi:10.1016/j.molcel.2012.05.009

Khurana, S., & Oberdoerffer, P. (2015). Replication Stress: A Lifetime of Epigenetic Change. *Genes (Basel), 6*(3), 858-877. doi:10.3390/genes6030858

Kidwell, M. G. (2002). Transposable elements and the evolution of genome size in eukaryotes. *Genetica, 115*(1), 49-63.

Kirkland, J. G., Raab, J. R., & Kamakaka, R. T. (2013). TFIIIC Bound DNA Elements in Nuclear Organization and Insulation. *Biochim Biophys Acta, 1829*(3-4), 418-424. doi:10.1016/j.bbagrm.2012.09.006

Kloc, A., Zaratiegui, M., Nora, E., & Martienssen, R. (2008). RNA interference guides histone modification during the S phase of chromosomal replication. *Curr Biol, 18*(7), 490-495. doi:10.1016/j.cub.2008.03.016

Klosin, A., Reis, K., Hidalgo-Carcedo, C., Casas, E., Vavouri, T., & Lehner, B. (2017). Impaired DNA replication derepresses chromatin and generates a transgenerationally inherited epigenetic memory. *Sci Adv, 3*(8), e1701143. doi:10.1126/sciadv.1701143

Kobayashi, T., & Ganley, A. R. (2005). Recombination regulation by transcription-induced cohesin dissociation in rDNA repeats. *Science, 309*(5740), 1581-1584. doi:10.1126/science.1116102

Kobayashi, T., Heck, D. J., Nomura, M., & Horiuchi, T. (1998). Expansion and contraction of ribosomal DNA repeats in Saccharomyces cerevisiae: requirement of replication fork blocking (Fob1) protein and the role of RNA polymerase I. *Genes Dev, 12*(24), 3821-3830.

Koc, A., Wheeler, L. J., Mathews, C. K., & Merrill, G. F. (2004). Hydroxyurea arrests DNA replication by a mechanism that preserves basal dNTP pools. *J Biol Chem, 279*(1), 223-230. doi:10.1074/jbc.M303952200

Køhler, J. B., Tammsalu, T., Jørgensen, M. M., Steen, N., Hay, R. T., & Thon, G. (2015). Targeting of SUMO substrates to a Cdc48–Ufd1–Npl4 segregase and STUbL pathway in fission yeast. *Nat Commun, 6*, 8827. doi:10.1038/ncomms9827

https://www.nature.com/articles/ncomms9827#supplementary-information

Kokoska, R. J., Stefanovic, L., Tran, H. T., Resnick, M. A., Gordenin, D. A., & Petes, T. D. (1998). Destabilization of Yeast Micro- and Minisatellite DNA Sequences by Mutations Affecting a Nuclease Involved in Okazaki Fragment Processing (rad27) and DNA Polymerase δ (pol3-t). *Mol Cell Biol, 18*(5), 2779-2788. doi:10.1128/mcb.18.5.2779

Kool, J., & Berns, A. (2009). High-throughput insertional mutagenesis screens in mice to identify oncogenic networks. *Nature Reviews Cancer, 9*, 389. doi:10.1038/nrc2647

Korbel, J. O., Urban, A. E., Affourtit, J. P., Godwin, B., Grubert, F., Simons, J. F., . . . Snyder, M. (2007). Paired-end mapping reveals extensive structural variation in the human genome. *Science, 318*(5849), 420-426. doi:10.1126/science.1149504

Krings, G., & Bastia, D. (2005). Sap1p binds to Ter1 at the ribosomal DNA of Schizosaccharomyces pombe and causes polar replication fork arrest. *J Biol Chem, 280*(47), 39135-39142. doi:10.1074/jbc.M508996200

Lander, E. S., Linton, L. M., Birren, B., Nusbaum, C., Zody, M. C., Baldwin, J., . . . Szustakowki, J. (2001). Initial sequencing and analysis of the human genome. *Nature, 409*(6822), 860-921. doi:10.1038/35057062

Lee, S. Y., Rozenzhak, S., & Russell, P. (2013). gammaH2A-binding protein Brc1 affects centromere function in fission yeast. *Mol Cell Biol, 33*(7), 1410-1416. doi:10.1128/mcb.01654-12

Li, F. (2011). Coordination of DNA Replication and Histone Modification by the Rik1-Dos2 Complex. *475*(7355), 244-248. doi:10.1038/nature10161

Li, F., Goto, D. B., Zaratiegui, M., Tang, X., Martienssen, R., & Cande, W. Z. (2005). Two novel proteins, dos1 and dos2, interact with rik1 to regulate heterochromatic RNA interference and histone modification. *Curr Biol, 15*(16), 1448-1457. doi:10.1016/j.cub.2005.07.021

Li, J., Wang, H.-T., Wang, W.-T., Zhang, X.-R., Suo, F., Ren, J.-Y., . . . Du, L.-L. (2019). Systematic analysis reveals the prevalence and principles of bypassable gene essentiality. *Nat Commun, 10*(1), 1002. doi:10.1038/s41467-019-08928-1

Liu, L. F., Desai, S. D., Li, T. K., Mao, Y., Sun, M., & Sim, S. P. (2000). Mechanism of action of camptothecin. *Ann N Y Acad Sci, 922*, 1-10. doi:10.1111/j.1749-6632.2000.tb07020.x

Liu, S., Xu, Z., Leng, H., Zheng, P., Yang, J., Chen, K., . . . Li, Q. (2017). RPA binds histone H3-H4 and functions in DNA replication–coupled nucleosome assembly. *Science, 355*(6323), 415-420. doi:10.1126/science.aah4712

Liu, V. F., Bhaumik, D., & Wang, T. S.-F. (1999). Mutator Phenotype Induced by Aberrant Replication. *Mol Cell Biol, 19*(2), 1126-1135. doi:10.1128/mcb.19.2.1126

Loeb, L. A., Springgate, C. F., & Battula, N. (1974). Errors in DNA Replication as a Basis of Malignant Changes. *Cancer Research, 34*(9), 2311-2321.

Lorenz, D. R., Mikheyeva, I. V., Johansen, P., Meyer, L., Berg, A., Grewal, S. I. S., & Cam, H. P. (2012). CENP-B Cooperates with Set1 in Bidirectional Transcriptional Silencing and Genome Organization of Retrotransposons. *Mol Cell Biol, 32*(20), 4215-4225. doi:10.1128/mcb.00395-12

Lorenzi, L. E., Bah, A., Wischnewski, H., Shchepachev, V., Soneson, C., Santagostino, M., & Azzalin, C. M. (2015). Fission yeast Cactin restricts telomere transcription and elongation by controlling Rap1 levels. *Embo j, 34*(1), 115-129. doi:10.15252/embj.201489559

Lundin, C., North, M., Erixon, K., Walters, K., Jenssen, D., Goldman, A. S., & Helleday, T. (2005). Methyl methanesulfonate (MMS) produces heat-labile DNA damage but no detectable in vivo DNA double-strand breaks. *Nucleic Acids Res, 33*(12), 3799-3811. doi:10.1093/nar/gki681

Lynch, M., Sung, W., Morris, K., Coffey, N., Landry, C. R., Dopman, E. B., . . . Hartl, D. L. (2008). A genome-wide view of the spectrum of spontaneous mutations in yeast. *Proceedings of the National Academy of Sciences, 105*(27), 9272-9277.

Mallet, P.-L., Larochelle, M., & Bachand, F. (2017). Multiple Transcriptional and Post-transcriptional Pathways Collaborate to Control Sense and Antisense RNAs of Tf2 Retroelements in Fission Yeast. *Genetics, 205*(2), 621-632. doi:10.1534/genetics.116.193870

Martienssen, R., & Moazed, D. (2015). RNAi and heterochromatin assembly. *Cold Spring Harb Perspect Biol, 7*(8), a019323. doi:10.1101/cshperspect.a019323

Mateo, L., & Gonzalez, J. (2014). Pogo-like transposases have been repeatedly domesticated into CENP-B-related proteins. *Genome Biol Evol, 6*(8), 2008-2016. doi:10.1093/gbe/evu153

McKinley, K. L., & Cheeseman, I. M. (2015). The molecular basis for centromere identity and function. *Nature Reviews Molecular Cell Biology, 17*, 16. doi:10.1038/nrm.2015.5

Mejía-Ramírez, E., Sánchez-Gorostiaga, A., Krimer, D. B., Schvartzman, J. B., & Hernández, P. (2005). The mating type switch-activating protein Sap1 Is required for replication fork arrest at the rRNA genes of fission yeast. *Mol Cell Biol, 25*(19), 8755-8761. doi:10.1128/MCB.25.19.8755-8761.2005

Mengoli, V., Bucciarelli, E., Lattao, R., Piergentili, R., Gatti, M., & Bonaccorsi, S. (2014). The analysis of mutant alleles of different strength reveals multiple functions of topoisomerase 2 in regulation of Drosophila chromosome structure. *PLoS Genet, 10*(10), e1004739. doi:10.1371/journal.pgen.1004739

Michel, A. H., Hatakeyama, R., Kimmig, P., Arter, M., Peter, M., Matos, J., . . . Kornmann, B. (2017). Functional mapping of yeast genomes by saturated transposition. *Elife, 6*, e23570.

Michel, B., Flores, M.-J., Viguera, E., Grompone, G., Seigneur, M., & Bidnenko, V. (2001). Rescue of arrested replication forks by homologous recombination. *Proceedings of the National Academy of Sciences, 98*(15), 8181-8188. doi:10.1073/pnas.111008798

Miller, E. L., Hargreaves, D. C., Kadoch, C., Chang, C. Y., Calarco, J. P., Hodges, C., . . . Crabtree, G. R. (2017). TOP2 synergizes with BAF chromatin remodeling for both resolution and formation of facultative heterochromatin. *Nat Struct Mol Biol, 24*(4), 344-352. doi:10.1038/nsmb.3384

Mischo, H. E., Gomez-Gonzalez, B., Grzechnik, P., Rondon, A. G., Wei, W., Steinmetz, L., . . . Proudfoot, N. J. (2011). Yeast Sen1 helicase protects the genome from transcription-associated instability. *Mol Cell, 41*. doi:10.1016/j.molcel.2010.12.007

Morrison, A., & Sugino, A. (1994). The 3'-->5' exonucleases of both DNA polymerases delta and epsilon participate in correcting errors of DNA replication in Saccharomyces cerevisiae. *Mol Gen Genet, 242*(3), 289-296.

Motamedi, M. R., Hong, E.-J. E., Li, X., Gerber, S., Denison, C., Gygi, S., & Moazed, D. (2008). HP1 Proteins Form Distinct Complexes and Mediate Heterochromatic Gene Silencing by Nonoverlapping Mechanisms. *Molecular Cell, 32*(6), 778-790. doi:https://doi.org/10.1016/j.molcel.2008.10.026

Muller, H. J., & Muller, H. (1930). Types of visible variations induced by X-rays in Drosophila. *Journal of Genetics, 22*(03).

Mundbjerg, K., Jørgensen, S. W., Fredsøe, J., Nielsen, I., Pedersen, J. M., Bentsen, I. B., . . . Andersen, A. H. (2015). Top2 and Sgs1-Top3 Act Redundantly to Ensure rDNA Replication Termination. *PLoS Genet, 11*(12), e1005697. doi:10.1371/journal.pgen.1005697

Murray, J. M., Watson, A. T., & Carr, A. M. (2016). Extraction of Chromosomal DNA from Schizosaccharomyces pombe. *Cold Spring Harb Protoc, 2016*(5). doi:10.1101/pdb.prot090985

Murray, J. M., Watson, A. T., and Carr, A.M. (2016). Transformation of Schizosaccharomyces Pombe: Electroporation Procedure. *Cold Spring Harbor Protocols*.

Murton, H. E., Grady, P. J. R., Chan, T. H., Cam, H. P., & Whitehall, S. K. (2016). Restriction of Retrotransposon Mobilization in Schizosaccharomyces pombe by Transcriptional Silencing and Higher-Order Chromatin Organization. *Genetics, 203*(4), 1669-1678. doi:10.1534/genetics.116.189118

Nakase, Y., & Matsumoto, T. (2018). The RHEB–mTOR axis regulates expression of Tf2 transposons in fission yeast. *Journal of Cell Science, 131*(22), jcs221457. doi:10.1242/jcs.221457

Nakayama, J.-i., Rice, J. C., Strahl, B. D., Allis, C. D., & Grewal, S. I. (2001). Role of histone H3 lysine 9 methylation in epigenetic control of heterochromatin assembly. *Science, 292*(5514), 110-113.

Nakayama, J., Rice, J. C., Strahl, B. D., Allis, C. D., & Grewal, S. I. (2001). Role of histone H3 lysine 9 methylation in epigenetic control of heterochromatin assembly. *Science, 292*(5514), 110-113. doi:10.1126/science.1060118

Nikolov, I., Taddei, A. (2015). Linking Replication Stress with Heterochromatin Formation.

Noguchi, C., & Noguchi, E. (2007). Sap1 promotes the association of the replication fork protection complex with chromatin and is involved in the replication checkpoint in Schizosaccharomyces pombe. *Genetics, 175*(2), 553-566. doi:10.1534/genetics.106.065334

Oliver, K. R., & Greene, W. K. (2009). Transposable elements: powerful facilitators of evolution. *Bioessays, 31*(7), 703-714.

Osman, F., & Whitby, M. C. (2009). Monitoring homologous recombination following replication fork perturbation in the fission yeast Schizosaccharomyces pombe. *Methods Mol Biol, 521*, 535-552. doi:10.1007/978-1-60327-815-7_31

Partridge, J. F. (2008). Centromeric chromatin in fission yeast. *Front Biosci, 13*, 3896-3905.

Pastuzyn, E. D., Day, C. E., Kearns, R. B., Kyrke-Smith, M., Taibi, A. V., McCormick, J., . . . Shepherd, J. D. (2018). The Neuronal Gene Arc Encodes a Repurposed Retrotransposon Gag Protein that Mediates Intercellular RNA Transfer. *Cell, 172*(1-2), 275-288.e218. doi:10.1016/j.cell.2017.12.024

Peng, J. C., & Karpen, G. H. (2008). Epigenetic regulation of heterochromatic DNA stability. *Curr Opin Genet Dev, 18*(2), 204-211. doi:10.1016/j.gde.2008.01.021

Pommier, Y., Barcelo, J. M., Rao, V. A., Sordet, O., Jobson, A. G., Thibaut, L., . . . Redon, C. (2006). Repair of topoisomerase I-mediated DNA damage. *Prog Nucleic Acid Res Mol Biol, 81*, 179-229. doi:10.1016/s0079-6603(06)81005-6

Pommier, Y., Sun, Y., Huang, S.-y. N., & Nitiss, J. L. (2016). Roles of eukaryotic topoisomerases in transcription, replication and genomic stability. *Nature Reviews Molecular Cell Biology, 17*, 703. doi:10.1038/nrm.2016.111

https://www.nature.com/articles/nrm.2016.111#supplementary-information

Prado, F., & Aguilera, A. (2005). Impairment of replication fork progression mediates RNA polII transcription-associated recombination. *Embo j, 24*(6), 1267-1276. doi:10.1038/sj.emboj.7600602

Provost, P., Silverstein, R. A., Dishart, D., Walfridsson, J., Djupedal, I., Kniola, B., . . . Ekwall, K. (2002). Dicer is required for chromosome segregation and gene silencing in fission yeast cells. *Proceedings of the National Academy of Sciences, 99*(26), 16648-16653.

Ranatunga, N. S., & Forsburg, S. L. (2016). Characterization of a Novel MMS-Sensitive Allele of Schizosaccharomyces pombe mcm4. *G3 (Bethesda), 6*(10), 3049-3063. doi:10.1534/g3.116.033571

Reveron-Gomez, N., Gonzalez-Aguilera, C., Stewart-Morgan, K. R., Petryk, N., Flury, V., Graziano, S., . . . Groth, A. (2018). Accurate Recycling of Parental Histones Reproduces the Histone Modification Landscape during DNA Replication. *Mol Cell, 72*(2), 239-249.e235. doi:10.1016/j.molcel.2018.08.010

Rey, O., Danchin, E., Mirouze, M., Loot, C., & Blanchet, S. (2016). Adaptation to Global Change: A Transposable Element–Epigenetics Perspective. *Trends in Ecology & Evolution, 31*(7), 514-526. doi:https://doi.org/10.1016/j.tree.2016.03.013

Reyes-Turcu, F. E., Zhang, K., Zofall, M., Chen, E., & Grewal, S. I. (2011). Defects in RNA quality control factors reveal RNAi-independent nucleation of heterochromatin. *Nat Struct Mol Biol, 18*(10), 1132-1138. doi:10.1038/nsmb.2122

Richet, N., Liu, D., Legrand, P., Velours, C., Corpet, A., Gaubert, A., . . . Ochsenbein, F. (2015). Structural insight into how the human helicase subunit MCM2 may act as a histone chaperone together with ASF1 at the replication fork. *Nucleic Acids Res, 43*(3), 1905-1917. doi:10.1093/nar/gkv021

Rothstein, R., Michel, B., & Gangloff, S. (2000). Replication fork pausing and recombination or "gimme a break". *Genes Dev, 14*(1), 1-10.

Rousset, F., Cui, L., Siouve, E., Becavin, C., Depardieu, F., & Bikard, D. (2018). Genome-wide CRISPR-dCas9 screens in E. coli identify essential genes and phage host factors. *PLoS Genet, 14*(11), e1007749. doi:10.1371/journal.pgen.1007749

Rowlands, H., Dhavarasa, P., Cheng, A., & Yankulov, K. (2017). Forks on the Run: Can the Stalling of DNA Replication Promote Epigenetic Changes? *Frontiers in Genetics, 8*(86). doi:10.3389/fgene.2017.00086

Rozenzhak, S., Mejía-Ramírez, E., Williams, J. S., Schaffer, L., Hammond, J. A., Head, S. R., & Russell, P. (2010). Rad3ATR decorates critical chromosomal domains with γH2A to protect genome integrity during S-phase in fission yeast. *PLoS Genet, 6*(7), e1001032.

Runge, K. W., & Zakian, V. A. (1996). TEL2, an essential gene required for telomere length regulation and telomere position effect in Saccharomyces cerevisiae. *Mol Cell Biol, 16*(6), 3094-3105. doi:10.1128/mcb.16.6.3094

Rustici, G., Mata, J., Kivinen, K., Lió, P., Penkett, C. J., Burns, G., . . . Bähler, J. (2004). Periodic gene expression program of the fission yeast cell cycle. *Nat Genet, 36*(8), 809.

Salim, D., Bradford, W. D., Freeland, A., Cady, G., Wang, J., Pruitt, S. C., & Gerton, J. L. (2017). DNA replication stress restricts ribosomal DNA copy number. *PLoS Genet, 13*(9), e1007006.

Sankar, T. S., Wastuwidyaningtyas, B. D., Dong, Y., Lewis, S. A., & Wang, J. D. (2016). The nature of mutations induced by replication–transcription collisions. *Nature, 535*(7610), 178-181. doi:10.1038/nature18316

Schmidt, B. H., Osheroff, N., & Berger, J. M. (2012). Structure of a topoisomerase II-DNA-nucleotide complex reveals a new control mechanism for ATPase activity. *Nat Struct Mol Biol, 19*(11), 1147-1154. doi:10.1038/nsmb.2388

Schultz. (1950). Interrelations of factors affecting heterochromatin-induced variegation in Drosophila. *Genetics*.

Sehgal, A., Lee, C. Y., & Espenshade, P. J. (2007). SREBP controls oxygen-dependent mobilization of retrotransposons in fission yeast. *PLoS Genet, 3*(8), e131. doi:10.1371/journal.pgen.0030131

Serero, A., Jubin, C., Loeillet, S., Legoix-Né, P., & Nicolas, A. G. (2014). Mutational landscape of yeast mutator strains. *Proceedings of the National Academy of Sciences, 111*(5), 1897-1902. doi:10.1073/pnas.1314423111

Shikata, M., Ishikawa, F., & Kanoh, J. (2007). Tel2 is required for activation of the Mrc1-mediated replication checkpoint. *J Biol Chem, 282*(8), 5346-5355. doi:10.1074/jbc.M607432200

Skourti-Stathaki, K., & Proudfoot, N. J. (2014). A double-edged sword: R loops as threats to genome integrity and powerful regulators of gene expression. *Genes Dev, 28*(13), 1384-1396.

Slater, M. L. (1973). Effect of Reversible Inhibition of Deoxyribonucleic Acid Synthesis on the Yeast Cell Cycle. *Journal of Bacteriology, 113*(1), 263-270.

Sohl, C. D., Ray, S., & Sweasy, J. B. (2015). Pools and Pols: Mechanism of a mutator phenotype. *Proceedings of the National Academy of Sciences, 112*(19), 5864-5865. doi:10.1073/pnas.1505169112

Spaller, T., Kling, E., Glöckner, G., Hillmann, F., & Winckler, T. (2016). Convergent evolution of tRNA gene targeting preferences in compact genomes. *Mob DNA, 7*(1), 17. doi:10.1186/s13100-016-0073-9

Spofford, J. B. (1967). Single-locus modification of position-effect variegation in Drosophila melanogaster. I. White variegation. *Genetics, 57*(4), 751-766.

Steglich, B., Strålfors, A., Khorosjutina, O., Persson, J., Smialowska, A., Javerzat, J. P., & Ekwall, K. (2015). The Fun30 Chromatin Remodeler Fft3 Controls Nuclear Organization and Chromatin Structure of Insulators and Subtelomeres in Fission Yeast. *PLoS Genet, 11*(3). doi:10.1371/journal.pgen.1005101

Stellfox, M. E., Bailey, A. O., & Foltz, D. R. (2013). Putting CENP-A in its place. *Cellular and molecular life sciences, 70*(3), 387-406.

Sugiyama, T., Cam, H., Verdel, A., Moazed, D., & Grewal, S. I. S. (2005). RNA-dependent RNA polymerase is an essential component of a self-enforcing loop coupling heterochromatin assembly to siRNA production. *Proc Natl Acad Sci U S A, 102*(1), 152-157. doi:10.1073/pnas.0407641102

Sugiyama, T., Cam, H. P., Sugiyama, R., Noma, K.-i., Zofall, M., Kobayashi, R., & Grewal, S. I. S. (2007). SHREC, an Effector Complex for Heterochromatic Transcriptional Silencing. *Cell, 128*(3), 491-504. doi:https://doi.org/10.1016/j.cell.2006.12.035

Sultana, T., van Essen, D., Siol, O., Bailly-Bechet, M., Philippe, C., Zine El Aabidine, A., . . . Cristofari, G. (2019). The Landscape of L1 Retrotransposons in the Human Genome Is Shaped by Pre-insertion Sequence Biases and Post-insertion Selection. *Molecular Cell, 74*(3), 555-570.e557. doi:https://doi.org/10.1016/j.molcel.2019.02.036

Sultana, T., Zamborlini, A., Cristofari, G., & Lesage, P. (2017). Integration site selection by retroviruses and transposable elements in eukaryotes. *Nature Reviews Genetics, 18*, 292. doi:10.1038/nrg.2017.7

https://www.nature.com/articles/nrg.2017.7#supplementary-information

Suski, C., & Marians, K. J. (2008). Resolution of converging replication forks by RecQ and topoisomerase III. *Mol Cell, 30*(6), 779-789. doi:10.1016/j.molcel.2008.04.020

Šviković, S., & Sale, J. E. (2017). The effects of replication stress on S phase histone management and epigenetic memory. *Journal of Molecular Biology, 429*(13), 2011-2029.

Takai, H., Xie, Y., de Lange, T., & Pavletich, N. P. (2010). Tel2 structure and function in the Hsp90-dependent maturation of mTOR and ATR complexes. *Genes Dev, 24*(18), 2019-2030. doi:10.1101/gad.1956410

Takeuchi, Y., Horiuchi, T., & Kobayashi, T. (2003). Transcription-dependent recombination and the role of fork collision in yeast rDNA. *Genes Dev, 17*(12), 1497-1506. doi:10.1101/gad.1085403

Talbert, P. B., & Henikoff, S. (2016). Histone variants on the move: substrates for chromatin dynamics. *Nature Reviews Molecular Cell Biology, 18*, 115. doi:10.1038/nrm.2016.148

https://www.nature.com/articles/nrm.2016.148#supplementary-information

Taneja, N., Zofall, M., Balachandran, V., Thillainadesan, G., Sugiyama, T., Wheeler, D., . . . Grewal, S. I. S. SNF2 Family Protein Fft3 Suppresses Nucleosome Turnover to Promote Epigenetic Inheritance and Proper Replication. *Molecular Cell*. doi:http://dx.doi.org/10.1016/j.molcel.2017.02.006

Thon, G., Cohen, A., & Klar, A. J. (1994). Three additional linkage groups that repress transcription and meiotic recombination in the mating-type region of Schizosaccharomyces pombe. *Genetics, 138*(1), 29-38.

Thon, G., & Klar, A. J. (1992). The clr1 locus regulates the expression of the cryptic mating-type loci of fission yeast. *Genetics, 131*(2), 287-296.

Ting, D. T., Lipson, D., Paul, S., Brannigan, B. W., Akhavanfard, S., Coffman, E. J., . . . Haber, D. A. (2011). Aberrant overexpression of satellite repeats in pancreatic and other epithelial cancers. *Science, 331*(6017), 593-596. doi:10.1126/science.1200801

Tong, X., Campbell, J. W., Balazsi, G., Kay, K. A., Wanner, B. L., Gerdes, S. Y., & Oltvai, Z. N. (2004). Genome-scale identification of conditionally essential genes in E. coli by DNA microarrays. *Biochem Biophys Res Commun, 322*(1), 347-354. doi:10.1016/j.bbrc.2004.07.110

Trojer, P., & Reinberg, D. (2007). Facultative Heterochromatin: Is There a Distinctive Molecular Signature? *Molecular Cell, 28*(1), 1-13. doi:10.1016/j.molcel.2007.09.011

Tubbs, A., & Nussenzweig, A. (2017). Endogenous DNA Damage as a Source of Genomic Instability in Cancer. *Cell, 168*(4), 644-656. doi:https://doi.org/10.1016/j.cell.2017.01.002

Uemura, T., & Yanagida, M. (1984). Isolation of type I and II DNA topoisomerase mutants from fission yeast: single and double mutants show different phenotypes in cell growth and chromatin organization. *Embo j, 3*(8), 1737-1744.

van Opijnen, T., & Camilli, A. (2013). Transposon insertion sequencing: a new tool for systems-level analysis of microorganisms. *Nature Reviews Microbiology, 11*, 435. doi:10.1038/nrmicro3033

Verdel, A., Jia, S., Gerber, S., Sugiyama, T., Gygi, S., Grewal, S. I., & Moazed, D. (2004). RNAi-mediated targeting of heterochromatin by the RITS complex. *Science, 303*(5658), 672-676.

Vesela, E., Chroma, K., Turi, Z., & Mistrik, M. (2017). Common Chemical Inductors of Replication Stress: Focus on Cell-Based Studies. *Biomolecules, 7*(1). doi:10.3390/biom7010019

Volpe, T. A., Kidner, C., Hall, I. M., Teng, G., Grewal, S. I. S., & Martienssen, R. A. (2002). Regulation of Heterochromatic Silencing and Histone H3 Lysine-9 Methylation by RNAi. *Science, 297*(5588), 1833-1837. doi:10.1126/science.1074973

Wang, T., Birsoy, K., Hughes, N. W., Krupczak, K. M., Post, Y., Wei, J. J., . . . Sabatini, D. M. (2015). Identification and characterization of essential genes in the human genome. *Science, 350*(6264), 1096-1101. doi:10.1126/science.aac7041

Weaver, D. C., Shpakovski, G. V., Caputo, E., Levin, H. L., & Boeke, J. D. (1993). Sequence analysis of closely related retrotransposon families from fission yeast. *Gene, 131*(1), 135-139. doi:https://doi.org/10.1016/0378-1119(93)90682-S

Wei, Y., Diao, L. X., Lu, S., Wang, H. T., Suo, F., Dong, M. Q., & Du, L. L. (2017). SUMO-Targeted DNA Translocase Rrp2 Protects the Genome from Top2-Induced DNA Damage. *Mol Cell, 66*(5), 581-596.e586. doi:10.1016/j.molcel.2017.04.017

Wessler, S. R. (2006). Transposable elements and the evolution of eukaryotic genomes. *Proceedings of the National Academy of Sciences, 103*(47), 17600-17601. doi:10.1073/pnas.0607612103

Williams, J. S., Williams, R. S., Dovey, C. L., Guenther, G., Tainer, J. A., & Russell, P. (2010). gammaH2A binds Brc1 to maintain genome integrity during S-phase. *Embo j, 29*(6), 1136-1148. doi:10.1038/emboj.2009.413

Win, T. Z., Goodwin, A., Hickson, I. D., Norbury, C. J., & Wang, S.-W. (2004). Requirement for Schizosaccharomyces pombe Top3 in the maintenance of chromosome integrity. *Journal of Cell Science, 117*(20), 4769-4778. doi:10.1242/jcs.01351

Xhemalce, B., Seeler, J. S., Thon, G., Dejean, A., & Arcangioli, B. (2004). Role of the fission yeast SUMO E3 ligase Pli1p in centromere and telomere maintenance. *Embo j, 23*(19), 3844-3853.

Xie, W., Gai, X., Zhu, Y., Zappulla, D. C., Sternglanz, R., & Voytas, D. F. (2001). Targeting of the yeast Ty5 retrotransposon to silent chromatin is mediated by interactions between integrase and Sir4p. *Mol Cell Biol, 21*(19), 6606-6614. doi:10.1128/mcb.21.19.6606-6614.2001

Xu, Y.-j., Khan, S., Didier, A. C., Wozniak, M., Liu, Y., Singh, A., & Nakamura, T. M. (2019). A tel2 mutation that destabilizes the Tel2-Tti1-Tti2 complex eliminates

Rad3[ATR] kinase signaling in the DNA replication checkpoint and leads to telomere shortening in fission yeast. *Mol Cell Biol*, MCB.00175-00119. doi:10.1128/mcb.00175-19

Yamada, T., Fischle, W., Sugiyama, T., Allis, C. D., & Grewal, S. I. (2005). The nucleation and maintenance of heterochromatin by a histone deacetylase in fission yeast. *Mol Cell, 20*(2), 173-185. doi:10.1016/j.molcel.2005.10.002

Yanagida, M. (1998). Fission yeast cut mutations revisited: control of anaphase. *Trends in Cell Biology, 8*(4), 144-149. doi:10.1016/S0962-8924(98)01236-7

Young Lee, S., & Russell, P. (2013). Brc1 links replication stress response and centromere function. *Cell Cycle, 12*(11), 1665-1671.

Zaratiegui, M., Castel, S., Irvine, D. V., Kloc, A., Ren, J., Li, F., . . . Martienssen, R. A. (2011). RNAi promotes heterochromatic silencing through replication-coupled release of RNA polII. *Nature, 479*(7371), 135-138. doi:10.1038/nature10501

Zaratiegui, M., Vaughn, M. W., Irvine, D. V., Goto, D., Watt, S., Bahler, J., . . . Martienssen, R. A. (2011). CENP-B preserves genome integrity at replication forks paused by retrotransposon LTR. *Nature, 469*(7328), 112-115. doi:10.1038/nature09608

Zhang, K., Mosch, K., Fischle, W., & Grewal, S. I. S. (2008). Roles of the Clr4 methyltransferase complex in nucleation, spreading and maintenance of heterochromatin. *Nature Structural &Amp; Molecular Biology, 15*, 381. doi:10.1038/nsmb.1406

https://www.nature.com/articles/nsmb.1406#supplementary-information

Zhang, W., Li, J., Suzuki, K., Qu, J., Wang, P., Zhou, J., . . . Belmonte, J. C. (2015). Aging stem cells. A Werner syndrome stem cell model unveils heterochromatin alterations as a driver of human aging. *Science, 348*(6239), 1160-1163. doi:10.1126/science.aaa1356

Zhang, X.-R., He, J.-B., Wang, Y.-Z., & Du, L.-L. (2018). A Cloning-Free Method for CRISPR/Cas9-Mediated Genome Editing in Fission Yeast. *G3 (Bethesda), 8*(6), 2067-2077. doi:10.1534/g3.118.200164

Zhao, H., & Russell, P. (2004). DNA binding domain in the replication checkpoint protein Mrc1 of Schizosaccharomyces pombe. *Journal of Biological Chemistry, 279*(51), 53023-53027.

Zhimulev, I., Belyaeva, E., Fomina, O., Protopopov, M., & Bolshakov, V. (1986). Cytogenetic and molecular aspects of position effect variegation in Drosophila melanogaster. *Chromosoma, 94*(6), 492-504.

Zhu, Q., Pao, G. M., Huynh, A. M., Suh, H., Tonnu, N., Nederlof, P. M., . . . Verma, I. M. (2011). BRCA1 tumour suppression occurs via heterochromatin-mediated silencing. *Nature, 477*(7363), 179-184. doi:10.1038/nature10371

Zou, S., Ke, N., Kim, J. M., & Voytas, D. F. (1996). The Saccharomyces retrotransposon Ty5 integrates preferentially into regions of silent chromatin at the telomeres and mating loci. *Genes Dev, 10*(5), 634-645. doi:10.1101/gad.10.5.634